CHALMERS

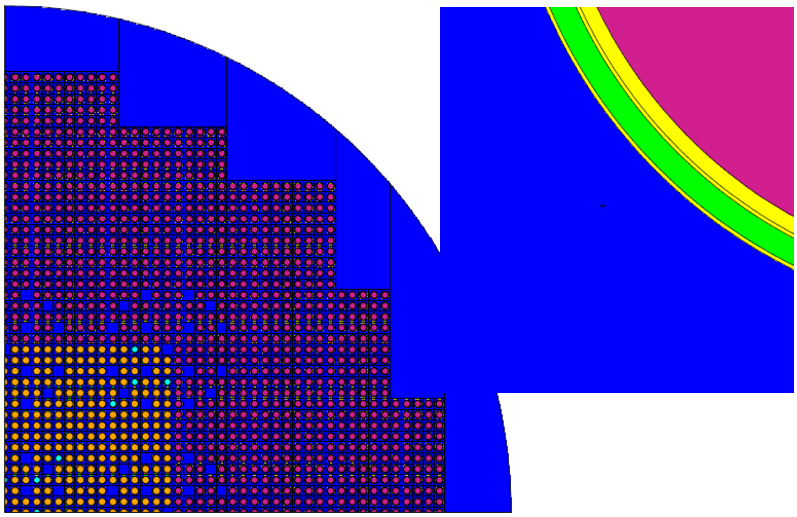

# MCNP5 criticality safety modeling and validation for LWR fuel cycle applications

Master of Science thesis in Nuclear Engineering

NICLAS HALLDIN
KARIN ROSENQVIST

Department of Applied Physics
*Division of Nuclear Engineering*
CHALMERS UNIVERSITY OF TECHNOLOGY
Gothenburg, Sweden, 2013

CTH-NT-274 ISSN 1653-4662

CTH-NT-274

# MCNP5 criticality safety modeling and validation for LWR fuel cycle applications

NICLAS C. HALLDIN

KARIN H. E. ROSENQVIST

Department of Applied Physics

CHALMERS UNIVERSITY OF TECHNOLOGY

Gothenburg, Sweden, 2013

MCNP5 criticality safety modeling and validation for LWR fuel cycle applications

NICLAS C. HALLDIN
KARIN H. E. ROSENQVIST



Master's thesis
CTH-NT-274
ISSN 1653-4662
Department of Applied Physics
Division of Nuclear Engineering
SE-412 96 Gothenburg
Sweden
Telephone: +46 (0)31-772 1000

Cover:

MCNP5 plots of heterogeneous and homogeneous systems

Chalmers Reproservice

Gothenburg, Sweden 2013

MCNP5 criticality safety modeling and validation for LWR fuel cycle applications

NICLAS C. HALLDIN and KARIN H. E. ROSENQVIST
Department of Applied Physics
Chalmers University of Technology

## Abstract

This thesis considers criticality safety in the production and storage stages of the light water reactor fuel cycle using the Monte Carlo N-Particle (MCNP) neutron transport code at Westinghouse Electric Sweden (WSE).

The fuel production process involves handling aqueous uranium solutions in different types of containers. The criticality safety handbook (KSH) is used as a quick way to assess if the geometry and materials of these containers are critically safe. Recent findings show that the composition of one absorber used in the KSH, polyvinyl chloride (PVC), is not conservative due to additives in the PVC that have not been accounted for. In addition, existing work on the KSH shows that the steel used in the containers cannot always be neglected in the computational models used. In light of this, the KSH is updated with a new PVC composition and steel is included when it is conservative to do so. The effect of the steel thickness on the neutron multiplication factor is evaluated for a number of uranium solutions and geometries. This parametric study also includes other parameters, such as the ratio of different components of the PVC.

The results show that the new PVC composition is more conservative than the old one for the cases studied while the addition of steel yields ambiguous results due to the complexity of the different mechanisms involved.

In the storage of nuclear fuel in new fuel racks and later in spent fuel pools, criticality must be avoided at all times. This is ensured by criticality safety analyses using e.g. MCNP. In order to be able to rely on the results, the code must be validated for the conditions of the system studied. In this thesis such a validation is done for MCNP5 version 1.51 for criticality calculations for common pressurized water reactor spent fuel storage conditions. This includes systems with soluble boron concentrations up to 3390 ppm and with solid absorbers present. The validation is performed against 101 heterogeneous critical experiments. From the calculations performed for these experiments the accuracy and precision of MCNP5 can be obtained and the upper subcritical limit (USL) may be determined. At WSE a B-term (B = 0.95 – USL) is added to the calculation results in criticality safety analyses to account for the bias of the code used.

The validation results show that the smallest and largest B-terms is seen for systems with and without absorbers present respectively. The latter result is unusually large due to the addition of an extra safety margin to account for a lack of data points and may be too conservative.

Keywords: MCNP, MCNP5, PWR, criticality safety, LWR, validation, criticality

**Acknowledgements**

We want to express our gratitude to those who have supported and encouraged us throughout our thesis work:

Christophe Demazière for establishing the contact with Westinghouse and being our examiner.

Stig Andersson for suggesting us to perform this project and for the tour at Tegnér.

Adam Libal, our supervisor and instructor at the Department of BWR and PWR Core Analysis for offering advice and counseling.

The factory personnel for their input on the criticality safety handbook.

Karolina Olofsson and Ulf Lindelöw, for having the patience needed to review all our Westinghouse reports.

Fellow co-workers at BT: Kalev Tammemäe for his nerdy anecdotes, Per Wiman for his random input on everything, our fellow thesis workers Oscar Puebla Garcia and Rashed Sarwar with whom we've spent many lunch breaks and probably a bunch of other people who we can't remember at this moment.

We would also like to thank our families and friends. Karin would especially like to thank her grandmother and her cat Herr Gose Katz Gubbson for helping her relax and forget about the thesis during the weekends. Niclas would especially like to thank his father Rickard Halldin that inspired him to pursue a career in the nuclear field and his mother Birgitta Rydquist for her encouraging words.

Niclas Halldin and Karin Rosenqvist

Västerås, May 2013

**List of abbreviations**

| | |
|---|---|
| **AOA** | Area of Applicability |
| **at%** | Atomic Percent |
| **B&W** | Babcock and Wilcox |
| **BFP** | Borated Flex Panel |
| **CSEWG** | Cross Section Evaluation Working Group |
| **EALF** | Energy corresponding to the Average neutron Lethargy causing Fission |
| **ENDF** | Evaluated Nuclear Data File |
| **IHECSBE** | International Handbook of Evaluated Criticality Safety Benchmark Experiments |
| $\mathbf{k_{eff}}$ | Effective neutron multiplication factor |
| **KSH** | Kriticitetssäkerhetshandbok (Criticality Safety Handbook) |
| **LEU** | Low Enriched Uranium |
| **LWR** | Light Water Reactor |
| **MCNP** | Monte Carlo N-Particle |
| **MOX** | Mixed Oxide Fuel |
| **PNL** | Pacific Northwest Laboratories |
| **ppm** | Parts per million |
| **PVC** | Polyvinyl chloride |
| **PWR** | Pressurized Water Reactor |

| | |
|---|---|
| **$UF_6$** | Uranium hexafluoride |
| **UNH** | Uranyl nitrate hexahydrate ($UO_2(NO_3)_2 \cdot 6H_2O$) |
| **$UO_2$** | Uranium dioxide |
| **$U_3O_8$** | Triuranium octoxide |
| **USL** | Upper Subcritical Limit |
| **WSE** | Westinghouse Electric Sweden AB |
| **wt%** | Weight Percent |

Plexiglas™ is a trademark of Atoglas

**1 INTRODUCTION ..... 1**

1.1 Purpose ..... 2
1.2 Scope ..... 2
1.3 Methodology ..... 3

**2 THEORETICAL BACKGROUND ..... 5**

2.1 Uranium fuel production ..... 5
2.2 Fuel storage ..... 5
2.3 Neutron absorbers ..... 6
*2.3.1 PVC ..... 6*
*2.3.2 Boron compounds ..... 6*
*2.3.3 Metal absorbers ..... 7*
2.4 The Monte Carlo method in nuclear engineering ..... 7
*2.4.1 MCNP ..... 8*
2.5 Determination of bias and bias uncertainty ..... 10
*2.5.1 Normality test ..... 12*
*2.5.2 Non-Parametric Treatment ..... 12*
*2.5.3 Determining a B-term from bias and bias uncertainty ..... 13*

**3 METHOD ..... 15**

3.1 KSH 12.3 ..... 15
*3.1.1 Scope ..... 15*
*3.1.2 Geometries and materials ..... 16*
3.2 KSH 12.6 ..... 19
*3.2.1 Scope ..... 19*
*3.2.2 Geometries and materials ..... 20*
3.3 Criticality code validation ..... 23
*3.3.1 Scope ..... 24*
*3.3.2 Geometries and materials ..... 24*
3.3.2.1 IHECSBE ..... 25
3.3.2.1.1 LEU-COMP-THERM-001 ..... 25
3.3.2.1.2 LEU-COMP-THERM-002 ..... 26
3.3.2.1.3 LEU-COMP-THERM-008 ..... 26
3.3.2.1.4 LEU-COMP-THERM-009 ..... 27
3.3.2.1.5 LEU-COMP-THERM-011 ..... 28
3.3.2.1.6 LEU-COMP-THERM-016 ..... 29
3.3.2.1.7 LEU-COMP-THERM-042 ..... 29
3.3.2.2 NUREG/CR-6361 ..... 29
3.3.2.2.1 BAW-1645 ..... 30
3.3.2.2.2 BAW-1231 ..... 31
3.3.2.2.3 BAW-1237 ..... 31
3.3.2.2.4 BAW-1810 ..... 32
3.3.2.2.5 EPRI NP-196 ..... 35
3.3.2.2.6 WCAP-3269 ..... 36
3.4 Calculation method ..... 39
*3.4.1 Statistical evaluation ..... 40*

**4 RESULTS AND DISCUSSION ..... 41**

4.1 KSH 12.3 ..... 41
*4.1.1 Infinite cylinders ..... 41*
*4.1.2 Finite cylinders ..... 42*
*4.1.3 Slabs infinite in two dimensions ..... 46*
*4.1.4 Slabs infinite in one dimension ..... 47*
*4.1.5 Comparison between the new and old BFP results ..... 50*
*4.1.6 Comparison between the new and old PVC results ..... 51*
*4.1.7 Parametric study ..... 52*
4.1.7.1 BFP ..... 52
4.1.7.2 PVC ..... 58
4.2 KSH 12.6 ..... 67
*4.2.1 $UO_2$ + $H_2O$ with a 30 cm water reflector ..... 68*
*4.2.2 UNH + $H_2O$ with a 30 cm water reflector ..... 69*
*4.2.3 $UO_2$ + $H_2O$ placed in a concrete corner ..... 70*
*4.2.4 Removing part of an absorber ..... 71*
*4.2.5 Comparison between the new and old PVC results ..... 72*
*4.2.6 Parametric study ..... 75*
4.3 VALIDATION RESULTS ..... 80
*4.3.1 Summary of calculation results ..... 83*
*4.3.2 Bias, bias uncertainty and normality check ..... 83*
*4.3.3 Trending analysis ..... 85*
4.3.3.1 Trend results for fresh fuel with strong absorbers ..... 85
4.3.3.2 Trend results for fresh fuel experiments without strong absorber ..... 87
*4.3.4 Non-parametric treatment ..... 89*
*4.3.5 Area of Applicability Definition ..... 89*

**5 CONCLUSION ..... 91**

5.1 THE CRITICALITY SAFETY HANDBOOK ..... 91
5.2 VALIDATION ..... 92

**REFERENCES ..... 95**

**APPENDIX I – CRITICAL CONDITIONS FOR THE VALIDATED BENCHMARKING EXPERIMENTS ..... I**

**APPENDIX II – TABLES OF RESULTS FOR KSH 12.3 AND 12.6 ..... VII**

**APPENDIX III - CROSS-SECTION LIBRARIES FOR 293.6 KELVIN ..... XIII**

# 1 Introduction

Westinghouse Electric Sweden AB (WSE) provides fuel for nuclear power plants around the world from their fuel factory located in Västerås. The criticality safety in the production and storage stages of the light water reactor fuel cycle using the Monte Carlo N-Particle (MCNP) neutron transport code is studied in this thesis.

As a part of the fuel production process, WSE handles enriched uranium which needs to be treated with care to avoid criticality accidents. At the fuel factory the criticality safety handbook (KSH or kriticitetssäkerhetshandboken) is used as a quick method to evaluate if a proposed installation will be below the criticality safety limit. The KSH covers $k_{eff}$ values for a number of geometries and reflectors with or without absorbers present. The absorbers used are either borated flex panel (BFP) or polyvinyl chloride (PVC), where boron and chlorine respectively absorb neutrons.

Analyses of the PVC used in the factory have shown a range of possible compositions. This means that parts of the KSH (12.3, 12.6) may no longer describe the actual installations as these are based on the theoretical PVC composition. To compensate for the uncertainty in the chlorine content of the PVC, excessive amounts of PVC have been used around tanks and pipes to ensure criticality safety. In addition to the uncertainties in the PVC composition, previous work on KSH 12.6 has revealed that it may be conservative to include steel-based structural materials in the computational models. This has necessitated an update of KSH 12.3, which presently does not include steel in any of the models.

In all stages of the fuel cycle unplanned criticality must be avoided. For this reason criticality safety analyses must be performed for fuel storage facilities. This includes new fuel racks as well as spent fuel that is stored in fuel pools. In order to perform the safety analyses for such arrangements, calculations using e.g. MCNP5 are needed.

In order to use MCNP5 v1.51 for fuel storage calculations it must first be extensively validated for the fuel storage conditions. There is a variety of different storage conditions to be considered. Due to uncertainties in the future storage of spent fuel, more fuel needs to be accommodated in the same installed capacity of spent fuel pools. To decrease the reactivity of the fuel, soluble boron or solid absorbers may need to be added and the fuel itself may contain burnable absorbers such as gadolinium. These conditions, among others, covered by a validation suite are summarized in its area of applicability (AOA).

WSE wants to produce a document detailing the complete methodology for spent fuel pools and new fuel rack criticality safety analysis using the codes MCNP5 and PHOENIX that may be presented to customers. As a part of this project there is a goal to extend the validated area of applicability of these codes for parameters associated with different absorbers.

## 1.1 Purpose

This thesis covers two different areas of the fuel cycle and therefore the purpose of the work is twofold. The first purpose of the thesis is to update two sections of the KSH (12.3 and 12.6) for which some of the content is no longer valid. The second purpose of the thesis is to validate MCNP5 v1.51 criticality calculations for spent fuel pool conditions and to determine the systematic error in such calculations.

## 1.2 Scope

Only KSH 12.3 and KSH 12.6 and the cases included in these handbooks, with a number of defined additions, are updated. In KSH 12.3, parametric studies will be performed in which different parameters are varied to assess the effect on $k_{eff}$.

In KSH 12.6, the PVC composition will be updated. Steel will be used in the model when it is conservative to do so, i.e. when the inclusion of steel yields a higher value of $k_{eff}$. Some parametric studies will be performed to complement the parametric studies in KSH 12.3 as defined in Section 3.

The validation is performed against evaluated criticality benchmark experiments. The benchmarking experiments to be studied are selected using the guidelines in [1]. All of the selected experiments contain fresh fuel and no experiments representing spent fuel are included.

This selection corresponds to an area of applicability of the validation report that covers safety analyses of Pressurized Water Reactor (PWR) uranium dioxide fuel but not Boiling Water Reactor (BWR) fuel or Mixed Oxide (MOX) fuel.

## 1.3 Methodology

The approach is to create and run MCNP5 input files for the different cases to be studied.

In KSH, repeated simulations are run for the different tank configurations to find a composition that maximizes the value of $k_{eff}$. The results are plotted in different ways to give an overview of which tank dimensions and configurations that are tolerable from a criticality safety standpoint.

The simulation step of the validation of MCNP5 v1.51 against selected benchmark experiments is followed by a statistical evaluation of the results. Using the method recommended in [1], the accuracy and precision of MCNP5 v1.51 is statistically determined.

# 2 Theoretical background

Throughout the fuel cycle there are stages where it is of the utmost importance to be able to ensure subcriticality. Before the fuel is utilized for power production, enriched uranium in different forms must be stored or handled. This is the case from the fuel production process to the storage of fresh fuel on site. After its use for power production, spent fuel remains that must be stored in a safe way before further handling. In some cases neutron absorbers must be used to achieve this. Criticality safety analyses are essential in these situations and such analyses are commonly performed using MCNP. Validation including statistical treatment is necessary to determine the precision and accuracy of MCNP5 in such calculations.

The following chapters detail the nuclear fuel production followed by nuclear fuel storage and the absorbers used. The neutron transport code used to simulate these installations and the statistical treatment performed to determine its calculation bias are also described.

## 2.1 Uranium fuel production

Nuclear fuel pellets that are to be shipped to various nuclear power plants around the world are produced at the WSE fuel factory. WSE is provided with uranium hexafluoride ($UF_6$) that is enriched with respect to uranium-235. From the $UF_6$, uranium dioxide ($UO_2$) powder is produced by wet chemical processing in several steps.

Another compound that is formed in the fuel production process is uranyl nitrate hexahydrate (UNH, $UO_2(NO_3)_2{\cdot}6H_2O$). UNH is formed upon dissolution of residues such as triuranium octoxide ($U_3O_8$) and $UO_2$ in nitric acid ($HNO_3$). The UNH is then converted to $UO_2$ in a number of steps.

After undergoing various processes to achieve the desired fuel properties, the $UO_2$ powder is pressed to pellets of a certain dimension. The pellets are put into fuel rods in a specified way, and the fuel rods are fixed into a fuel assembly that holds the rods in a grid pattern in the reactor. [2]

## 2.2 Fuel storage

The fuel produced at WSE will be transported to the nuclear power plant to be loaded into the core. Fresh unirradiated fuel will usually be stored in fresh fuel storage racks. Fuel storage will also become an issue after the irradiated fuel is taken out of the reactor. After being used in a nuclear reactor, the fuel elements are stored in pools in order for the

radioactivity and the associated decay heat to decrease before further handling in reprocessing plants or storage in final repositories. These storage facilities must fulfill a number of requirements ensuring e.g. subcriticality under normal and accident conditions [3]. Different solid or soluble absorbers may be used to decrease the reactivity of the fuel.

## 2.3 Neutron absorbers

Neutron absorbers are utilized to control reactivity and avoid criticality. Strong neutron absorbers all have a high microscopic capture cross section $\sigma_c$ in common. This section gives a general overview of the absorbers used in the cases studied.

### 2.3.1 PVC

PVC is one of the most widely produced plastics in the world [4]. Its molecular formula is $(C_2H_3Cl)_n$ and the structure is shown in Figure 2-1 [5].

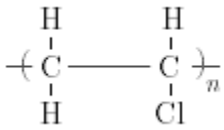

**Figure 2-1.** The chemical structure of PVC.

Chlorine, which is part of the PVC structure, has a high neutron absorption cross section of 33.5 barns [6]. Because of this, PVC is often used as a cost-effective neutron absorber at the WSE fuel factory.

Previous calculations in the KSH in which PVC is included has erroneously assumed that the theoretical composition reflects the actual composition of PVC. In reality, the composition of PVC will vary due to various additives that are added to achieve certain desired physical properties [7]. Current calculations overestimate the amount of neutron absorbing chlorine atoms in the PVC, suggesting that PVC is not as good of an absorber as anticipated.

### 2.3.2 Boron compounds

The boron isotope B-10 shows a large cross section for absorbing neutrons in the (n, α) reaction [8]. For this reason boron containing compounds are frequently used as solid and soluble neutron absorbers. In this thesis boron is present as a solid absorber in the form of BFP, Boral (boron carbide + aluminum) or borated steel. BFP (also known as “BoraFlex” or “BoroFlex”) consists of a silicone rubber binder combined with boron carbide and is used as an absorber placed around tanks in the fuel production. Boral or

borated stainless steel may be used as absorber plates in fuel storage. Soluble boron may be present in the form of dissolved boric acid or borax in PWR spent fuel pools. [9]

### 2.3.3 Metal absorbers

A number of metals are used as solid neutron absorbers. Indium, cadmium, silver and gadolinium are used in the cases investigated. The alloy Ag-In-Cd is used in control rods for PWRs. This combination of absorbers is used due to the overlapping absorption spectrums with cadmium being a good thermal absorber and indium and silver displaying significant resonance absorption in the epithermal region. In cases with higher enriched fuel these control rods may be stored together with the assemblies in the spent fuel pool to decrease reactivity [10]. Cadmium is also sometimes used on its own in absorber plates. [8], [9]

Gadolinium is added in the form of $Gd_2O_3$ as a burnable absorber in fuel rods. This is due to the large capture cross sections of the isotopes Gd-155 and Gd-157. As neutrons are captured these gadolinium isotopes are transmuted to nuclides with smaller capture cross sections and "burn out", hence the term "burnable absorber". [11]

## 2.4 The Monte Carlo method in nuclear engineering

The Monte Carlo method is used to make a theoretical duplication of a stochastic process, such as neutron transport. Sampling is done from appropriate probability distributions, and a numerical answer to a certain problem is obtained by statistical means. Since the simulation is stochastic, the answer may differ each time the simulation is run. This is in contrast to deterministic methods where the same answer is produced every time. [12]

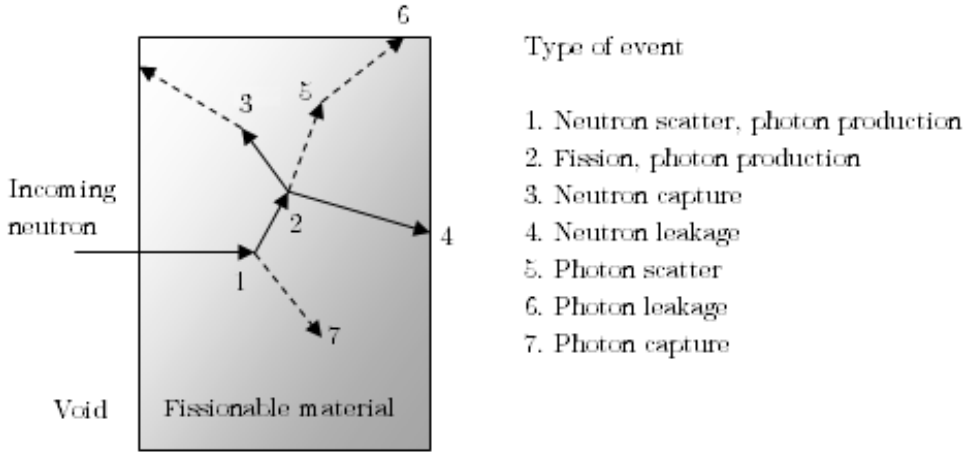


**Figure 2-2.** Example of a random history of a neutron interaction. Reproduced from [12]

Neutron transport problems are solved by simulating the particle collisions instead of solving the transport equation. This is possible since the total macroscopic cross section $\Sigma_T$ can be interpreted as the probability of first interaction per unit distance, $s$, traveled by a neutron (for infinitesimal path lengths):

$$p(s)ds = e^{-\Sigma_T s}\Sigma_T ds \quad (1)$$

The interactions depend on neutron energy and the composition of the system, and the direction and energy of any emerging neutron(s) are determined stochastically from sets of random numbers. [12], [13]

A history, as shown in Figure 2-2, consists of the interactions of a neutron emitted from a source and all neutrons created as a result of the interactions of the original neutron. After sufficiently many histories have been studied the characteristics of the system may be evaluated from the statistical average of the neutron histories. The amount of neutron histories that are used to make such a statistical average is a trade-off between computing time and precision. [8], [12]

Monte Carlo methods are particularly well-suited for complex problems that cannot be modeled very well with deterministic computer codes. Unlike deterministic codes, probabilistic codes do not require averaging approximations of position, energy and time that would have affected the computational results. [12]

There will always be a statistical error $\sigma_{calc}$ associated with Monte Carlo calculation results that is dependent on the number of neutron histories collected. This is a drawback in the sense that for problems where a high precision is required many histories must be collected causing the calculations to be computationally intensive and thus time-consuming. [12], [13]

The results will be an average of contributions from many histories and the precision will depend on the number of histories and the method used. The accuracy, and conversely, the systematic error will be a function of the code used and how the problem is modeled by the user. [12]

### 2.4.1 MCNP

The current analysis methodology employs the MCNP5 v1.51 computer code and the ENDF 7.0 cross section library.

The MCNP code is a general transport code using a pseudo-stochastic version of the Monte Carlo method. As a consequence repeated runs of the same input file will give the same results unless another random number seed is selected. [12]

MCNP may be used to study neutron, electron or photon transport or any combination of those. For neutron transport problems, the MCNP code may be used to follow the neutrons from the cradle (by fission) to the grave (by capture or escape) as shown in Figure 2-2. This makes it possible to simulate fissile systems such as aqueous solutions of uranium in the nuclear fuel production process or fuel assemblies stored in spent fuel pools. [12]

The system is modeled by creating an input deck describing the geometry and material composition of the system based on a set of cards, with the terms card and deck referring to the punched card system once used for writing the input file. The model is made up of a collection of cell cards that in turn rely on surface and material cards to be fully defined. [12]

Material cards are used to define the material composition of a cell. This is done by entering the relative abundance of each nuclide in the material and stating which cross section library that should be used for that nuclide. [12]

Thermal cards may supplement material cards to give an appropriate treatment of the interactions between thermal neutrons and the material. At low energies molecular binding in the material and crystalline effects in the material will affect the cross section for neutron interaction. By using a thermal card, the cross section data for thermal energies will be taken from data libraries that account for this effect using the *S(α,β)* scattering treatment. Thermal cards are only available for selected nuclides in materials of special interest e.g. hydrogen in light water. Without a thermal card the standard free-gas-treatment will be used even at thermal energies. [12]

Surface cards are used to define surfaces. These surfaces are in turn used to construct the geometry specifications for different cells by combining the surface cards using logical operators.

Cell cards are used to define the cells constructed from the surface cards. Each cell is filled by a material defined in one of the material cards or void. The system is modeled as the collection of all such cells combined with cards that are specific for the type of problem.

For criticality calculations, cards are added to define the number of fission generations to study and the properties of the original fission source points.

The `kcode` card defines the number of fission generations ($k_{eff}$ cycles) and the number of neutrons per generation to study. A fission generation only covers a part of a history as any neutrons created through fission by the original neutron will be part of the next cycle.

The use of a `kcode` card will also cause MCNP to give information relevant for criticality calculations as an output: average $k_{eff}$ with its estimated standard deviation, the energy corresponding to the average neutron lethargy causing fission (EALF), percentage of fissions caused by thermal, intermediate and fast neutrons, average number of neutrons produced per fission. [12]

The `ksrc` or `sdef` cards (or a srctp file) will determine the number of initial fission points to be used and where in the system these are placed. At these predefined source points, fission will occur in the very first generation if placed within cells containing fissile material. These fission events will in turn cause more fission that will generate the source points in the next generation. After a number of generations the pattern for the fission source points will have reached the correct distribution for the problem and at this point source convergence is reached. All generations before fission source convergence is reached should be disregarded in any criticality calculations. [12]

Other similar codes exist, e.g. KENO that is part of the SCALE code package, based on the Monte Carlo method [14].

## 2.5 Determination of bias and bias uncertainty

The bias and bias uncertainty are determined using the methodology presented in [1]. The obtained $k_{eff}$ values first need to be normalized to account for simplification in the benchmark model or deviations from critical conditions ($k_{exp} \neq 1.0$) for the modeled experiment. This is done according to:

$$k_{norm} = \frac{k_{calc}}{k_{exp}} \quad (2)$$

This normalization is based on assumptions only valid for small deviations from critical and should never be used if it makes the resulting bias smaller. The normalized $k_{eff}$ values are then used in all subsequent statistical analyses.

In order to include both the experimental uncertainty $\sigma_{exp}$ and the estimated standard deviation for the calculation $\sigma_{calc}$ in the weighted mean a combined uncertainty is created from the root-sum-square of $\sigma_{exp}$ and $\sigma_{calc}$:

$$\sigma_t = \sqrt{\sigma_{calc}^2 + \sigma_{exp}^2} \quad (3)$$

For a data set of size $n$ including the i:th element $k_{norm,i}$ with the associated combined uncertainty $\sigma_t(i) = \sigma_i$ the variance about the mean is given by:

$$s^2 = \frac{\left(\frac{1}{n-1}\right)\Sigma\frac{1}{\sigma_i^2}\left(k_{norm,i}-\bar{k}_{norm}\right)^2}{\frac{1}{n}\Sigma\frac{1}{\sigma_i^2}} \quad (4)$$

The weighted mean $\bar{k}_{norm}$ used is defined as:

$$\bar{k}_{norm} = \frac{\Sigma\frac{1}{\sigma_i^2}k_{norm,i}}{\Sigma\frac{1}{\sigma_i^2}} \quad (5)$$

The average total uncertainty is given by:

$$\bar{\sigma}^2 = \frac{n}{\Sigma\frac{1}{\sigma_i^2}} \quad (6)$$

The square root of the pooled variance $S_P$ is the square root of the sum of the variance about the mean and the average total uncertainty:

$$S_P = \sqrt{s^2 + \bar{\sigma}^2} \quad (7)$$

The best estimate, untrended, bias is defined as:

$$Bias = \begin{cases} \bar{k}_{norm} - 1.0 \; if \; \bar{k}_{norm} < 1.0 \\ 0.0 \qquad\quad if \; \bar{k}_{norm} \geq 1.0 \end{cases} \quad (8)$$

A positive bias is set to zero as it is not conservative to take credit for any positive deviations from criticality in the calculated values.

In addition it is possible to define a safety margin known as the upper subcritical limit (USL). The USL states the maximum allowed $k_{eff}$ for a certain fissile configuration for future criticality safety calculations with MCNP5. If the MCNP5 output is below the USL it ensures that criticality is avoided. The upper subcritical limit (USL) is defined as:

$$USL = 1.0 + Bias - \sigma_{bias} - \Delta_{SM} - \Delta_{AOA} \quad (9)$$

In this equation the experimental $k_{eff}$ is assumed to be 1.0, bias is the negative deviation from critical and $\sigma_{bias}$ is the statistical uncertainty associated with the bias. Two different subcritical margins may be added based on the situation: the subcritical margin set by regulations $\Delta_{SM}$ and an additional subcritical margin $\Delta_{AOA}$ that is added for extensions outside the AOA.

In addition the USL may be determined from the lower tolerance limit or lower tolerance band $K_L$:

$$USL = K_L - \Delta_{SM} - \Delta_{AOA} \quad (10)$$

For WSE applications inside the area of applicability $\Delta_{SM} = 0.05$ and $\Delta_{AOA} = 0$ [15].

### 2.5.1 Normality test

To ensure a statistical treatment suitable for the distribution of the data set, a normality test is performed. The computer program USLSTATS is used to test the data sets for normality. The program is described in Appendix C of NUREG/CR-6361 "Criticality Benchmark Guide for Light-Water-Reactor Fuel in Transportation and Storage Packages" (henceforth only referred to as NUREG/CR-6361) [16]. From the $\chi^2$ (chi-square) goodness-of-fit test in the USLSTATS output it is decided whether the combination of experiments is normally distributed. Dividing the data points into five bins and selecting a 0.95 confidence level the data set is concluded normal for $\chi^2 \leq 9.49$. For sets with few data points (less than 50) an additional test for normality, the Shapiro-Wilk test is needed to ensure a reliable test result. If the data set turns out to follow a normal distribution, a one-sided tolerance limit or tolerance band can be used to determine bias and bias uncertainty. As neither data set featured in this report is normally distributed a non-parametric treatment is needed.

### 2.5.2 Non-Parametric Treatment

For non-normal distributions of data $K_L$ will be determined according to:

$$K_L = k_{norm}^{min} - uncertainty\ for\ k_{norm}^{min} - NPM \quad if\ \bar{k}_{norm} \leq 1.0 \quad (11)$$

$$K_L = 1.0 - S_P - NPM \quad if\ \bar{k}_{norm} > 1.0$$

$$k_{norm}^{min} = minimum\ normalized\ k_{norm}$$

$$uncertainty\ for\ k_{norm}^{min} = \sigma_i(\ k_{norm,i} = k_{norm}^{min})$$

$$NPM - non\ parametric\ margin$$

NPM is a function of sample size $n$ and degree of confidence $\beta$ that the desired fraction $q$ of the population lies above the smallest value:

$$\beta = 1 - q^n \quad (12)$$

NPM can be obtained from Table 2-1 as a function of $\beta$. In this report a value of $q = 0.95$ is used.

**Table 2-1.** Non-parametric margins. Data from [1]

| Degree of confidence β for q = 0.95 (95 % of the population) | Non-parametric margin (NPM) |
|---|---|
| > 90 % | 0.00 |
| > 80 % | 0.01 |
| > 70 % | 0.02 |
| > 60 % | 0.03 |
| > 50 % | 0.04 |
| > 40 % | 0.05 |
| ≤ 40 % | Additional data needed (less than 10 data points) |

From the value of $K_L$ the bias may be determined as:

$$Bias = K_L - 1.0 + \sigma_{bias} \quad (13)$$

### 2.5.3 Determining a B-term from bias and bias uncertainty

In the criticality safety analyses performed at the WSE fuel factory a B-term is used that combines the bias and bias uncertainty [15]. This term is calculated as:

$$B = 1 - K_L \quad (14)$$

This B-term is used in criticality safety calculations to determine if the $k_{eff}$ of an installation is below the critically safe limit $k_{eff} = 0.95$. To ensure that this is the case the following inequality must be fulfilled by the calculated $k_{eff}$ value $k_{calc}$ with the associated standard deviation $\sigma_{calc}$ [17]:

$$k_{calc} + 3\sigma_{calc} + B < 0.95 \quad (15)$$

# 3 Method

The specific methodology for the modeling of each of the different systems featured in this thesis is presented in the subsequent subchapters. This is followed by the calculations described in Section 3.4.

## 3.1 KSH 12.3

The scope, geometries and materials used in KSH 12.3 are presented below.

### 3.1.1 Scope

The geometrical shapes that are studied in KSH 12.3 are infinite and finite cylinders, as well as slabs infinite in one or two dimensions. The content of each system is a mixture of $UO_2$ + $H_2O$.

Each of the geometries is reflected by either 30 cm water or 50 cm concrete which is sufficient to provide total reflection [18].

The absorbers that are used are either 0.64 cm BFP or 0.9/1.3 cm PVC for cylinders and slabs respectively. For the cases where BFP is used as an absorber, a 0.4/0.5 cm thick steel tank contains the $UO_2$ + $H_2O$ mixture for cylinders and slabs respectively. Also, a 0.1 cm thick steel enclosure is used around the absorber. When PVC is used as an absorber, no steel is used in the model for reasons explained in the parametric study (see Section 4.1.7).

KSH 12.3 also contains parametric studies for infinite geometries of critically safe dimensions with absorbers. The following parameters have been varied to study the effect on $k_{eff}$:

- Steel layer thickness between the $UO_2$ + $H_2O$ mixture and the absorber
- Water column thickness between the $UO_2$ + $H_2O$ mixture or steel tank (for PVC and BFP respectively) and the absorber

Additionally, the following parameters have been varied for PVC:

- Weight fraction of chlorine
- Atomic ratio between hydrogen and carbon
- Density
- Thickness

### 3.1.2 Geometries and materials

The geometries that are studied in KSH 12.3 are cylinders and slabs, see Figure 3-1 below.

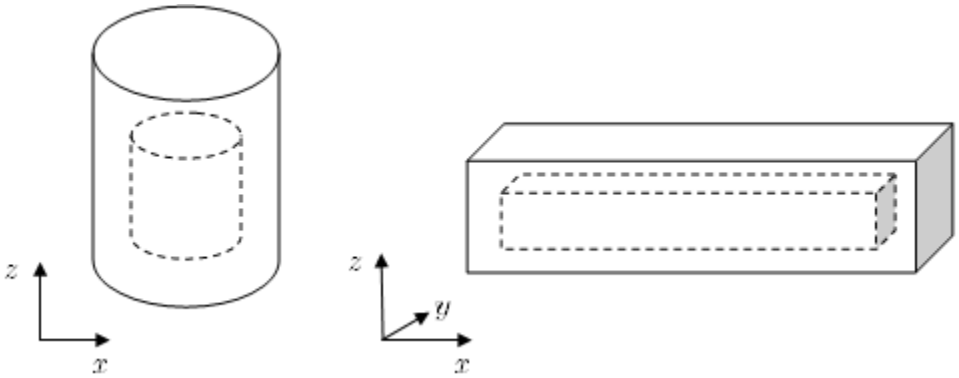


**Figure 3-1.** A schematic representation of the geometries studied in KSH 12.3; cylinders and slabs surrounded by a reflector. The coordinates $z$ and $x$ refer to the height and diameter for cylinders. For slabs, $z$, $y$ and $x$ refer to the height, depth and width respectively.

When BFP is used as an absorber, several layers of steel are incorporated into the model. This is shown in the MCNP plots in Figure 3-2 and Figure 3-3 below.

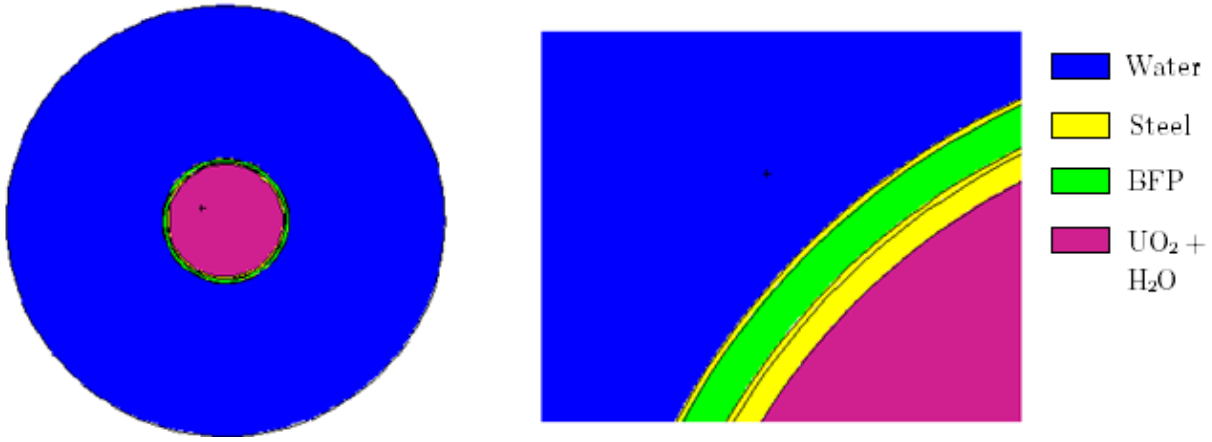


**Figure 3-2.** Example of a cylindrical geometry reflected by water with BFP as an absorber, with a steel tank between the $UO_2$ mixture and the absorber as well as a steel enclosure around the absorber. The picture to the right shows an enlarged portion of the cross section in the left picture.

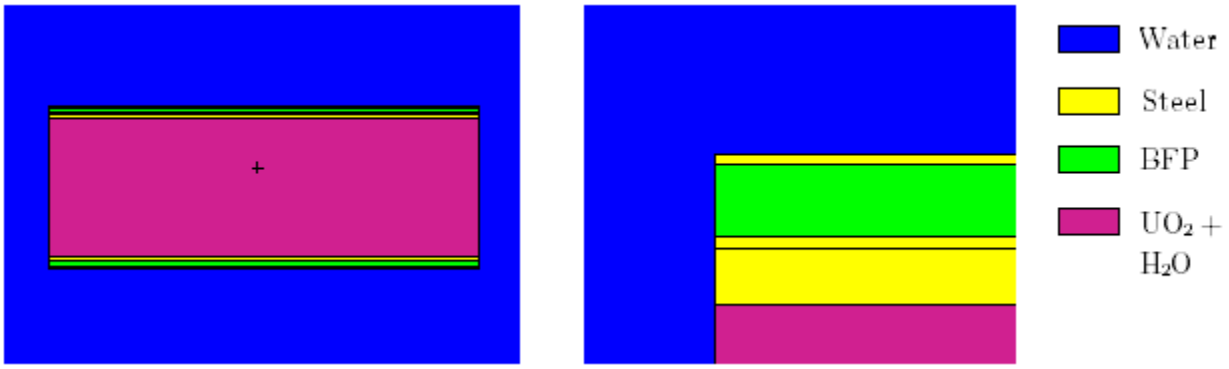


**Figure 3-3.** Example of a slab geometry reflected by water with BFP as an absorber, with a steel tank between the $UO_2$ mixture and the absorber as well as a steel enclosure around the absorber. The picture to the right shows an enlarged portion of the top left corner of the cross section in the left picture (the entire reflector is not visible).

As seen in Figure 3-3, the steel tank does not cover the short sides (the sides without absorber) of the slab geometry models with BFP. This is conservative compared to having steel around the entire slab.

The PVC setup shown in Figure 3-4 and Figure 3-5 is similar to that of BFP, except that it is not conservative to include steel and for this reason it has been excluded. This is explained further in the parametric study in Section 4.1.7.2.

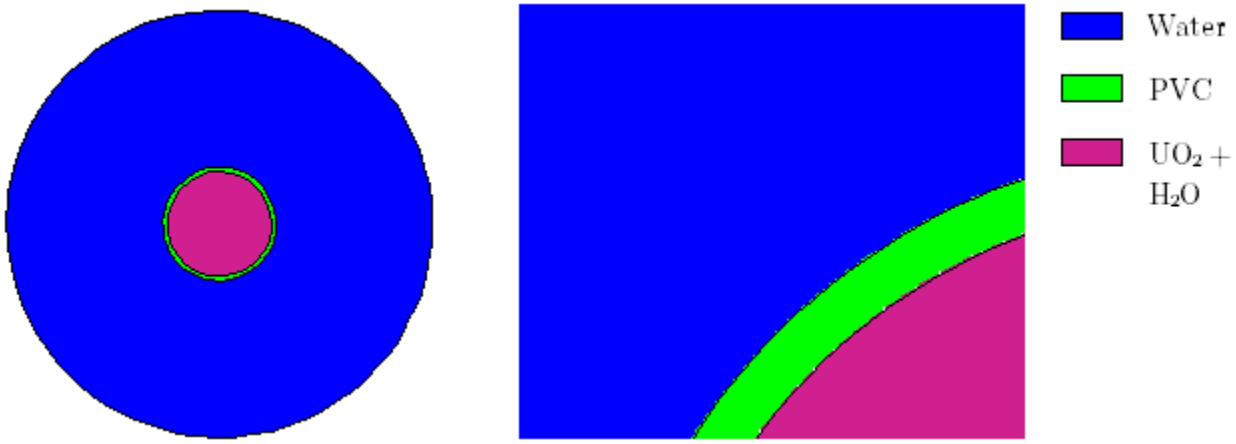


**Figure 3-4.** Example of a cylindrical geometry reflected by water with PVC as an absorber. The picture to the right shows an enlarged portion of the cross section in the left picture.

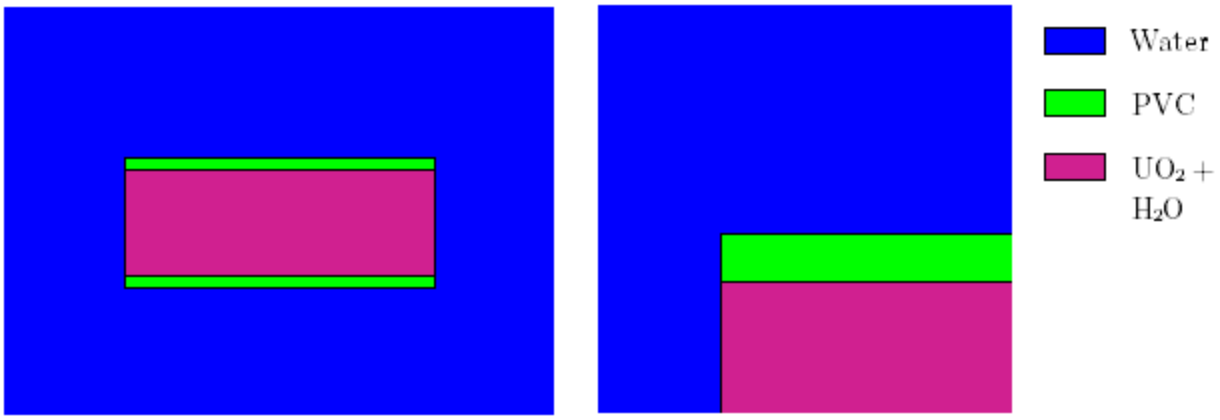


**Figure 3-5.** Example of a slab geometry reflected by water with PVC as an absorber. The picture to the right shows an enlarged portion of the top left corner in the left picture.

A summary of the materials used in KSH 12.3 is presented in Table 3-1 below.

**Table 3-1.** Materials that are used in KSH 12.3.

| Material | Density (g/cm$^3$) | Composition |
|---|---|---|
| BFP | 1.01 | KSH 9 rev. 3 [19] |
| Concrete | 2.30 | KSH 9 rev. 3 [19] |
| $H_2O$ | 1.00 | Stoichiometric |
| PVC | 1.30 | 70 wt% hydrogen + carbon |
| | | 30 wt% chlorine |
| | | H/C atom ratio 1.5 [20] |
| Steel (SS-EN 10250-4 -1.4301) | 7.92 | KSH 9 rev. 3 [19] |
| $UO_2$ + $H_2O$ mixture | Variable | Variable |

The $UO_2$ powder is insoluble in water, but for the calculations that are performed in KSH 12.3 (and KSH 12.6) a homogeneous and uniform[1] suspension of $UO_2$ in water is assumed. The uranium is further assumed to be 5 percent enriched in weight (wt%) with respect to uranium-235.

The composition of the $UO_2$ mixture has been varied to achieve optimal moderation, meaning that the hydrogen to uranium ratio is varied to maximize $k_{eff}$. This is a conservative assumption, since in reality the uranium concentration is typically either too high or too low to have optimal moderation and thus the actual value of $k_{eff}$ will be lower than the calculated value [21].

[1] A homogeneous and uniform suspension refers to a suspension with a composition that is the same in the entire volume

The water reflector and any possible water columns are conservatively assumed to have a density of 1 g/cm$^3$. The PVC composition has been estimated with the help of experimental measurements of the PVC used in the fuel factory, as well as with conservative assumptions.

## 3.2 KSH 12.6

The scope, geometries and materials used in KSH 12.6 are presented below.

### 3.2.1 Scope

In KSH 12.6, both finite and infinite (in two dimensions) slabs containing either $UO_2$ + $H_2O$ or UNH + $H_2O$ are studied. For some of the cases, the effect on $k_{eff}$ upon removing a piece of the absorber is studied. The reflectors used are either a 30 cm water reflector or a composite system of water and concrete ("concrete corner") which represents the case when the slab is placed in a corner with 50 cm concrete on three sides and 50 cm water on the other three sides.

The cases included in KSH 12.6 are summarized in Table 3-2 below.

**Table 3-2.** An overview of the systems in KSH 12.6. The cases included are marked with "X" and the cases not included are marked with "-".

| Uranium mixture | | $UO_2$ + $H_2O$ | | UNH + $H_2O$ |
|---|---|---|---|---|
| Reflector | | Water | Concrete corner | Water |
| Absorber | BFP on one side | X | - | X |
| | BFP on two sides | X | - | X |
| | PVC on one side | X | X | X |
| | PVC on two sides | X | X | X |
| Removed part of an absorber | BFP on one side | X | - | - |
| | BFP on two sides | X | - | - |
| | PVC on one side | X | - | - |
| | PVC on two sides | X | - | - |

As a complement to the parametric studies in KSH 12.3, KSH 12.6 also contains parametric studies in which the effect on $k_{eff}$ from different parameters is studied. In KSH 12.6, the parameters being varied are both the steel thickness of the tank that contains the uranium mixture and also the thickness of a water column between the tank and the absorber to simulate flooding conditions. The parametric studies are performed for both finite and infinite (in two dimensions) slabs containing UNH + $H_2O$, reflected by 30 cm water with 1.3 cm thick PVC absorbers on both sides of the slab.

### 3.2.2 Geometries and materials

As mentioned previously, only slabs are studied in KSH 12.6. The slabs have a quadratic base area $A$ of a certain side length $s$ and thickness $z$, except for the infinite systems which have an infinite base area. The general setup is shown in Figure 3-6:

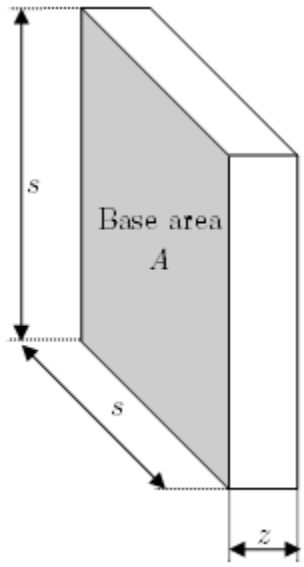


**Figure 3-6.** A slab with a quadratic base area.

The grey area in Figure 3-6 is covered with absorber and steel (when appropriate). The white sides have neither absorber nor steel, just as in KSH 12.3. The thickness is varied with millimeter precision to find when $k_{eff} + 3\sigma + B$ equals at least 0.95 which is the criticality safety limit. The closest underlying value of the thickness corresponding to the criticality safety limit is used as a safety precaution.

As in KSH 12.3, the absorbers used are either BFP or PVC with a thickness of 0.64 cm and 1.3 cm respectively. For the cases with BFP, the steel tank is 0.6 cm thick with a 0.1 cm thick steel enclosure around the absorber. For all the cases with PVC, the models have been simulated both with and without a 0.6 cm thick steel tank to conservatively cover different configurations with up to 0.6 cm steel. In Figure 3-7 and Figure 3-8 the two reflector types are shown.

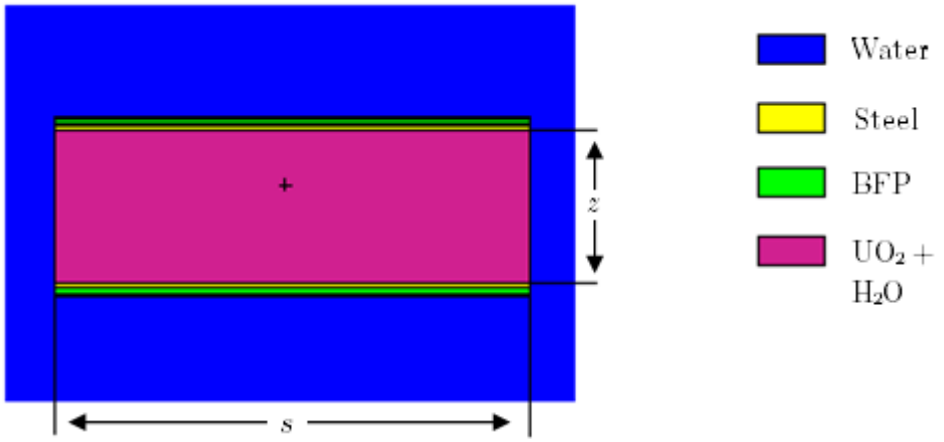


**Figure 3-7.** Example of a slab geometry with BFP as an absorber on two sides, with a steel tank between the $UO_2$ mixture and the absorber as well as a steel enclosure around the absorber. The system is surrounded by a water reflector (the entire reflector is not visible in the picture).

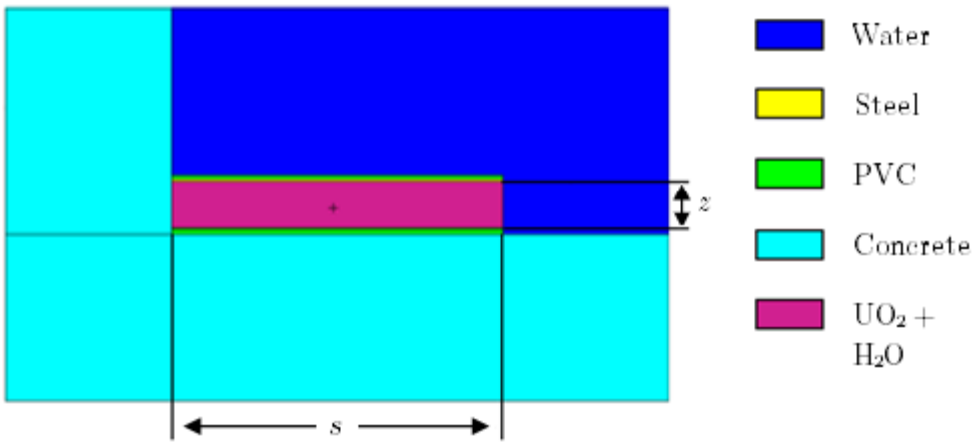


**Figure 3-8.** Example of a slab geometry with PVC as an absorber on two sides, with steel between the $UO_2$ mixture and the absorber. The system is placed in a concrete corner with a water reflector on the sides that are not facing the concrete.

In Figure 3-9 and Figure 3-10 a close up of a corner of the slab is shown. As in KSH 12.3, the short side without absorber (denoted $z$ in Figure 3-6) is not covered with steel.

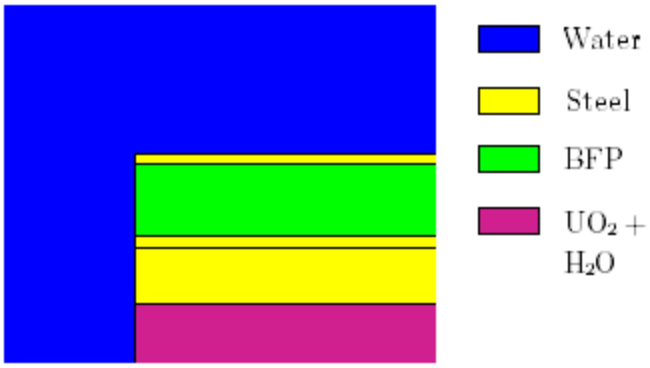


**Figure 3-9.** Example of a slab geometry with BFP as an absorber with a steel enclosure as well as a steel tank containing the $UO_2$ mixture. The picture shows an enlargement of a corner of the slab.

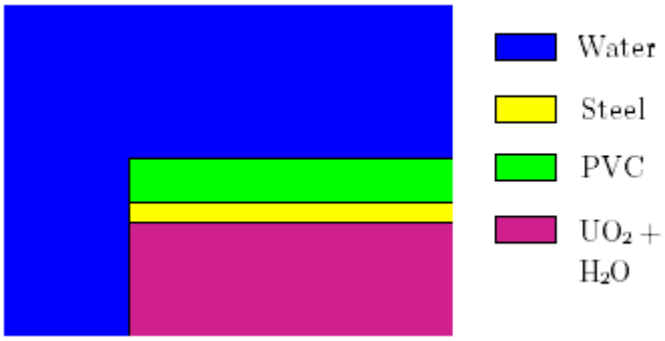


**Figure 3-10.** Example of a slab geometry with PVC as an absorber and a steel tank containing the $UO_2$ mixture. The picture shows an enlargement of a corner of the slab.

To assess the effect on $k_{eff}$ upon removing a part of the absorber to make room for various instruments, an analysis has been performed in which the area of a circular hole in the absorber is varied. To conservatively cover cases when an object is protruding from the hole, the hole is modeled as a $UO_2$ + $H_2O$ cylinder. The cylinder is not covered in steel. An example is shown in Figure 3-11.

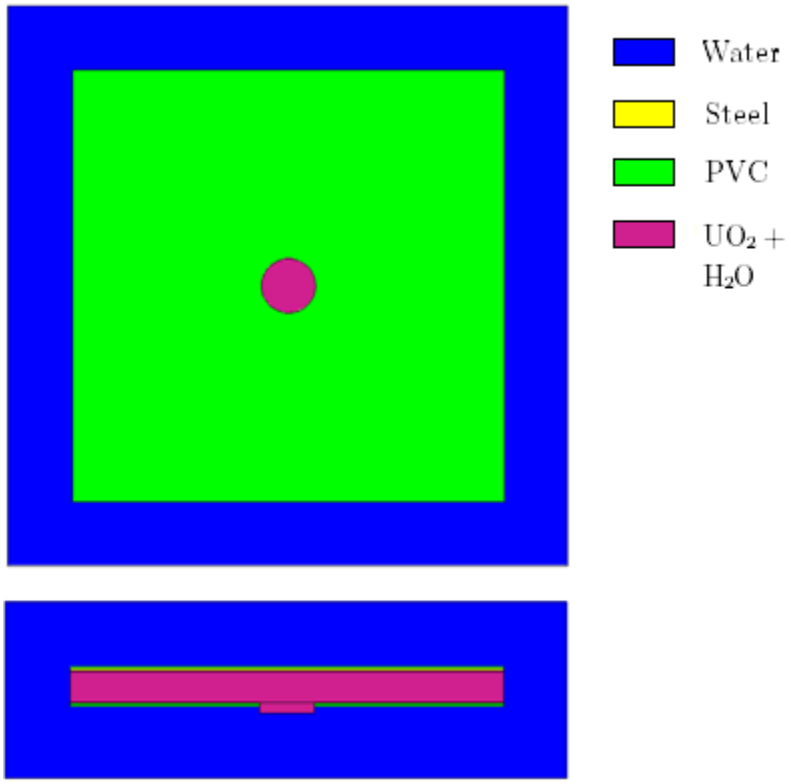


**Figure 3-11.** Example of a slab with a circular hole in the absorber. The hole in the absorber has been replaced with a 5 cm thick $UO_2$ + $H_2O$ mixture. The figure shows a slab with a side length of 200 cm and an area of the hole of 5 $dm^2$.

The same material compositions and assumptions as in KSH 12.3 (see Table 3-1) are used, with the addition of UNH + $H_2O$. Unlike $UO_2$, UNH is soluble in water. The calculations performed in KSH 12.6 however assume a uniform and homogeneous suspension of UNH crystals in water. This assumption has been shown to be conservative due to a higher concentration of hydrogen and a lower concentration of oxygen and nitrogen for a given uranium concentration [22]. The composition of UNH + $H_2O$ is also varied to find optimal moderation.

## 3.3 Criticality code validation

The approach for the MCNP5 v1.51 validation is to create and run input files for all cases in the selected validation suite described in Section 3.1.1. Experiments that have been part of an earlier WSE validation report [15] are used without modifications. With this exception MCNP5 input files from [23] are used for the experiments from the International Handbook of Evaluated Criticality Safety Benchmark Experiments (IHECSBE). For these files the cross section libraries are updated and thermal cards are added for the components in uranium oxide. For the other reference no MCNP5 input

files have been available and the experiments have been modeled based on experimental reports, handbook information and KENO input files. A description of the critical experiments may be found in Section 3.3.2.

The validation is aimed at a quantification of the bias, defined as the difference between the calculated and the experimental $k_{eff}$ value. A statistical analysis is performed that is described in Section 3.4.1.

### 3.3.1 Scope

The experiments featured in the validation suite have been selected based on the recommendations in [1]. Based on this methodology IHECSBE is chosen as the primary source of criticality benchmark experiments. To ensure adequate coverage of all the important parameters selected experiments from NUREG/CR-6361 [16] are included. Experiments covering spent fuel have been excluded from this validation suite.

The included benchmark experiments have been selected based on the parameters to be validated. These are meant to cover the parameters associated with spent fuel analyses. For this reason the chosen experiments share the following features:

- Fuel material: $UO_2$ pellets
- Moderator/reflector: $H_2O$ near standard temperature and pressure
- Structural materials: Al-, SS-, Zr-based.
- Absorbers: B, Gd, Ag, In, Cd

Spent fuel storage without burnable absorbers and depletion credited is covered by this validation suite as these conditions can be conservatively modeled as fresh fuel without burnable absorbers placed in a storage pool. Despite the fact that the validation suite includes only fresh fuel experiments the most common way of storing fresh fuel, dry storage in new fuel racks, is not covered. The reason for this is that dry storage conditions differ from the experimental conditions in this validation suite where all experiments are performed in water filled tanks simulating fuel pool conditions. The validation is adequate to cover most PWR square-pitched fuel designs without MOX.

### 3.3.2 Geometries and materials

This section gives an overview of the critical experiments modeled and the models created. The material compositions stated in IHECSBE and NUREG/CR-6361 are used if available. In other cases standard material compositions as defined in the Standard Composition Library for SCALE are used [14]. Case specific assumptions made are

described in the following Section 3.3.2. Details about the calculations are found in Section 3.4.

The soluble boron concentration is given in parts per million (ppm), as reported in the reference used. However the different experiments use different definitions of ppm boron. The older definition is based on mass boron per moderator volume while the new definition corresponds to a mass fraction. Near a moderator density of 1 g/cm$^3$ the difference will be at most a few ppm. In the cases taken from IHECSBE this difference is included in the experimental uncertainty [24], [29].

#### 3.3.2.1 IHECSBE

A number of experiments with thermal (THERM) compound (COMP) systems containing low enriched uranium (LEU) are included from this handbook. The experimental suites included are all named LEU-COMP-THERM-XXX with XXX being a number identifier. The handbook describes each experiment in detail including an estimation of the uncertainty in the benchmark model $k_{eff}$. This estimation may range from a stringent calculation of the standard deviation to a rough estimate depending on the data available. For all IHECSBE cases this uncertainty has been used as the experimental uncertainty. Critical conditions for these cases are available in Appendix I.

##### 3.3.2.1.1 LEU-COMP-THERM-001

These experiments are performed in a large water filled tank at the Pacific Northwest Laboratories (PNL) using aluminum clad $UO_2$ fuel rods placed in square-pitched clusters. Criticality is reached by varying the separation between clusters. A general setup for the series of experiments is shown in Figure 3-12 for the cases with three clusters. The absorber plates shown in the picture are not included in this experimental suite and nor is soluble boron. Cases 1-8 are included in this benchmark suite. The simplifying assumptions made when modeling these experiments are consistent with the benchmark model presented in [25].

Because the acrylic lattice plates are omitted the benchmark-model $k_{eff}$ is 0.9998 ± 0.0030 for cases 1-6 and 8. Case 7 has got a slightly larger estimated uncertainty in the benchmark-model $k_{eff,}$ 0.0031. For this case the benchmark $k_{eff}$ is 0.9998 ± 0.0031. [25]

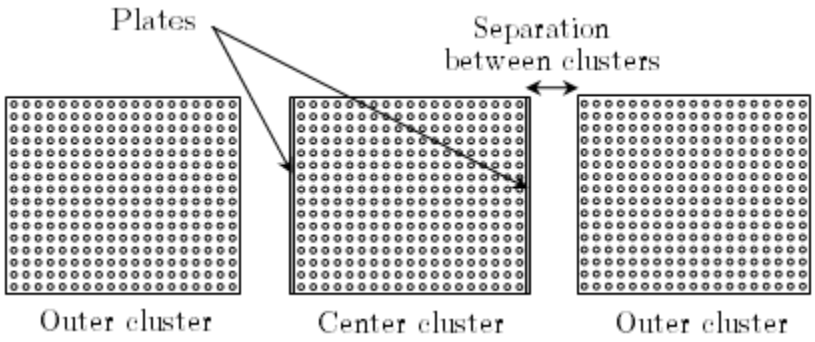


**Figure 3-12.** Experimental layout for cases with three clusters where no steel wall is present. Reproduced from [26]

#### 3.3.2.1.2 LEU-COMP-THERM-002

These experiments are performed in a large water filled tank at the PNL using aluminum clad $UO_2$ fuel rods in square-pitched clusters. The separation between the clusters is varied until criticality is obtained. A general setup for the series of experiments is shown in Figure 3-12 for the cases with three clusters. The absorber plates shown in the picture are not included in this experimental suite and nor is soluble boron. Cases 1-5 are included in this benchmark suite. Simplifying assumptions made when modeling these experiments are consistent with the benchmark model presented in [27].

Because the acrylic lattice plates are omitted the benchmark model $k_{eff}$ is 0.9997 ± 0.0020 for cases 1-3. For case 4 the benchmark model $k_{eff}$ is 0.9997 ± 0.0018 and for case 5 the benchmark model $k_{eff}$ is 0.9997 ± 0.0019. [27]

#### 3.3.2.1.3 LEU-COMP-THERM-008

These experiments are performed in a large water filled tank at the Babcock and Wilcox's (B&W's) Lynchburg Research Center with aluminum clad $UO_2$ fuel rods placed in square-pitched clusters. Criticality is obtained by varying the boron concentration [24]. A general setup for the series of experiments is shown in Figure 3-13. Soluble boron and in some cases alumina/aluminum perturbing rods are included in this experimental suite. Cases 1-3, 11-12, 14 and 16-17 are included in this benchmark suite.

The simplifying assumptions made when modeling these experiments are consistent with the benchmark model presented in [24] with the exception that the upper grids have been retained. The experimental uncertainty for the benchmark model (without upper grids) is used for simplicity and is based on the assumption that the effect of omitting the grids would be greater than the possible uncertainty in the grid position.

Because the experimental system was reported to be slightly supercritical the benchmark $k_{eff}$ is 1.0007 ± 0.0012. [24]

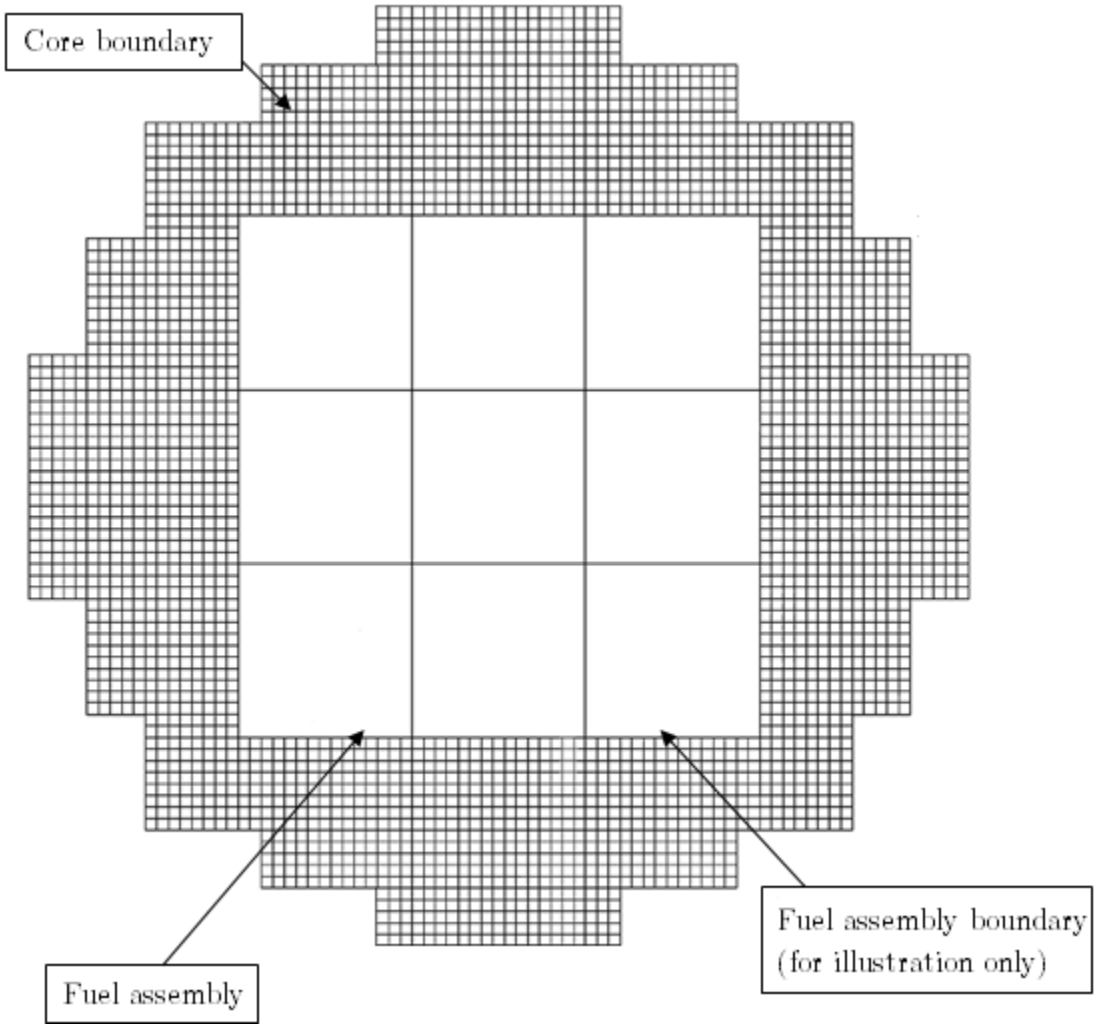


**Figure 3-13.** Core layout for the experimental suite LEU-COMP-THERM-008. The layout of the central region (3 x 3 assemblies) is different for each experiment. Reproduced from [24].

#### 3.3.2.1.4 LEU-COMP-THERM-009

These experiments are performed in a large water filled tank at PNL with aluminum clad $UO_2$ fuel rods in square-pitched clusters. Criticality is reached by varying the separation between the clusters. A general setup for the series of experiments is shown in Figure 3-12. No soluble boron is included in these experiments. Solid absorbers are included in some cases, e.g. in the form of Boral or borated stainless steel. Cases 1-9, 16-23 and 26-27 are included in this benchmark suite. Case 1 is included in the previous WSE validation report [15]. The simplifying assumptions made when modeling these experiments are consistent with the benchmark model presented in [28].

#### 3.3.2.1.5 LEU-COMP-THERM-011

These experiments are performed in a large water filled tank at the B&W Lynchburg Research Center with square-pitched clusters of aluminum clad $UO_2$ fuel rods. Criticality is obtained by varying the water level. Soluble boron is included in these experiments. Cases 1-9 are included in this benchmark suite. The different core loadings used are presented in Figure 3-14 and Figure 3-15. Cases 1, 2 and 5 of these are included in the previous WSE validation report [15] and additional data about the experimental suite may be found there. The simplifying assumptions made when modeling these experiments are consistent with the benchmark model presented in [29].

With systematic errors accounted for the benchmark $k_{eff}$ is $1.0010 \pm 0.0018$ for Case 1 and $1.0009 \pm 0.0032$ for Cases 2 – 9. [29]

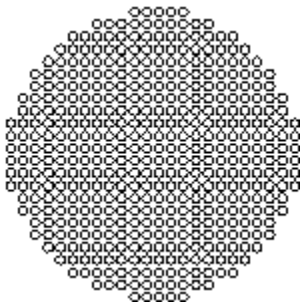

**Figure 3-14.** Loading diagram for Case 1 (Core I) of experimental suite LEU-COMP-THERM-011.

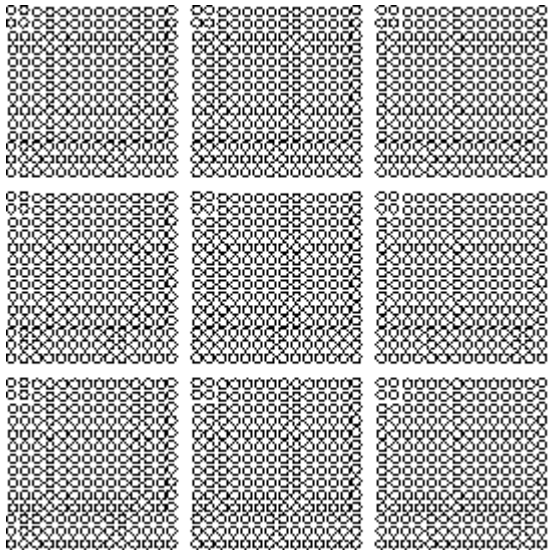

**Figure 3-15.** Loading diagram for Case 2-9 (Core II and III) in experimental suite LEU-COMP-THERM-011, nine arrays separated by 0-4 pin pitch.

#### 3.3.2.1.6 LEU-COMP-THERM-016

These experiments are performed at PNL with aluminum clad $UO_2$ fuel rods in square-pitched clusters placed in a large water filled tank. The separation between the clusters is varied until criticality is obtained. A general setup for the series of experiments is shown in Figure 3-12. No soluble boron is included in these experiments. Cases 1-14, 21-27 and 31-32 are included in the benchmark suite. Case 1 of these is included in the previous WSE report [15]. The simplifying assumptions made when modeling these experiments are consistent with the benchmark model presented in [26].

#### 3.3.2.1.7 LEU-COMP-THERM-042

These experiments are performed in a large water filled tank at PNL containing square-pitched clusters of aluminum clad $UO_2$ fuel rods. Criticality is reached by varying the separation between clusters. A general setup for the series of experiments is shown in Figure 3-16. These experiments do not include any form of soluble boron. Absorber plates are included in the experiments and the clusters are placed between stainless steel reflector walls. The absorber plates have been placed directly against the outer cell boundaries of the center cluster without any gap in between. Cases 1-3 and 5 are included in this benchmark suite. The simplifying assumptions made when modeling these experiments are consistent with the benchmark model presented in [30].

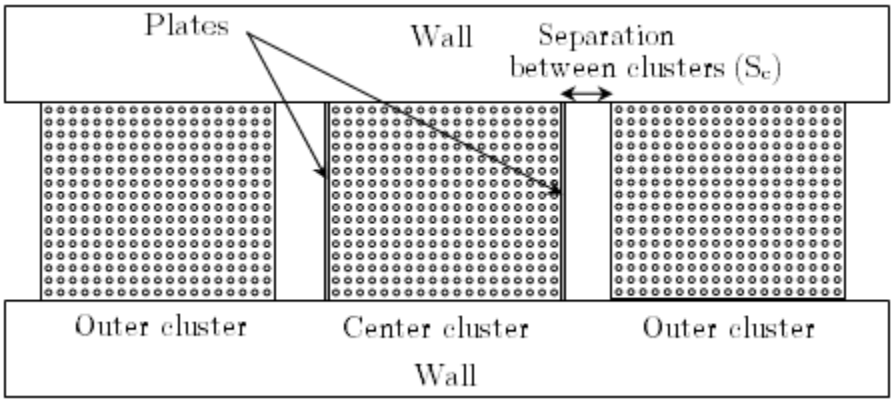


**Figure 3-16.** Cases with three clusters. Reproduced from [30]

### 3.3.2.2 NUREG/CR-6361

NUREG/CR-6361 is a guide to be used for performing criticality benchmark calculations for Light Water Reactor (LWR) fuel applications. Critical conditions for all the experiments from this guide included in the benchmark suite can be found in Appendix I.

The description of the included experiments is sparser in this guide than in the IHECSBE. For this reason the provided sample KENO input deck has been used to provide data that

is not given in the guide. As there is no data on experimental uncertainties, these have been estimated from similar experiments in the IHECSBE using the guidelines in [1].

#### 3.3.2.2.1 BAW-1645

These experiments are performed at B&W with square-pitched clusters of aluminum clad $UO_2$ fuel rods in a large water filled tank with soluble boron and aluminum absorber plates present. Cases BW1645SO1 and -SO2 are included in the benchmark suite.

Due to lacking information in NUREG/CR-6361 regarding the arrangement of the cluster, the KENO input deck has been used as the main source of information giving the arrangement seen in Figure 3-17. This is in line with the information given in the experiment description and Figure 2.25 in NUREG/CR-6361 [16]. Although difficult to distinguish from Figure 3-17 the corner rods of each cluster are solid aluminum rods. The model has been simplified by omitting the mid grids due to lack of data regarding position and composition. The critical conditions for the experiments are found in Appendix I.

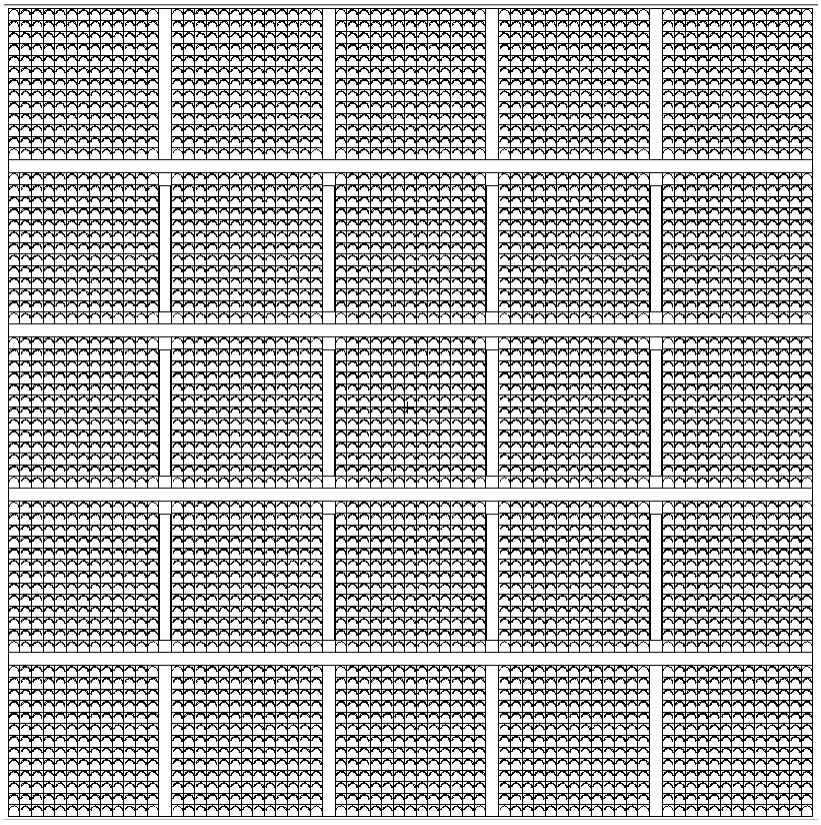

**Figure 3-17.** Core layout for experiments BW1645SO1 and BW1645SO2. The absorber plates are placed between the clusters in the three middle rows.

#### 3.3.2.2.2 BAW-1231

These experiments are performed at B&W with square-pitched cores of $UO_2$ fuel rods in a large water filled tank with soluble boron present. Cases BW1231B1 and -B2 are included in this benchmarking suite. The core layout for these experiments is seen in Figure 3-18.

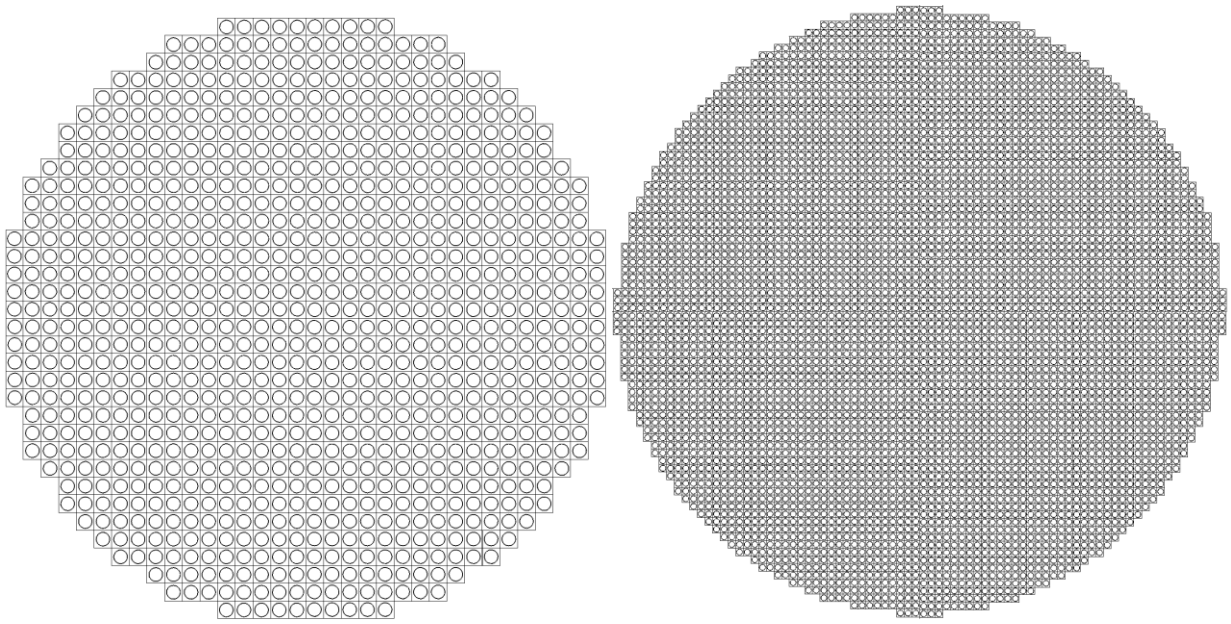

**Figure 3-18.** Core geometry for the experiment BW1231B1 (left) and BW1231B2 (right).

#### 3.3.2.2.3 BAW-1237

This experiment (BW1237M) is performed at B&W with a square-pitched core of $UO_2$ fuel rods in a large water filled tank. Soluble boron is included in this experiment. The core layout may be seen in Figure 3-19.

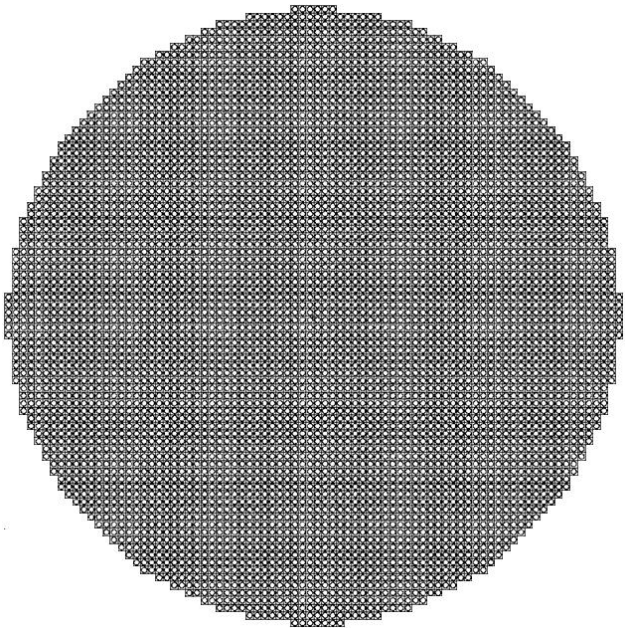

**Figure 3-19.** Core layout for the criticality experiment BAW1237M

#### 3.3.2.2.4 BAW-1810

These experiments are performed at B&W with a square-pitched core of fuel rods in a large water filled tank. Three different types of fuel are used: 2.459 wt% and 4.020 wt% pure $UO_2$ fuel and 1.944 wt% $UO_2$ fuel with 4 wt% $Gd_2O_3$. Soluble boron, and in one of the experiments, Ag-In-Cd absorber rods are included in these experiments. Cases BW1810A through BW1810I are included in the benchmark suite. The core layouts for these cases are presented in Figure 3-20 through Figure 3-24.

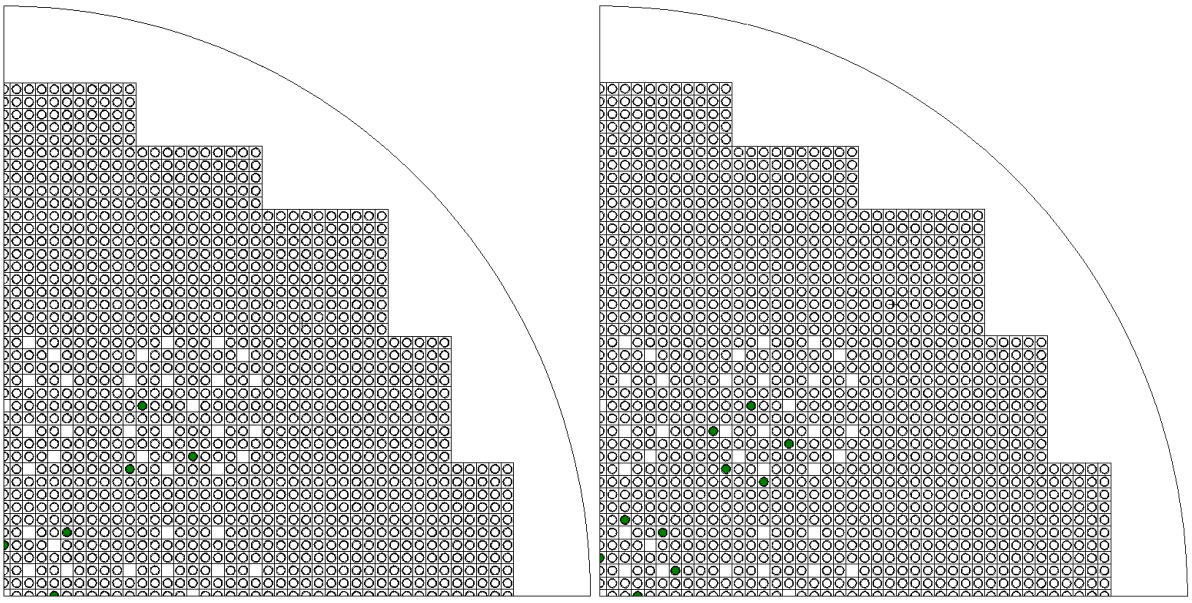

**Figure 3-20.** Quarter core layout for the criticality experiments BW1810A (left) and BW1810B (right). Green rods contain burnable absorber.

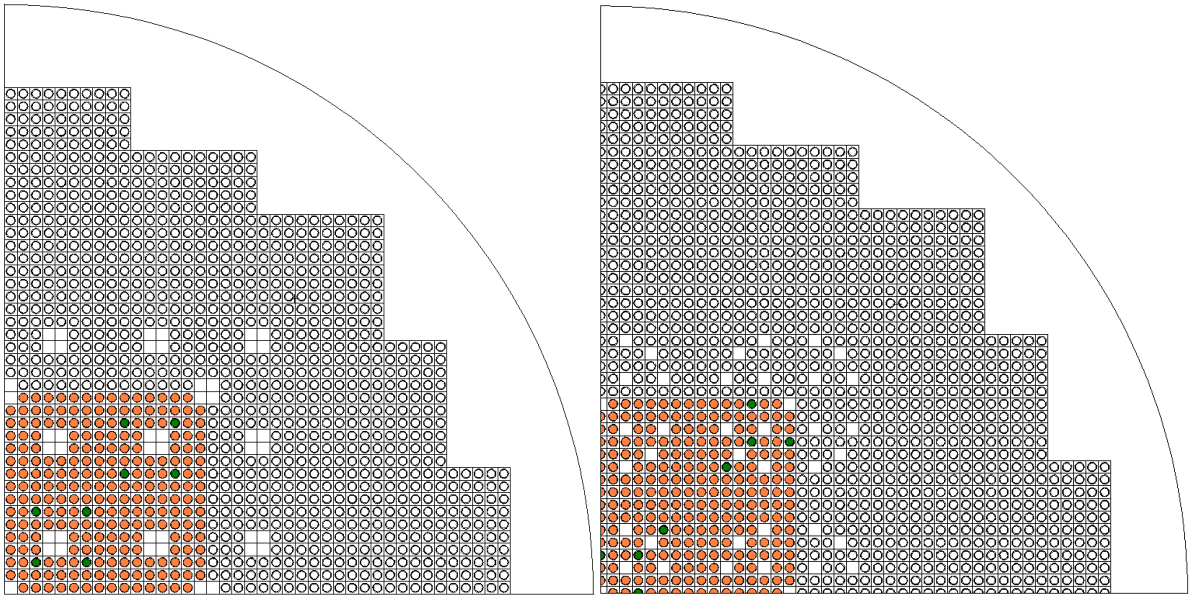

**Figure 3-21.** Quarter core layout for the criticality experiments BW1810C (left) and BW1810D (right). Green rods contain burnable absorber. The orange region contain fuel rods of a higher enrichment (4.020 wt%) than the surrounding grey rods (2.459 wt%).

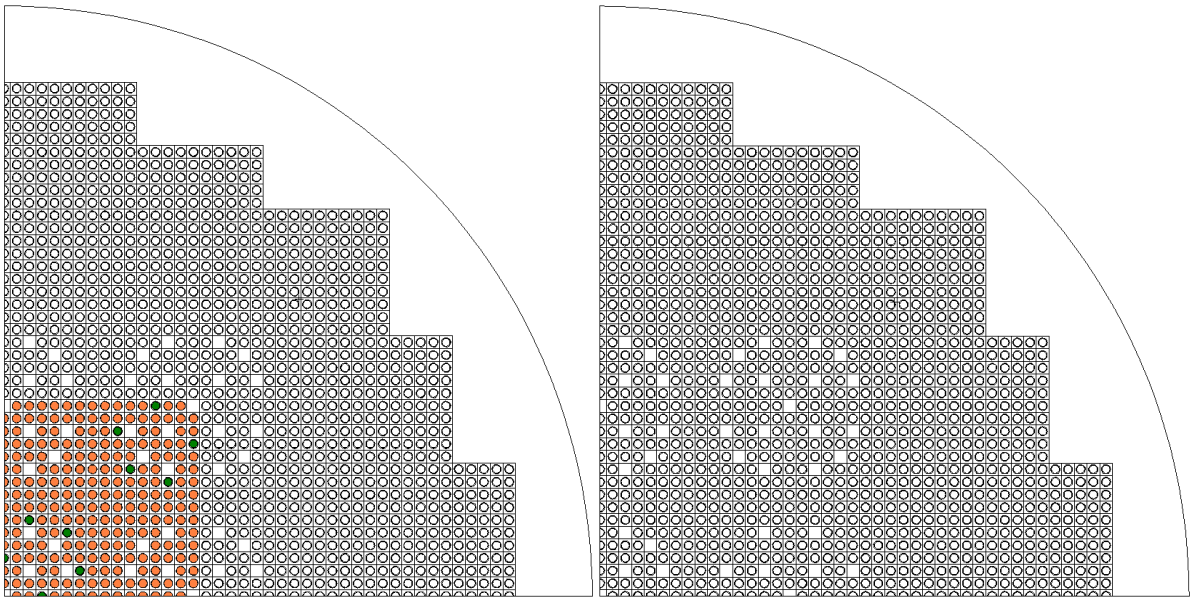

**Figure 3-22.** Quarter core layout for the criticality experiments BW1810E (left) and BW1810F (right). Green rods contain burnable absorber. The orange region contain fuel rods of a higher enrichment (4.020 wt%) than the surrounding grey rods (2.459 wt%).

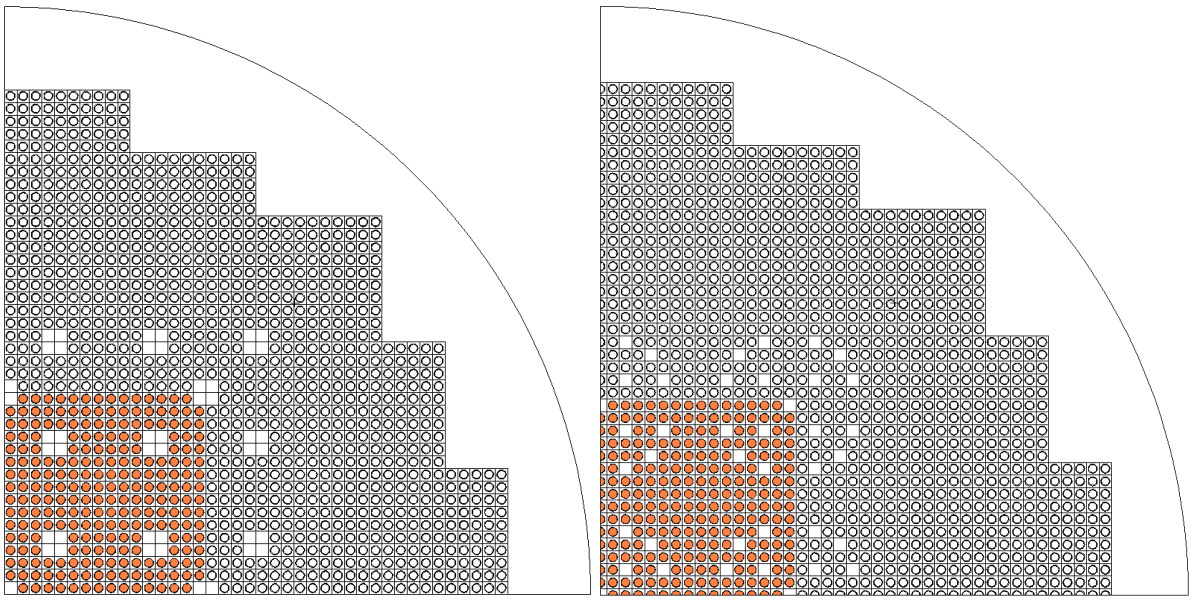

**Figure 3-23.** Quarter core layout of the criticality experiments BW1810G (left) and BW1810H (right). The orange region contain fuel rods of a higher enrichment (4.020 wt%) than the surrounding grey rods (2.459 wt%).

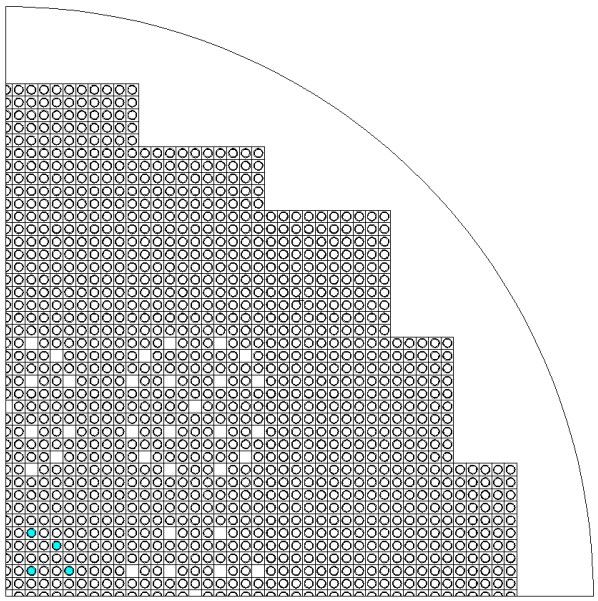

**Figure 3-24.** Quarter core layout of the criticality experiment BW1810I. Turquoise rods are Ag-In-Cd absorber rods.

#### 3.3.2.2.5 EPRI NP-196

These experiments are performed with a square-pitched core of fuel rods in a large water filled tank. Soluble boron is included in some of these experiments. Cases EPRU65, EPRU65B, EPRU75, EPRU75B, EPRU87 and EPRU87B are included in this validation suite. The core layouts of these experiments are found in Figure 3-25 through Figure 3-27.

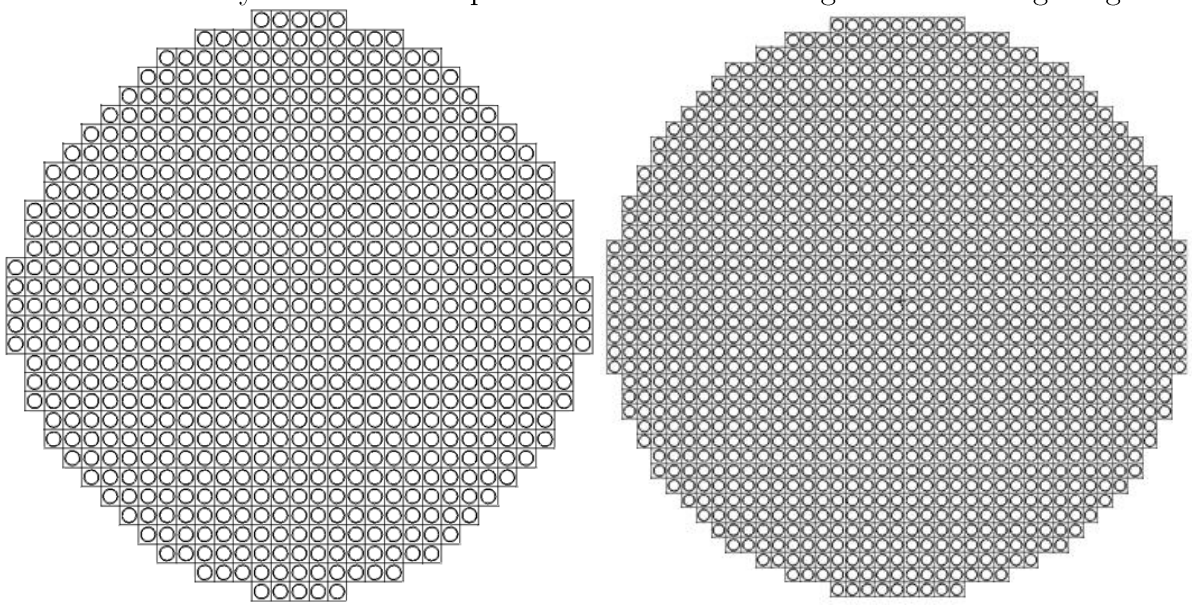

**Figure 3-25.** Core layout for the experiments EPRU65 (left) and EPRU65B (right).

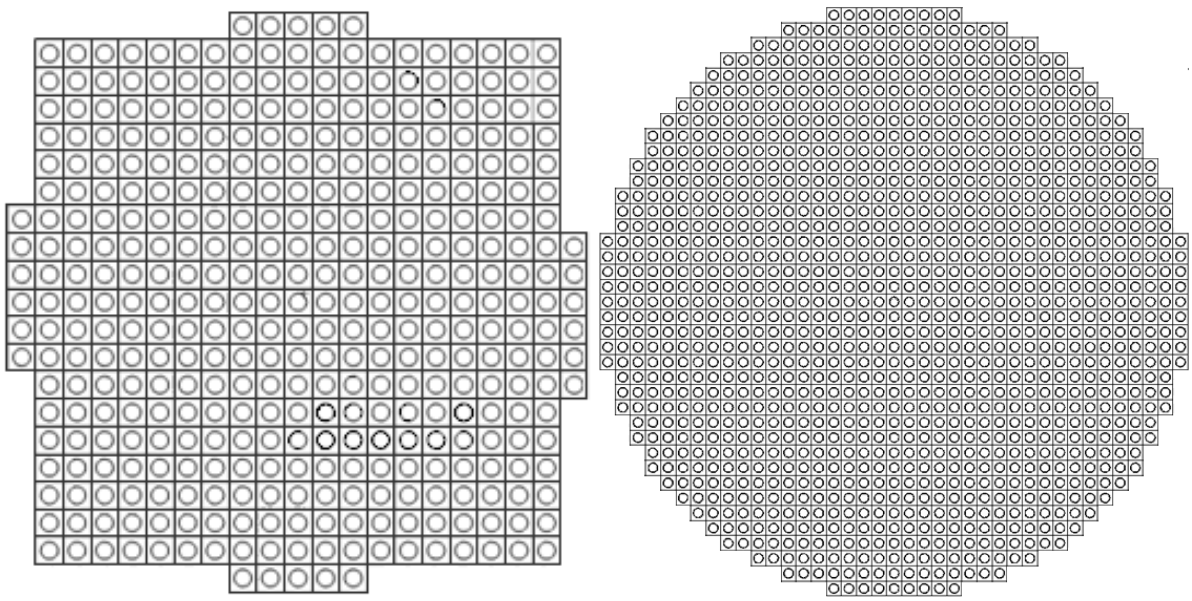

**Figure 3-26.** Core layout for the experiments EPRU75 (left) and EPRU75B (right).

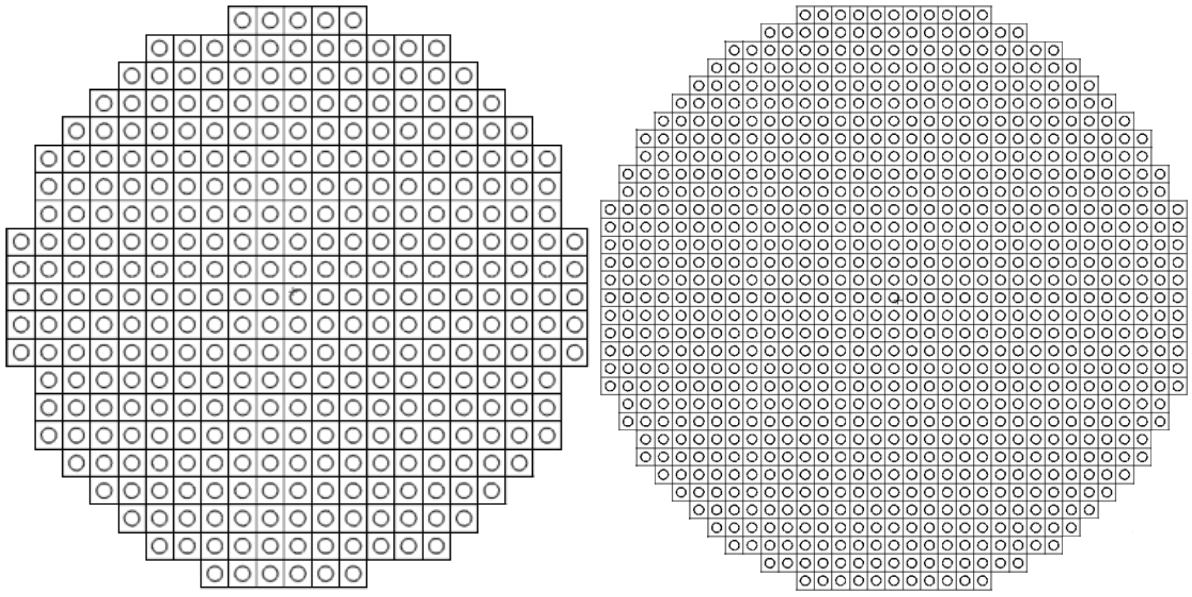

**Figure 3-27.** Core layout for the experiment EPPRU87 (left) and EPRU87B (right).

#### 3.3.2.2.6 WCAP-3269

These experiments are performed at Westinghouse Electric Corporation with square-pitched clusters of $UO_2$ fuel rods in a large water filled tank. In these experiments Ag-In-Cd absorber rods are included. Cases W3269A, W3269B1, W3269B2, W3269B3 and W3269C are included in this validation suite. The core layouts of these experiments are

displayed in Figure 3-28 through Figure 3-32. The models created are based primarily on the data given in [31]. For this reason some of the fuel rod dimensions used deviate from those given in NUREG/CR-6361 [16].

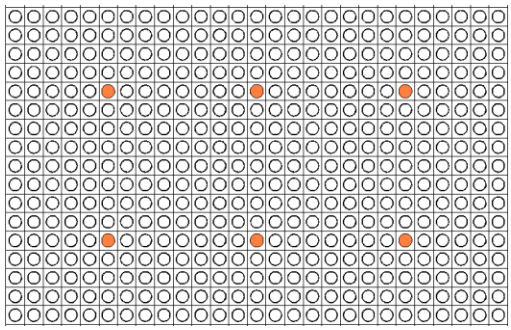

**Figure 3-28.** Core configuration for the experiment W3269A. Orange rods are absorber rods.

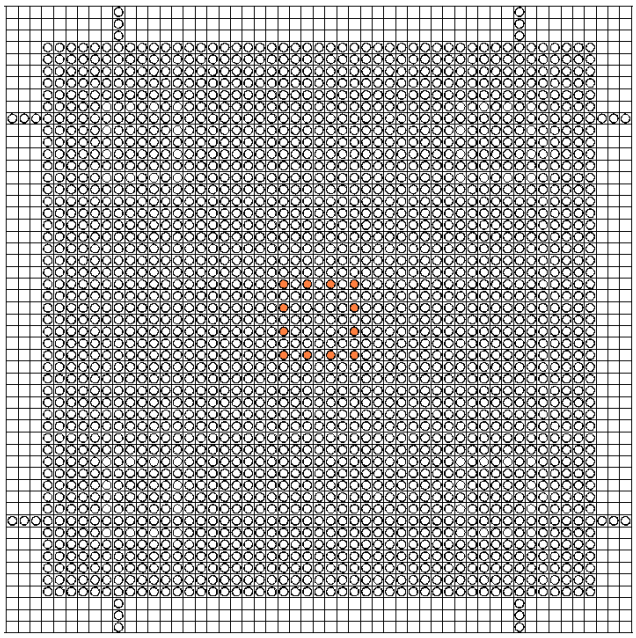

**Figure 3-29.** Core configuration for the experiment W3269B1. Orange rods are absorber rods. The rods extending outside the assembly are part of fuel follower control rod crosses that were fully inserted throughout the experiment.

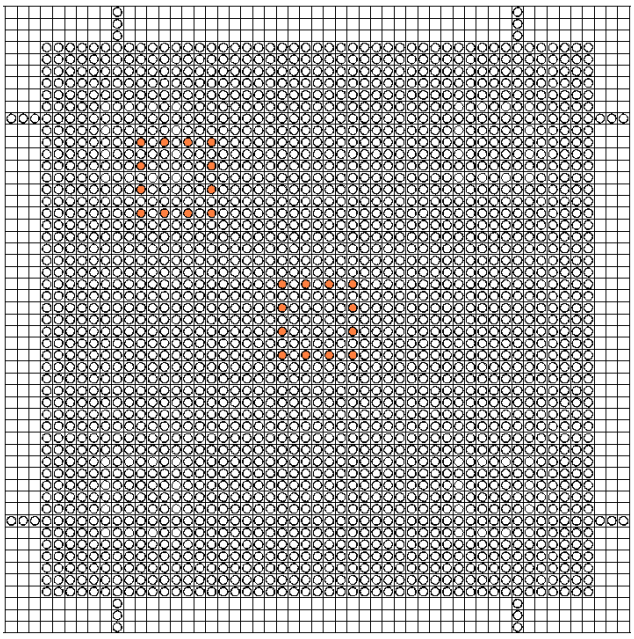

**Figure 3-30.** Core configuration for the experiment W3269B2. Orange rods are absorber rods. The rods extending outside the assembly are part of fuel follower control rod crosses that were fully inserted throughout the experiment.

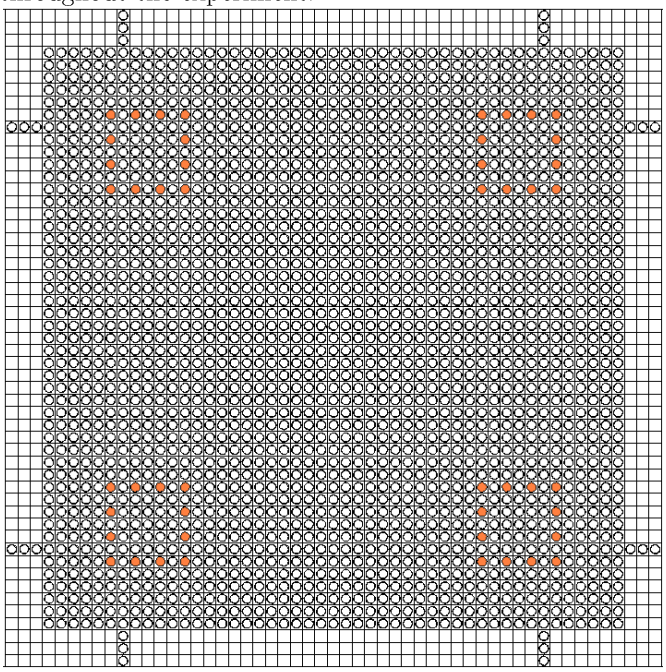

**Figure 3-31.** Core configuration for the experiment W3269B3. Orange rods are absorber rods. The rods extending outside the assembly are part of fuel follower control rod crosses that were fully inserted throughout the experiment.

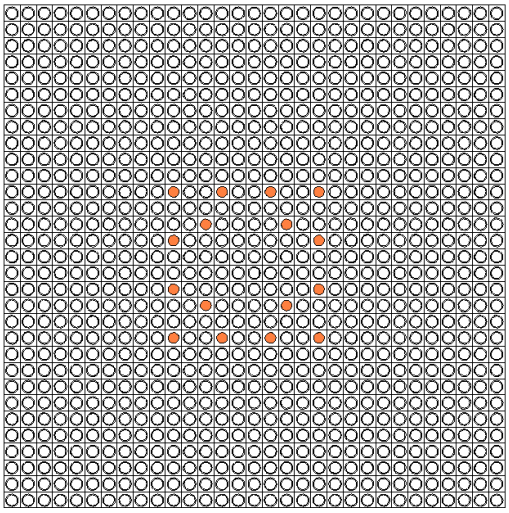

**Figure 3-32.** Core configuration for the experiment W3269C. Orange rods are absorber rods.

## 3.4 Calculation method

All calculations are performed on systems with the following hardware and software characteristics:

- Intel Xeon 3.0 GHz and 3.166 GHz
- MCNP5 Version 1.51
- Suse Linux 9.0

The cross-sections used in the calculations are taken from the ENDF70/B-VII library with the *S(α, β)*-scattering cross sections taken from endf70sab/endf7.0. ENDF stands for Evaluated Nuclear Data Files, and the libraries are produced by the Cross Section Evaluation Working Group (CSEWG) [32]. The source data files used are endf70a through endf70j from B-VII.0 for 293.6 K. These files are selected as all cases run are assumed to be at room temperature. All the cross-section and *S(α,β)* libraries used in the calculations are displayed in Appendix III. The nuclides displayed in the tables are used in at least one experiment included in the validation suite.

The number of cycles and the number of neutrons for each cycle determines the level of precision in the results. More cycles will give a better estimate of the mean $k_{eff}$. More neutrons per cycle will also give a higher precision with a lower standard deviation.

The number of cycles and neutrons per cycle in the calculations can be found in Table 3-3. During the first cycles the spatial source distribution will change from the initial to the correct distribution, as described in Section 2.4.1. Because source convergence has to

be reached in order to calculate a correct $k_{eff}$, the results from the first cycles are skipped when calculating the average $k_{eff}$. The number of skipped cycles may also be found in Table 3-3.

**Table 3-3.** MCNP settings.

| Data source | Skipped cycles | Total cycles | Neutrons per cycle |
|---|---|---|---|
| IHECSBE | 200 | 1200 | 50000 |
| NUREG/CR-6361 | 200 | 1200 | 50000 |
| KSH | 150-400 | 500-1000 | 50000-70000 |

### 3.4.1 Statistical evaluation

For the validation of MCNP5 v1.51 the simulations are followed by statistical analyses. The experiments are placed into two different groups covering frequently encountered situations in storage of spent LWR fuel:

- Experiments which contain fresh fuel and strong absorbers.
- Experiments which contain fresh fuel without strong absorbers.

These fresh fuel experiments may be used for validation for spent fuel pool conditions. This is due to the possibility of conservatively modeling spent fuel as fresh fuel without burnable absorbers. Experiments like these are also sometimes used in validation for fresh fuel storage calculations. This is not done at WSE where a B-term taken from the WSE validation report [15] is used for fresh fuel storage criticality safety calculations.

The strong absorbers in this validation suite are boron, gadolinium and cadmium containing compounds including the alloy Ag-In-Cd. Experiments containing absorber plates of other materials e.g. aluminum or stainless steel are considered to be without strong absorbers.

The subsequent data analysis for each group includes: determining the USL and the associated B-term, testing for normality and identifying trends using the method described in Section 2.5.

# 4 Results and discussion

The results for the different parts of the thesis work are presented and discussed in the subsequent subchapters.

## 4.1 KSH 12.3

The results in KSH 12.3 are divided into subchapters according to the geometry being studied. The simulations have been run with enough precision to ensure that the standard deviation $\sigma$ has been less than 20 pcm. The B-term (see Section 2.5.3) is 0.0122 for the conditions being used. The term $k_{eff}$ refers to the calculated value of $k_{eff}$, $k_{calc}$.

### 4.1.1 Infinite cylinders

The first geometry being studied is a cylinder with an infinite height. Depending on the ratio between the diameter and the height of a cylinder, the cylinder may not need to be more than a couple of meters in height to be considered infinite in terms of reactivity. The results for infinite cylinders with different configurations are shown in Figure 4-1.

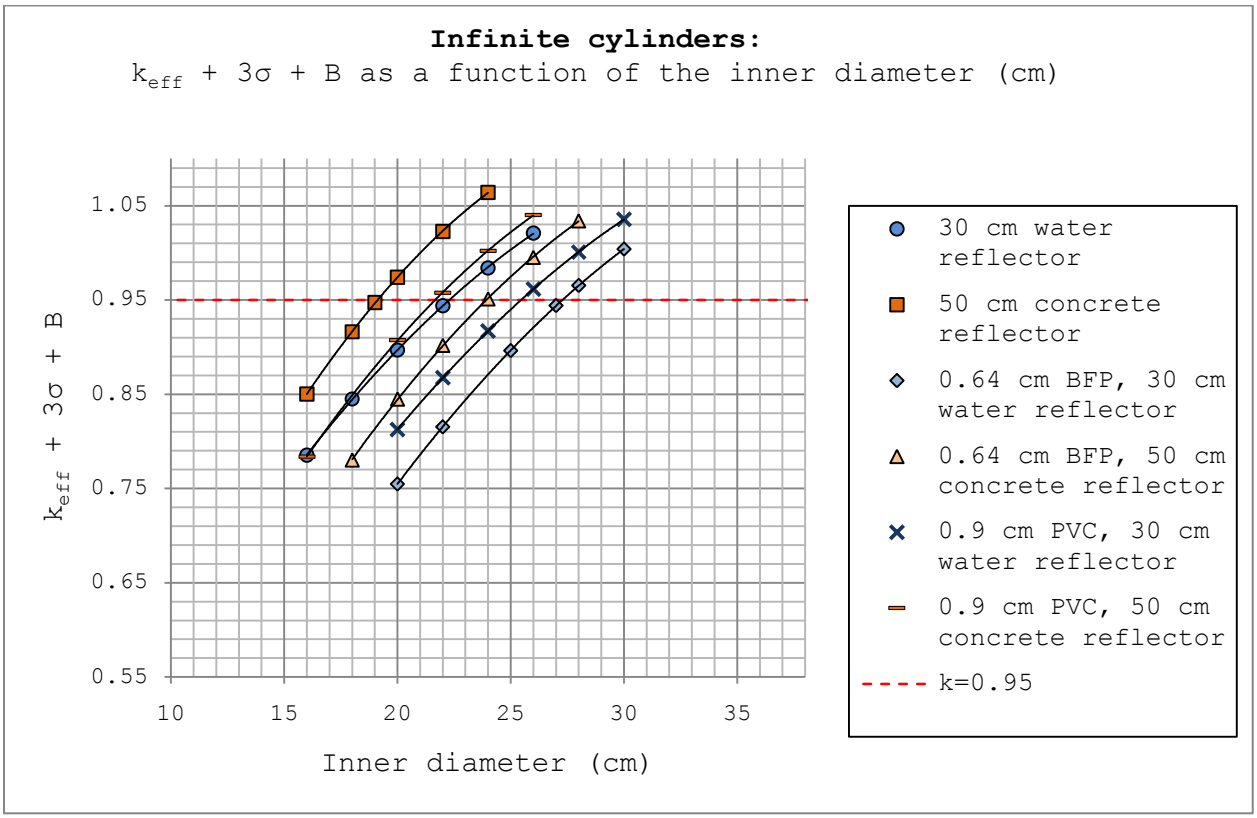


**Figure 4-1.** Infinite cylinders with and without absorbers, surrounded by water or concrete reflectors.

Figure 4-1 shows that the largest inner diameter of the cylinder that can be permitted is when BFP is used as an absorber with a 30 cm water reflector, roughly 27 cm. The smallest inner diameter that can be permitted is the case when no neutron absorber is used and the system is reflected by concrete, roughly 19 cm. This is an anticipated result considering the neutron absorption properties of BFP and the more reflecting (and less absorbing) properties of concrete compared to water [33].

The results for critically safe inner diameters for infinite cylinders are tabulated in Table A2-1 in Appendix II.

### 4.1.2 Finite cylinders

The finite cylinders can be used when the critically safe inner diameter for the infinite cylinders needs to be exceeded by restricting the height of the cylinder. The results in Figure 4-2 through Figure 4-7 show how $k_{eff}$ is affected by altering the height of the cylinders, for different absorbers and reflectors.

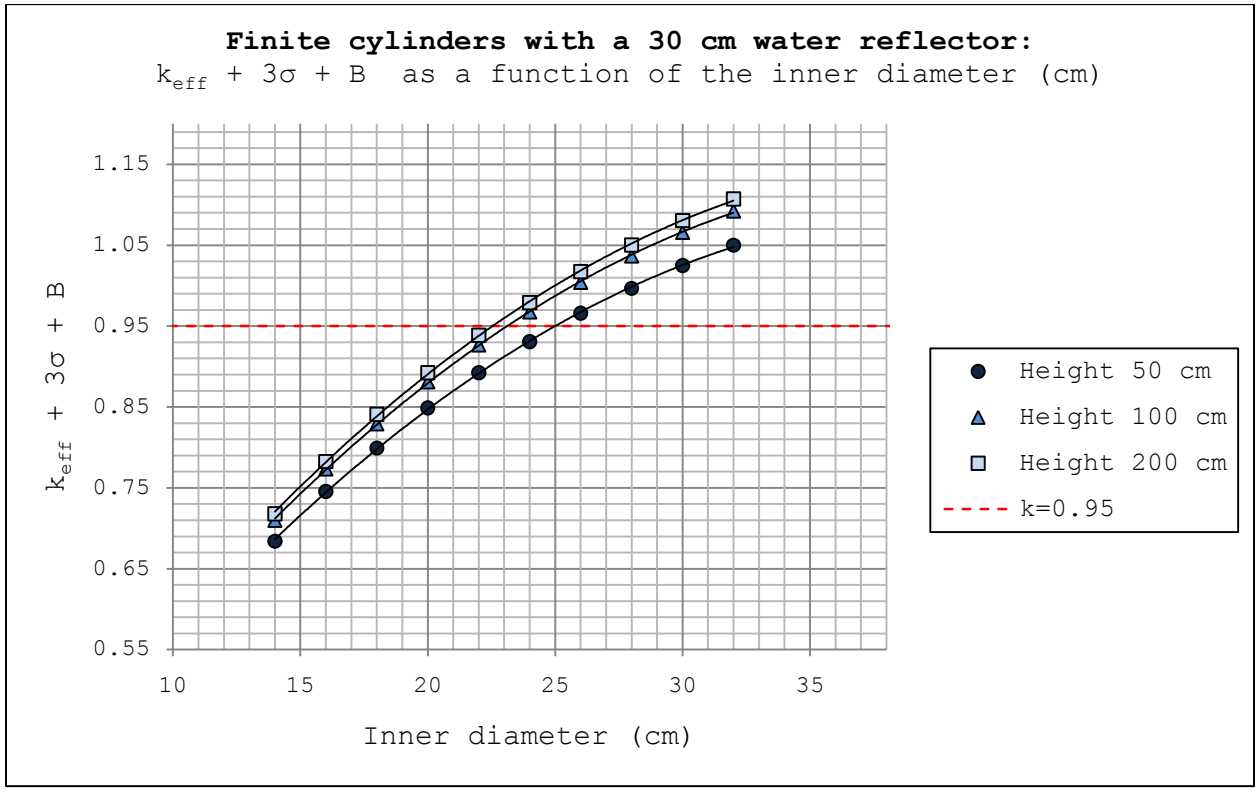


**Figure 4-2.** Cylinders of different heights, reflected by 30 cm water.

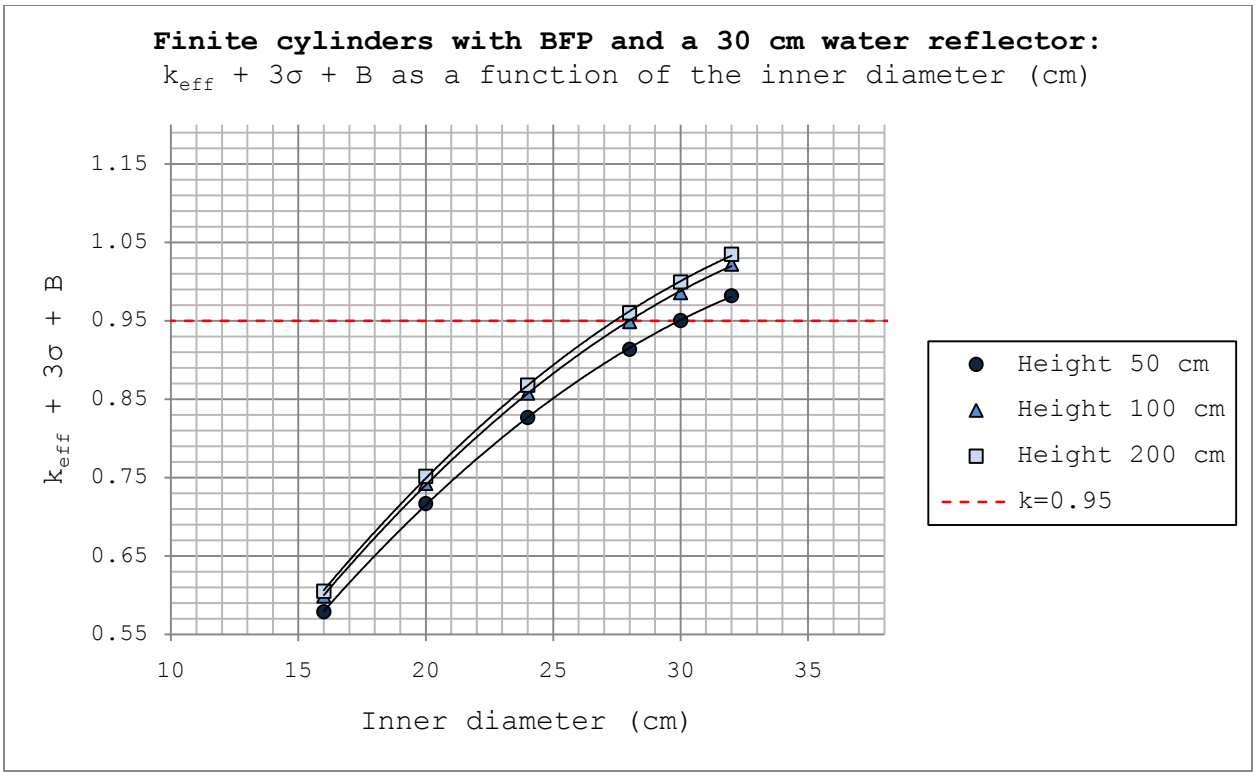


**Figure 4-3.** Cylinders of different heights with BFP as an absorber, reflected by 30 cm water.

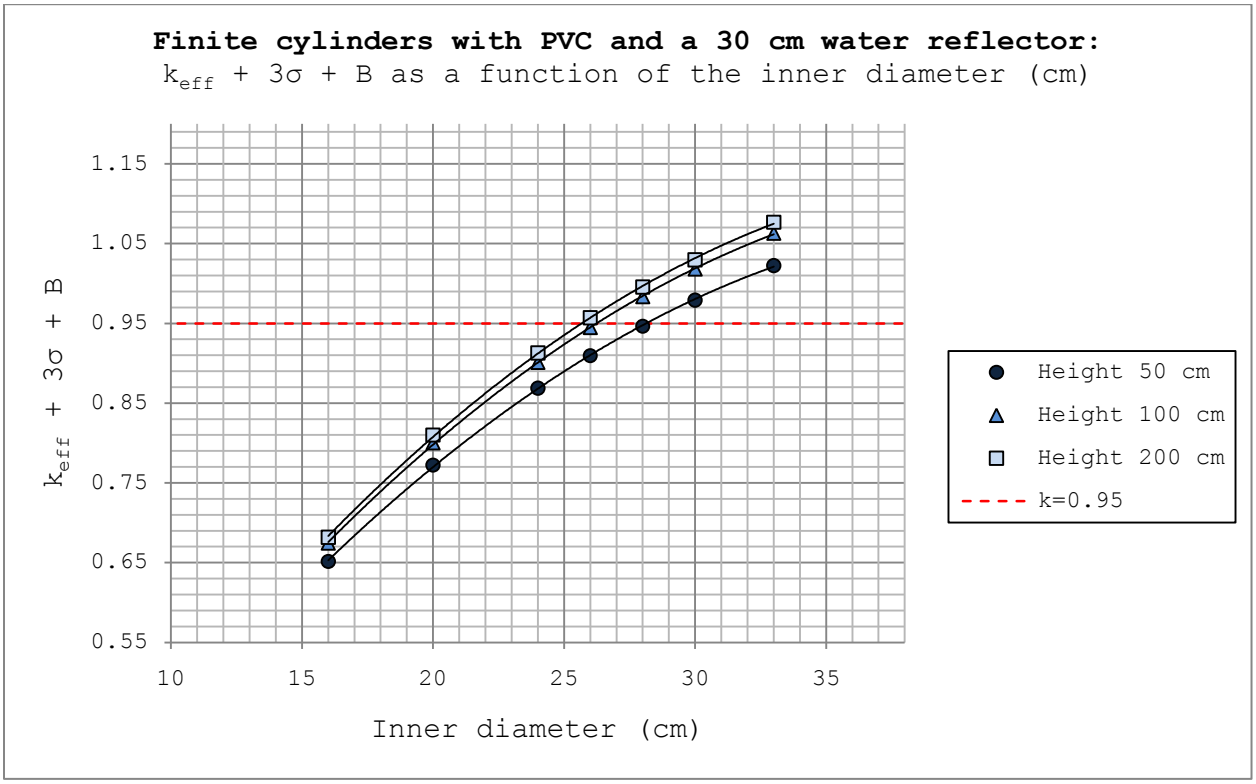


**Figure 4-4.** Cylinders of different heights with PVC as an absorber, reflected by 30 cm water.

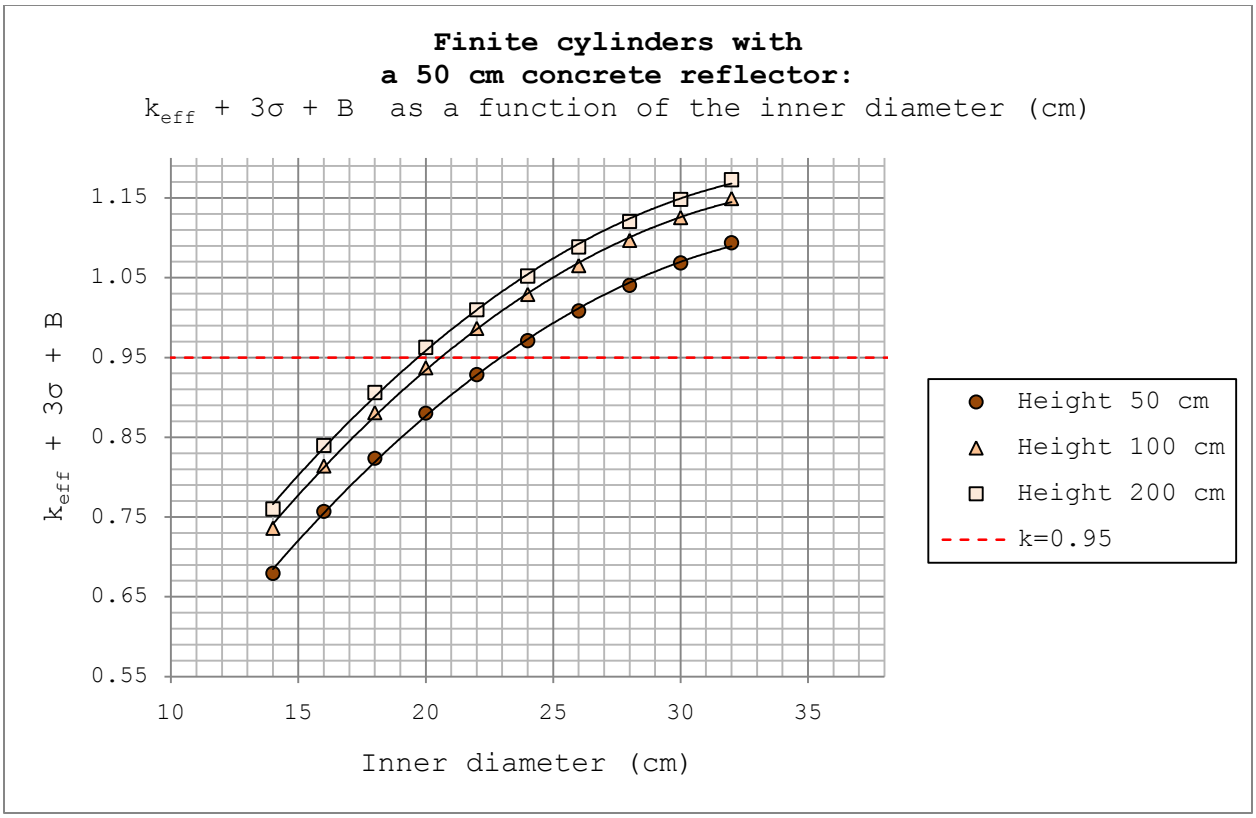


**Figure 4-5.** Cylinders of different heights, reflected by 50 cm concrete.

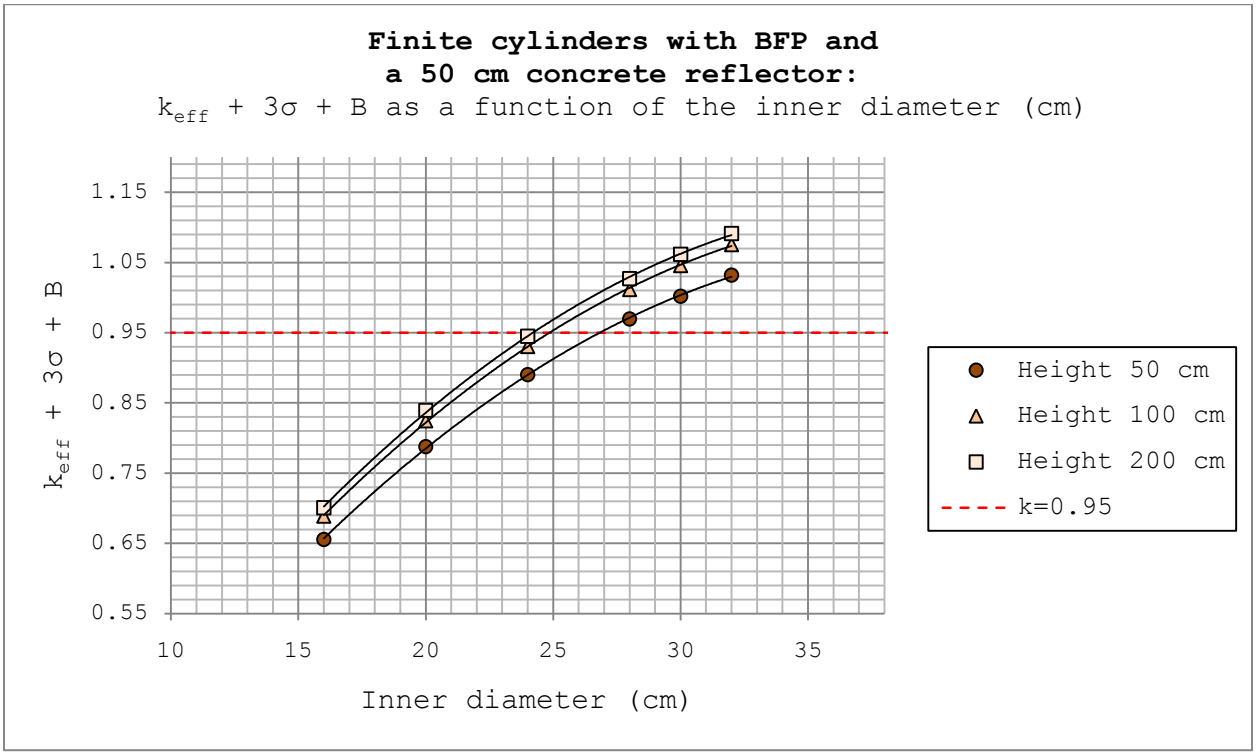


**Figure 4-6.** Cylinders of different heights with BFP as an absorber, reflected by 50 cm concrete.

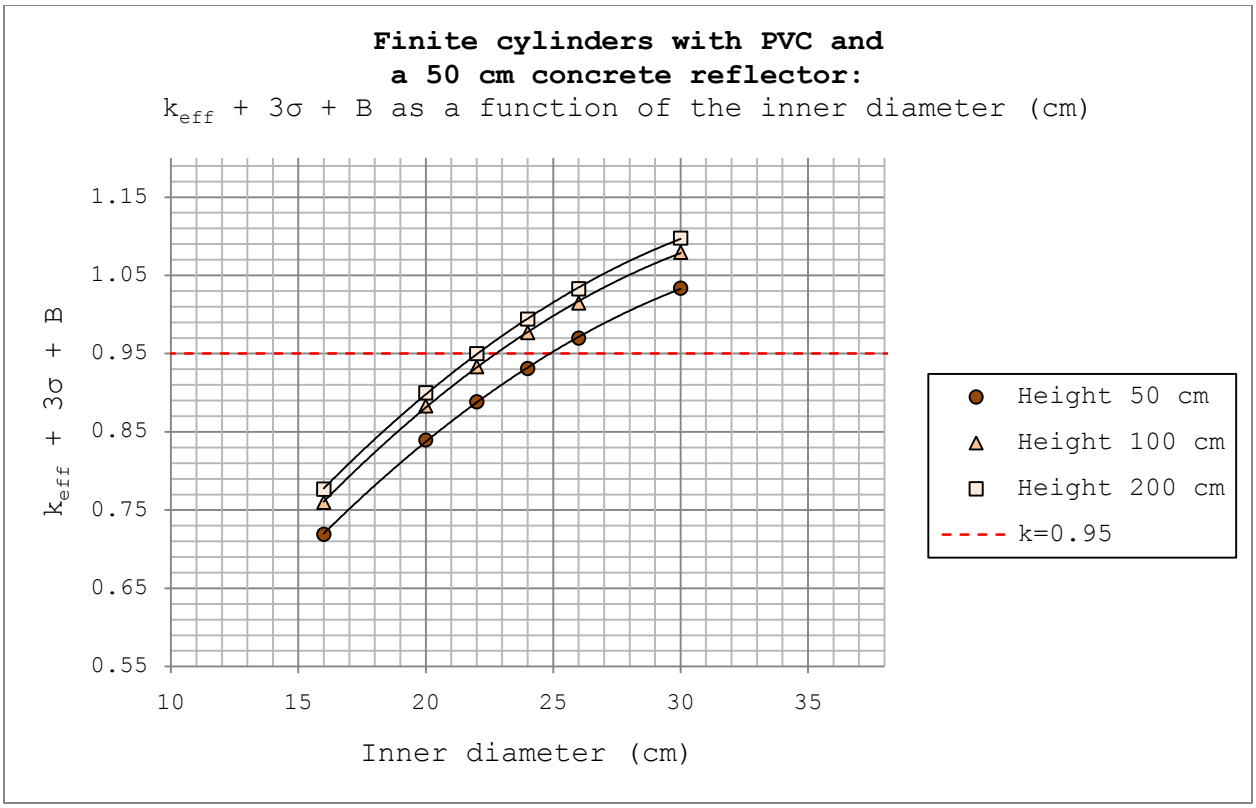


**Figure 4-7.** Cylinders of different heights with PVC as an absorber, reflected by 50 cm concrete.

There are a lot of similarities between the curves for the finite cylinders. Increasing the height of the cylinder gives a vertical displacement of the curve, decreasing the allowed inner diameter. It can also be observed that the distance between the curves decreases even though the difference in height between the curves increases. This is in agreement with the earlier comment on how cylinders can be regarded as infinite in terms of reactivity when they reach a certain height. Increasing the height further will eventually lead to an overlap in the curves due to decreasing differences in reactivity.

Just as for the case with the infinite cylinders, adding an absorber gives a horizontal displacement of the curve to the right, allowing a larger inner diameter for a given height. It can also be seen that the water reflector permits a larger inner diameter than the concrete reflector with all other conditions being the same.

The results for critically safe inner diameters for finite cylinders are tabulated in Table A2-2 through A2-4 in Appendix II.

### 4.1.3 Slabs infinite in two dimensions

Just as with infinite cylinders, the slabs infinite in two dimensions provide a single dimension for which the slab can be said to the critically safe. The results for slabs infinite in two dimensions are shown in Figure 4-8 below.

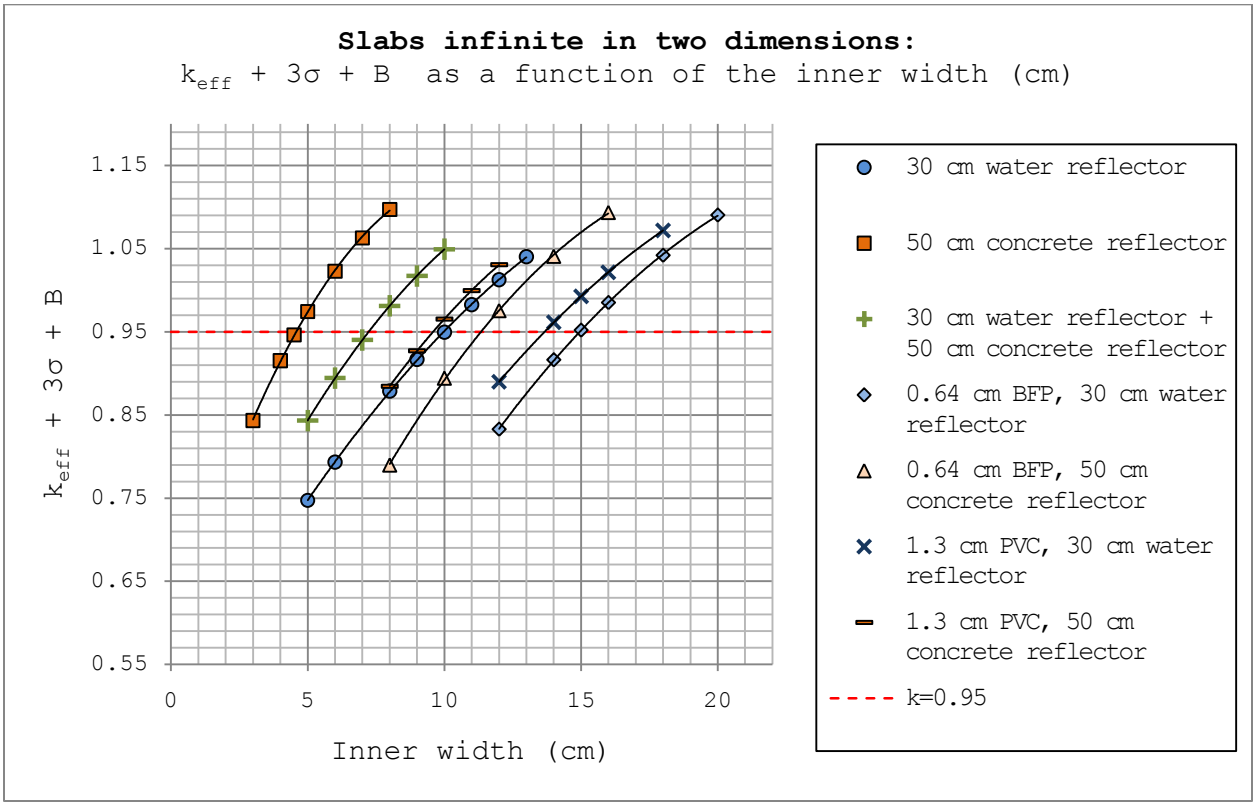


**Figure 4-8.** Slabs infinite in depth and height with and without absorbers, surrounded by water and/or concrete reflectors.

The trend in the curves is reminiscent of the case with the infinite cylinders. The least slab width is tolerated when no absorber is used and concrete is used as a reflector, about 4.5 cm. If a BFP absorber is used and the system is reflected by water, the tolerated slab width is instead about 14.9 cm. This is, again, a testament to the neutron absorbing capabilities of BFP as well as the neutron reflecting capabilities of concrete.

The results for critically safe inner widths for slabs infinite in two dimensions are tabulated in Table A2-5 in Appendix II.

### 4.1.4 Slabs infinite in one dimension

Analogous to the case with infinite and finite cylinders, the inner width of a slab may need to be exceeded by restricting the depth of the slab. The results in Figure 4-9 through Figure 4-14 show how $k_{eff}$ is affected by altering the depth of the slabs, for different absorbers and reflectors.

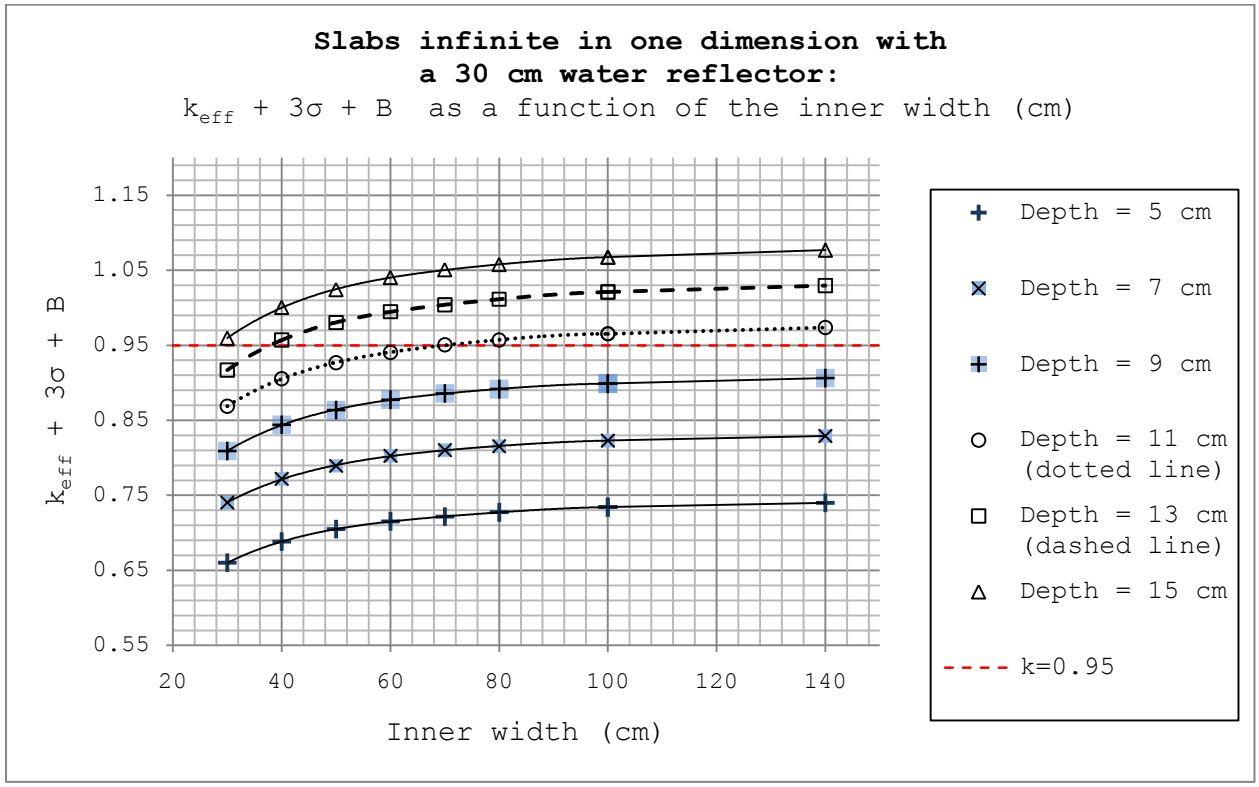


**Figure 4-9.** Slabs infinite in height, reflected by 30 cm water.

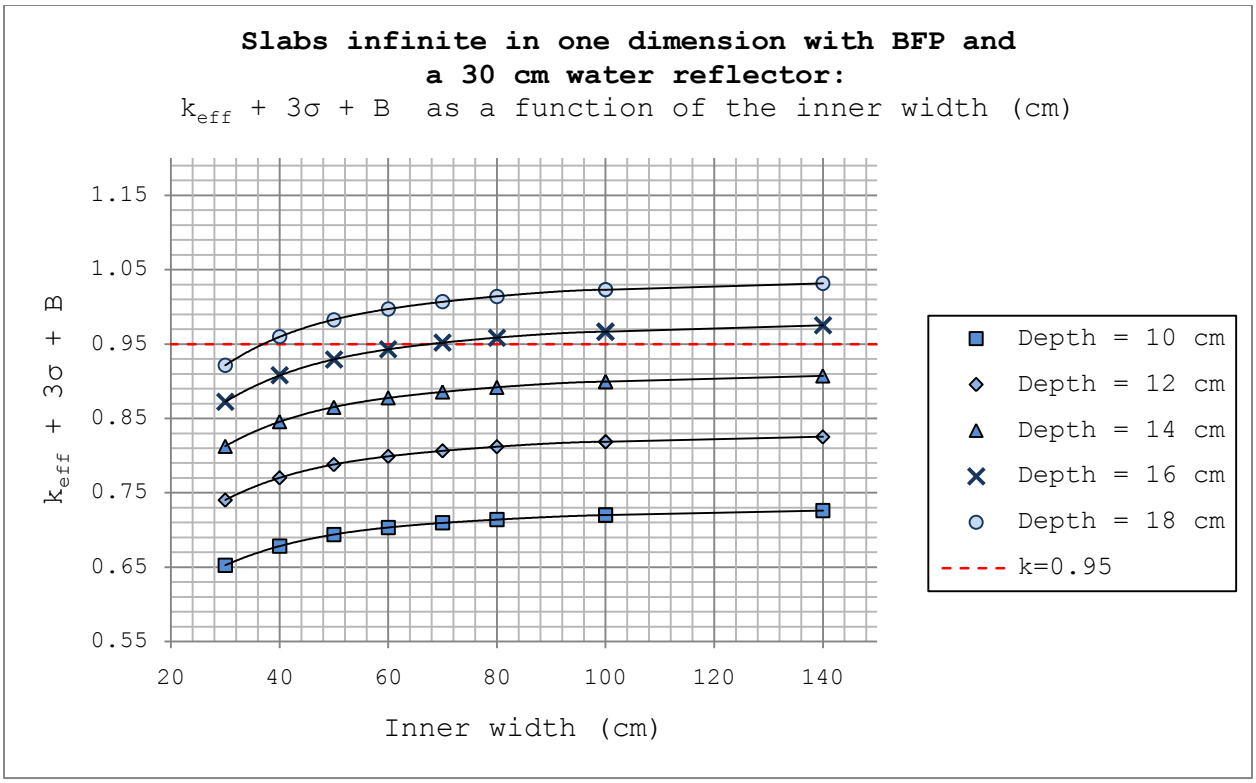


**Figure 4-10.** Slabs infinite in height with BFP as an absorber, reflected by 30 cm water.

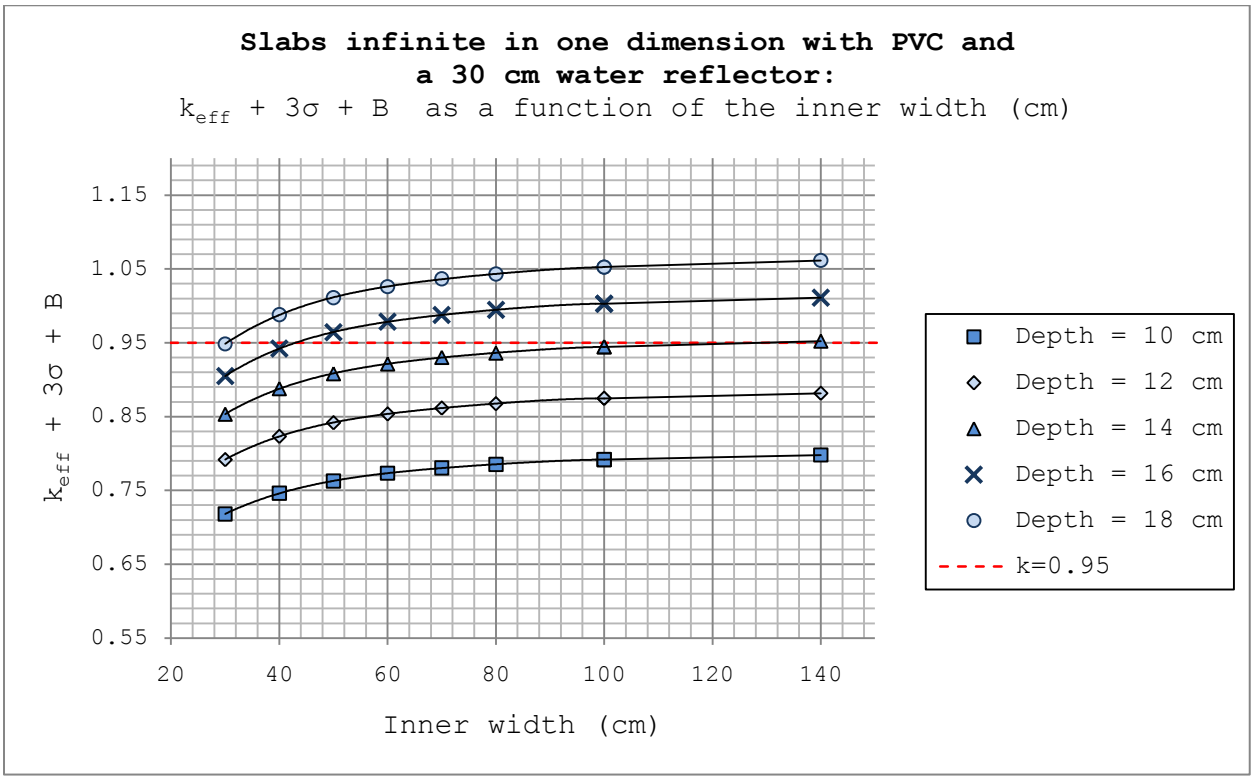


**Figure 4-11.** Slabs infinite in height with PVC as an absorber, reflected by 30 cm water.

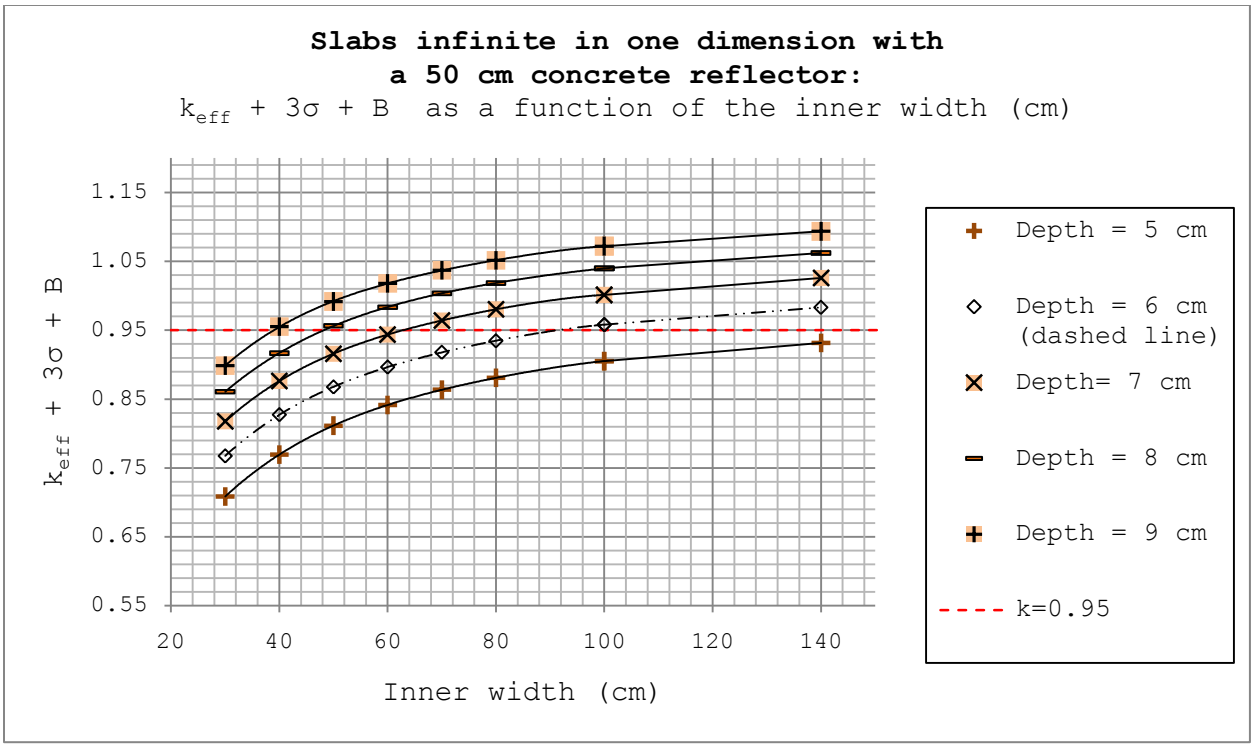


**Figure 4-12.** Slabs infinite in height, reflected by 50 cm concrete.

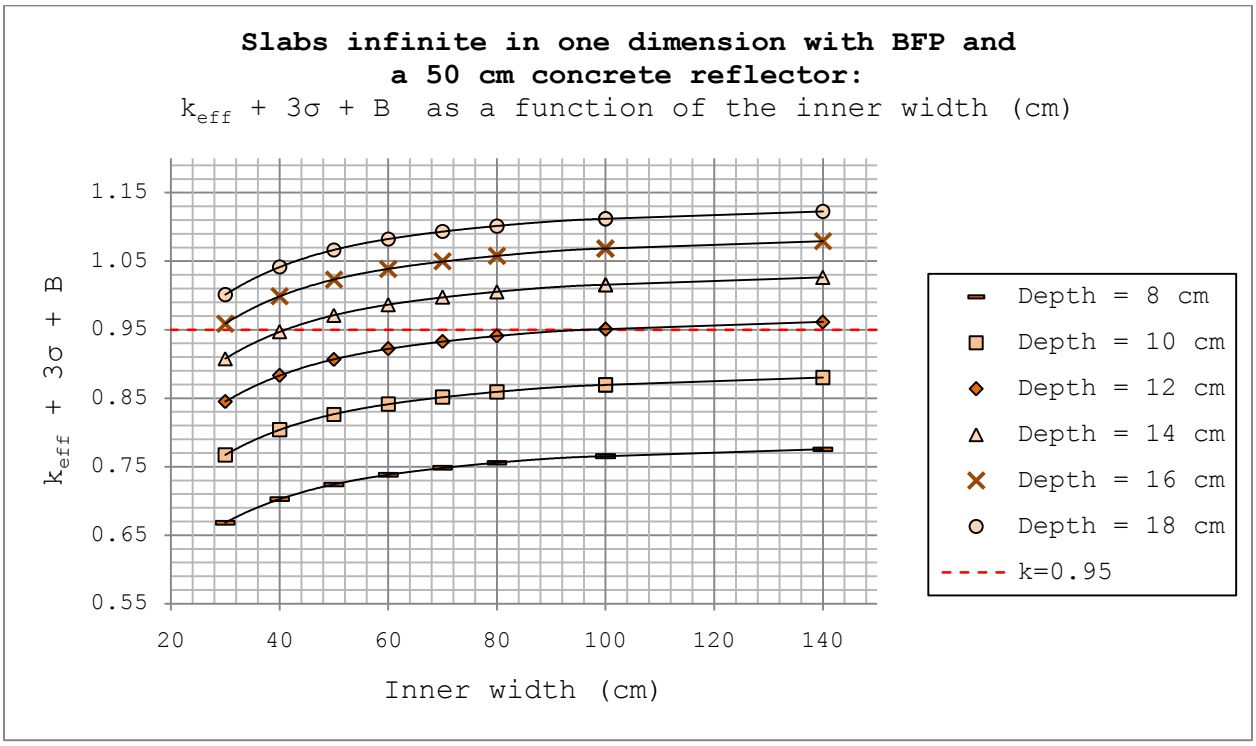


**Figure 4-13.** Slabs infinite in height with BFP as an absorber, reflected by 50 cm concrete.

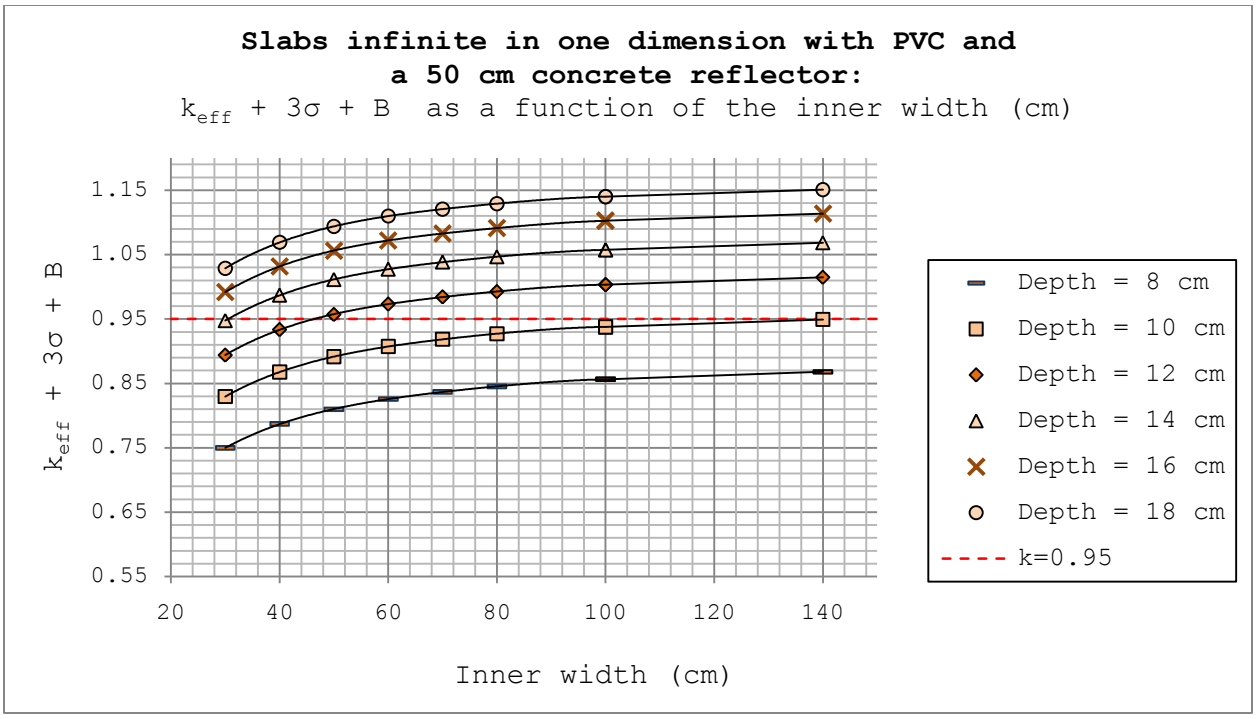


**Figure 4-14.** Slabs infinite in height with PVC as an absorber, reflected by 50 cm concrete.

The results for critically safe inner widths for slabs infinite in one dimension are tabulated in Table A2-6 through A2-11 in Appendix II.

### 4.1.5 Comparison between the new and old BFP results

Since it would be difficult to get an overview of all the data points in all the simulations made in KSH 12.3, an arbitrary selection of results with the new and the old BFP setup is presented in Table 4-1.

**Table 4-1.** Comparison in reactivity between the old and new BFP results of KSH 12.3.

| Systems with BFP | Diameter or Width (cm) | KSH 12.3 (old) ($k_{eff} + 3\sigma_{old}$) | KSH 12.3 (new) ($k_{eff} + 3\sigma_{new} + B$) | Difference new-old (pcm) |
|---|---|---|---|---|
| Infinite cylinder, concrete refl. | 24 | 0.940 | 0.951 | + 1100 |
| Infinite cylinder, water refl. | 28 | 0.940 | 0.965 | + 2500 |
| Finite cylinder, concrete refl., height 50 cm | 24 | 0.875 | 0.890 | + 1500 |
| Finite cylinder, water refl., height 50 cm | 24 | 0.800 | 0.827 | + 2700 |
| Slab infinite in two dimensions, concrete refl. | 12 | 0.930 | 0.975 | + 4500 |
| Slab infinite in two dimensions, water refl. | 12 | 0.775 | 0.833 | + 5800 |

It is worth mentioning a number of differences between the simulations. Steel has been added to the BFP model, but the thickness of BFP is still 0.64 cm for both the new and the old versions of KSH 12.3. The old version of KSH 12.3 is based on simulations made

in KENO with older cross section libraries. The magnitude of the standard deviation in the old simulations $\sigma_{old}$ is unknown, but it is likely higher than the standard deviation in the new version $\sigma_{new}$ since the simulations were made in the 90's when less computing power was available. However, a rather large B-term has been added to the results in the new version. In the old methodology with KENO, no B-term was used and it is therefore not included in the old results.

Comparisons for slabs infinite in one dimension have not been made since the old simulations erroneously used absorber on all four sides of the slab whereas the real installations only use absorber on two sides.

As anticipated from existing work on KSH 12.6, the addition of steel in the model with BFP gives a higher value of $k_{eff}$ due to increased neutron reflection which thus leads to more restrictions in the allowed dimensions for new installations.

### 4.1.6 Comparison between the new and old PVC results

A selection of comparisons between the new and old results with PVC is presented in Table 4-2.

**Table 4-2.** Comparison in reactivity between the old and new PVC composition of KSH 12.3.

| Systems with PVC | Diameter or Width (cm) | KSH 12.3 (old) ($k_{eff} + 3\sigma_{old}$) | KSH 12.3 (new) ($k_{eff} + 3\sigma_{new} + B$) | Difference new-old (pcm) |
|---|---|---|---|---|
| Infinite cylinder, concrete refl. | 22 | 0.935 | 0.958 | + 2300 |
| Infinite cylinder, water refl. | 28 | 0.975 | 1.001 | + 2600 |
| Finite cylinder, concrete refl., height 50 cm | 30 | 1.020 | 1.034 | + 1400 |
| Finite cylinder, water refl., height 50 cm | 20 | 0.740 | 0.772 | + 3200 |
| Slab infinite in two dimensions, concrete refl. | 10 | 0.949 | 0.965 | + 1600 |
| Slab infinite in two dimensions, water refl. | 18 | 1.025 | 1.072 | + 4700 |

The same general claims about the differences mentioned for BFP in Section 4.1.5 applies to PVC as well. The old version uses 1.0 cm PVC for all geometries whereas the new version uses 0.9/1.3 cm for cylinders and slabs respectively.

As anticipated from the decrease in chlorine concentration, the new PVC composition leads to more restrictions in the allowed dimensions of new systems.

### 4.1.7 Parametric study

As mentioned in Section 3, a number of parametric studies have been performed for infinite cylinders and slabs infinite in two dimensions having critically safe dimensions and different absorbers. Both concrete and water reflectors are considered for BFP whereas with PVC only water reflectors are studied.

The results in the parametric studies are presented in a different way than the rest of the report; they show the difference in $k_{eff} + 3\sigma + B$ from 0.95 by varying a certain parameter. The intersection of the curves with the k = 0.95 line thus represents the basic configuration which all previous simulations in the report are based on.

It is also worth mentioning that the interval in which the parameters are varied covers a broader range than what can be expected in the actual installations in the fuel factory.

#### 4.1.7.1 BFP

The combined thickness of the steel layers (both the tank and one side of the enclosure) that separate the $UO_2$ + $H_2O$ mixture and the absorber (marked with red crosses in Figure 4-15) has been varied to assess the effect of the steel thickness on $k_{eff}$. The results for the infinite cylinders are shown in Figure 4-16 and Figure 4-17. The corresponding results for slabs infinite in two dimensions are shown in Figure 4-18 and Figure 4-19.

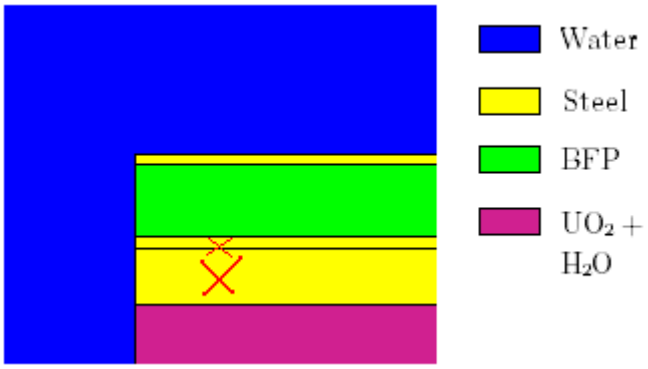


**Figure 4-15**. Close up of a cross section of an infinite cylinder with BFP as an absorber. The red crosses marks the steel layers whose thickness has been varied.

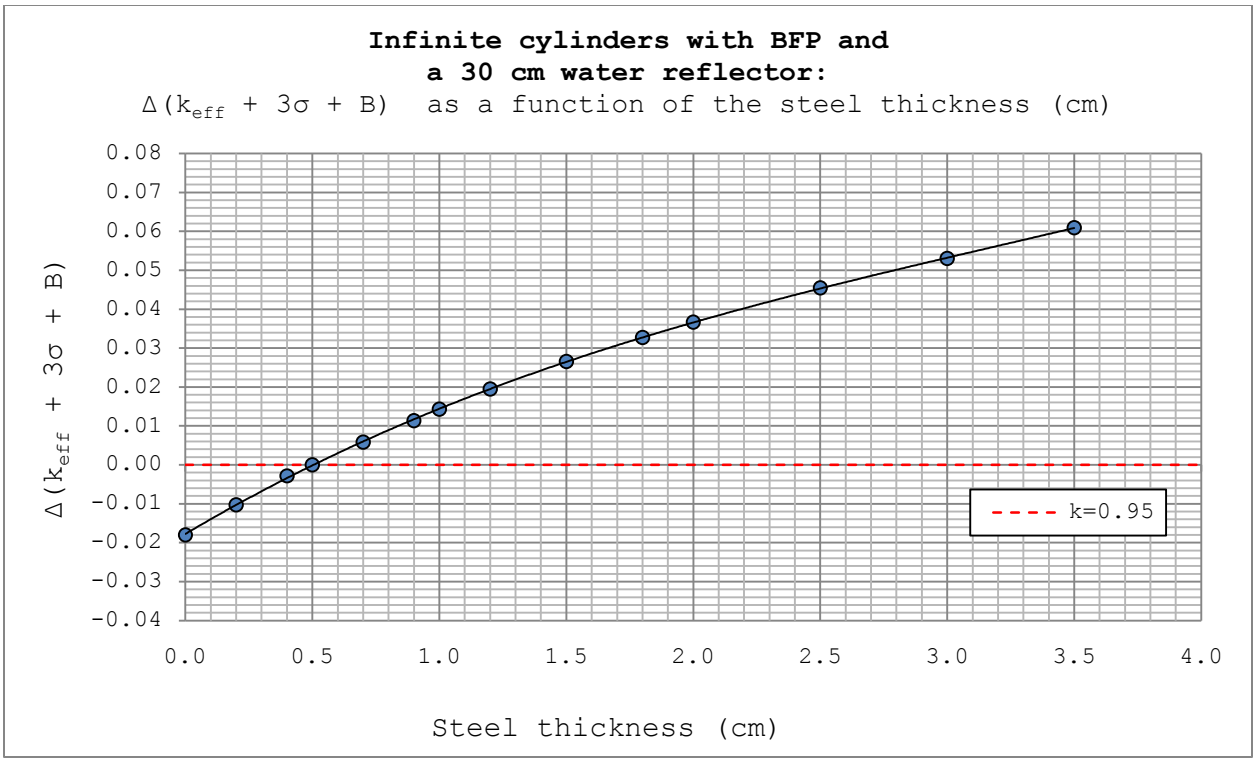


**Figure 4-16.** An infinite cylinder with BFP as an absorber, reflected by 30 cm water.

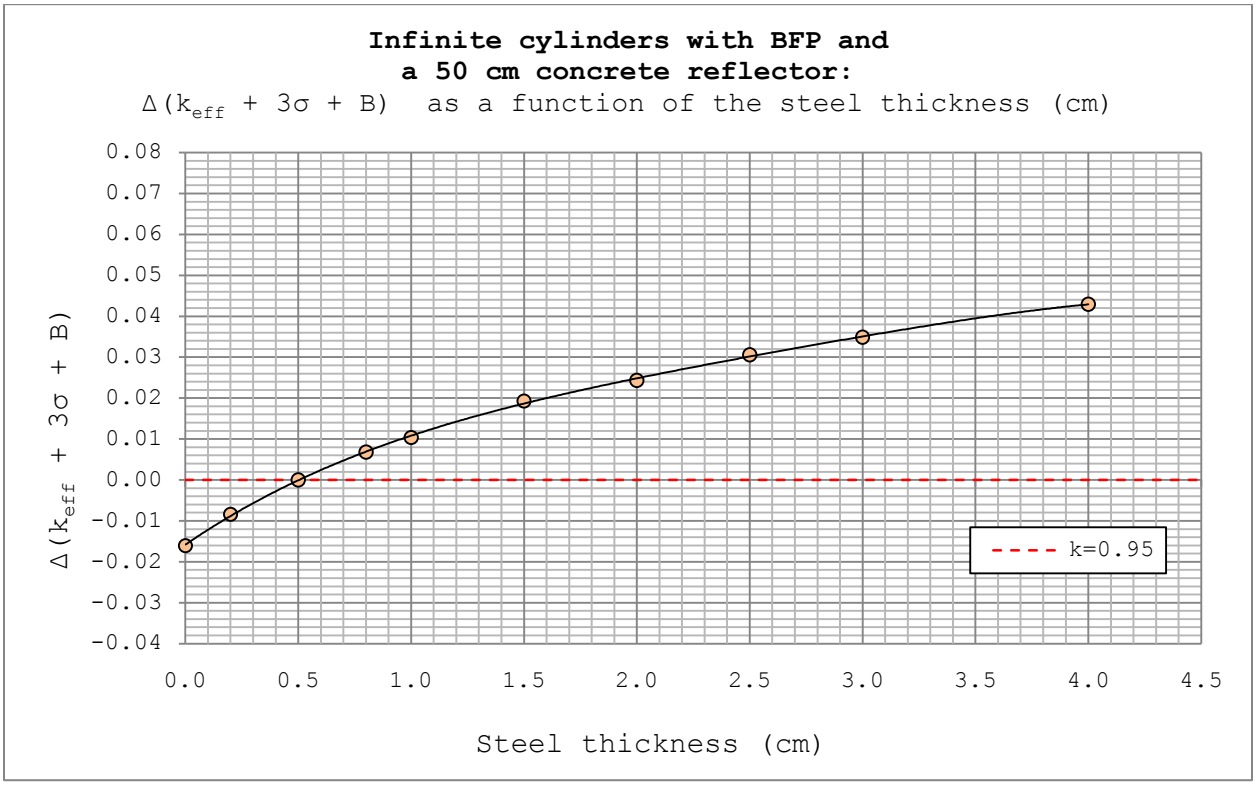


**Figure 4-17.** An infinite cylinder with BFP as an absorber, reflected by 50 cm concrete.

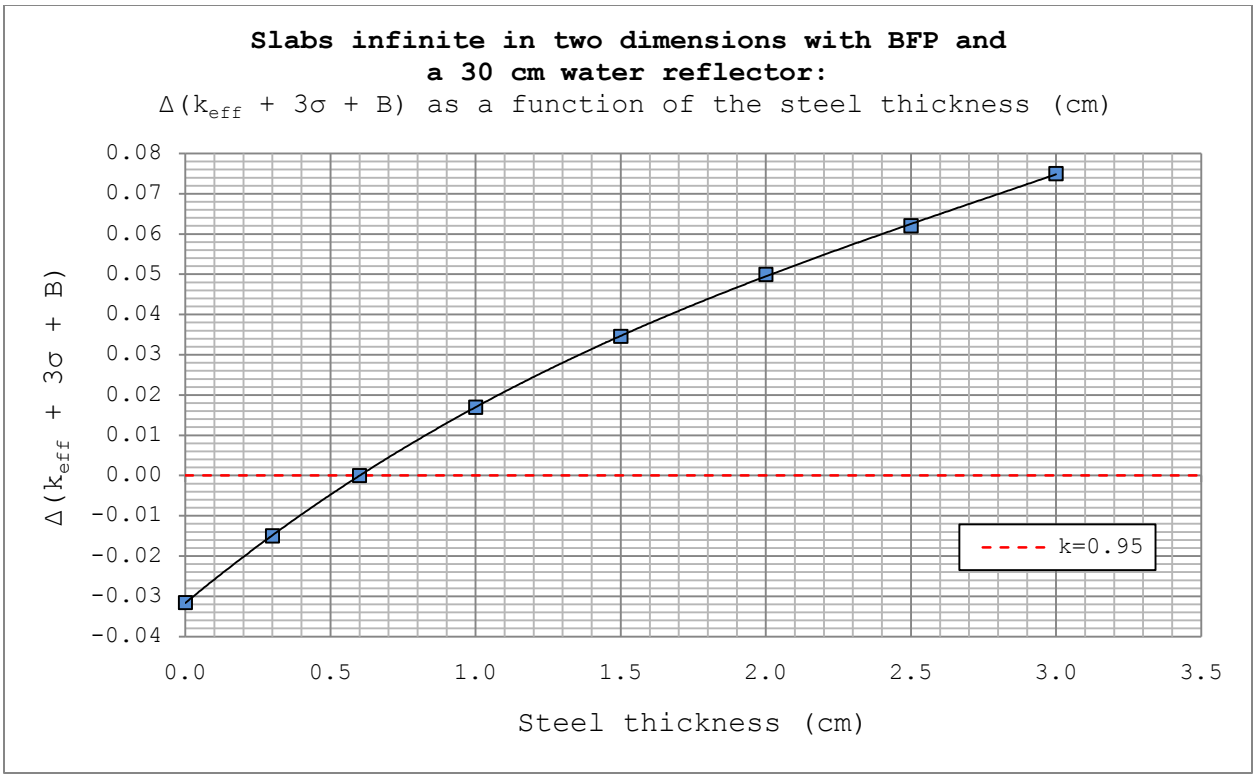


**Figure 4-18.** A slab infinite in depth and height with BFP as an absorber, reflected by 30 cm water.

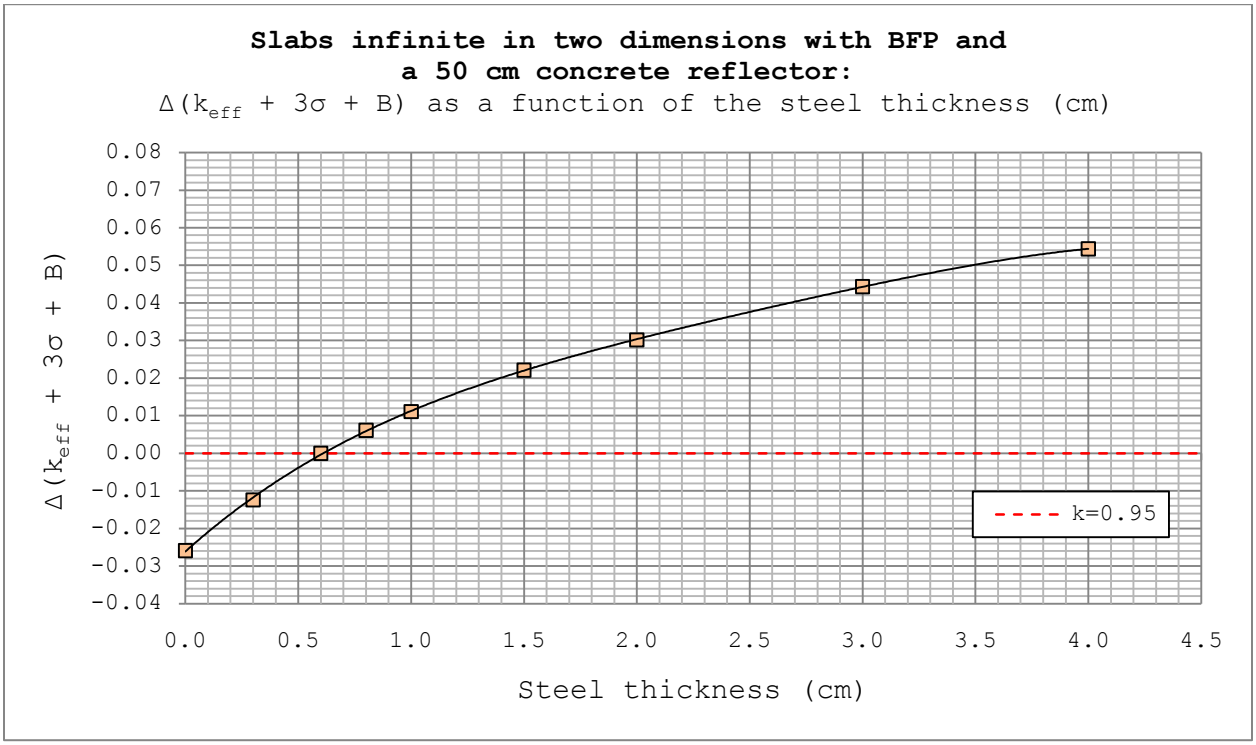


**Figure 4-19.** A slab infinite in depth and height with BFP as an absorber, reflected by 50 cm concrete.

As seen in the previous figures, $k_{eff}$ increases with an increasing steel thickness for both cylinders and slabs. The steel acts as a reflector, reflecting neutrons back into the $UO_2$ mixture causing fission. The probability for reflection increases with an increasing steel thickness and the effect is greater when water is used as a reflector for both geometries.

In the physical installations at the fuel factory, there is often an empty space between the tank and the absorber. To assess the effect on $k_{eff}$ in the event of flooding of this space, the thickness of a water column (marked with a red cross in Figure 4-20) has been varied.

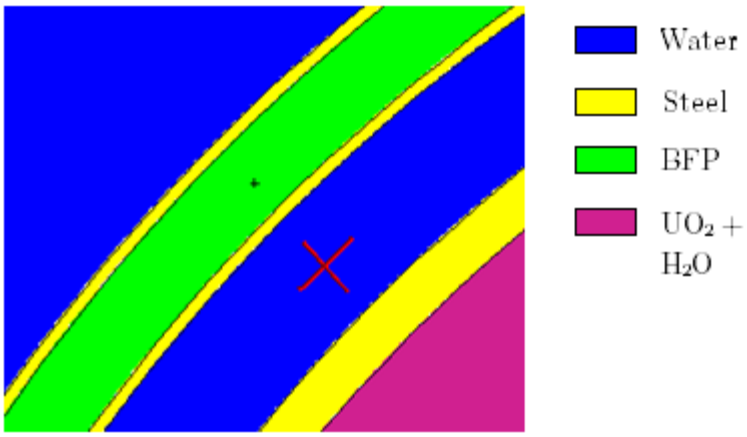


**Figure 4-20.** Close up of a cross section of an infinite cylinder with BFP as an absorber. The red cross marks the water column whose thickness has been varied.

The results for infinite cylinders are shown in Figure 4-21 and Figure 4-22. The corresponding results for slabs infinite in two dimensions are shown in Figure 4-23 and Figure 4-24.

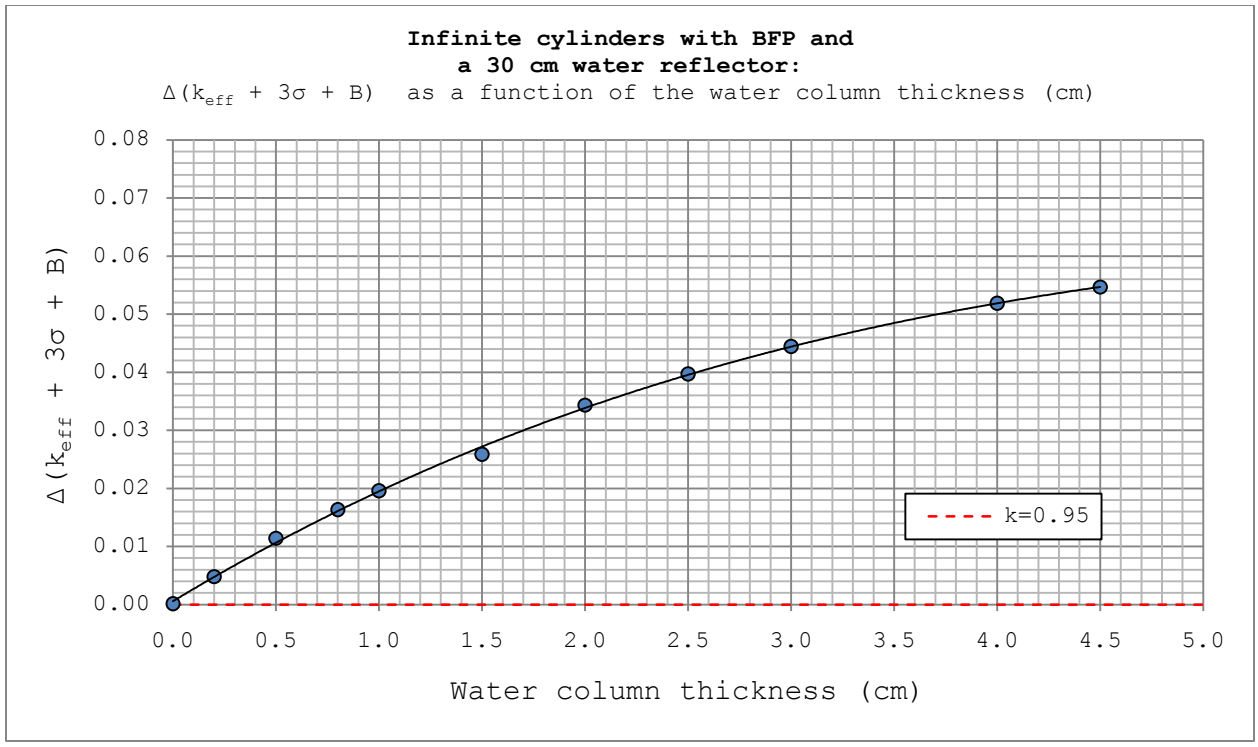


**Figure 4-21.** An infinite cylinder with BFP as an absorber, reflected by 30 cm water.

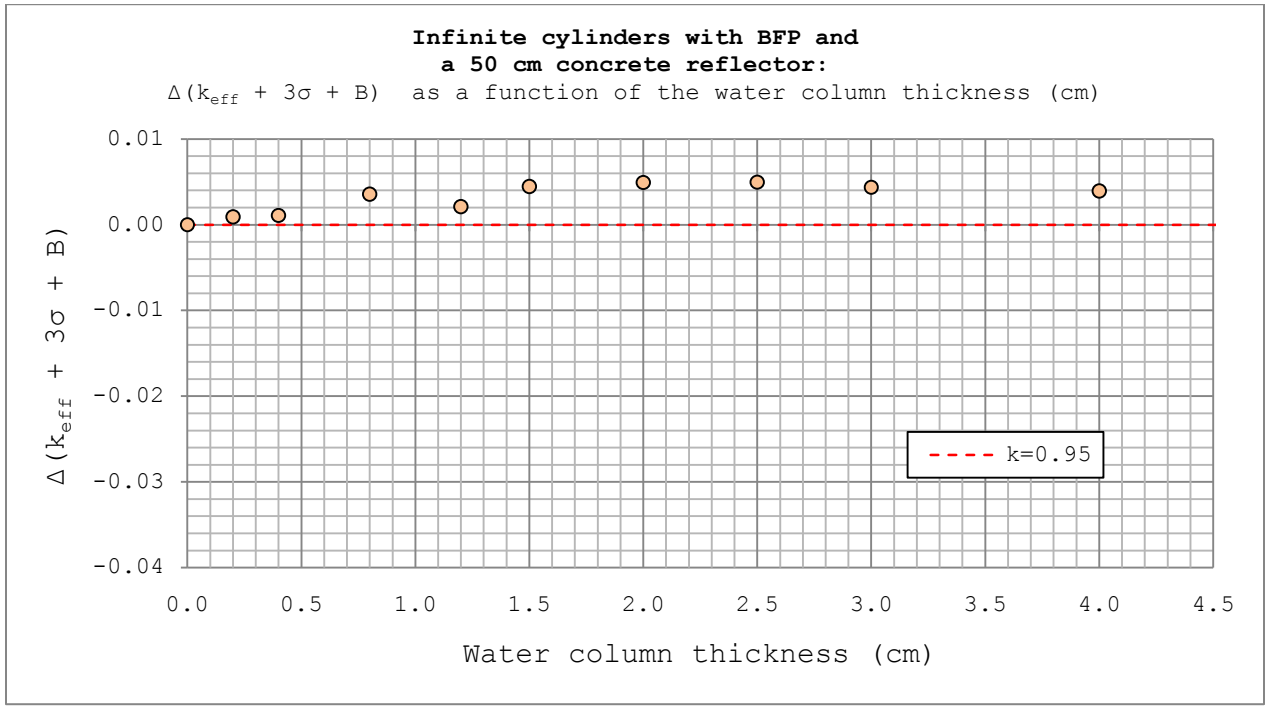


**Figure 4-22.** An infinite cylinder with BFP as an absorber, reflected by 50 cm concrete.

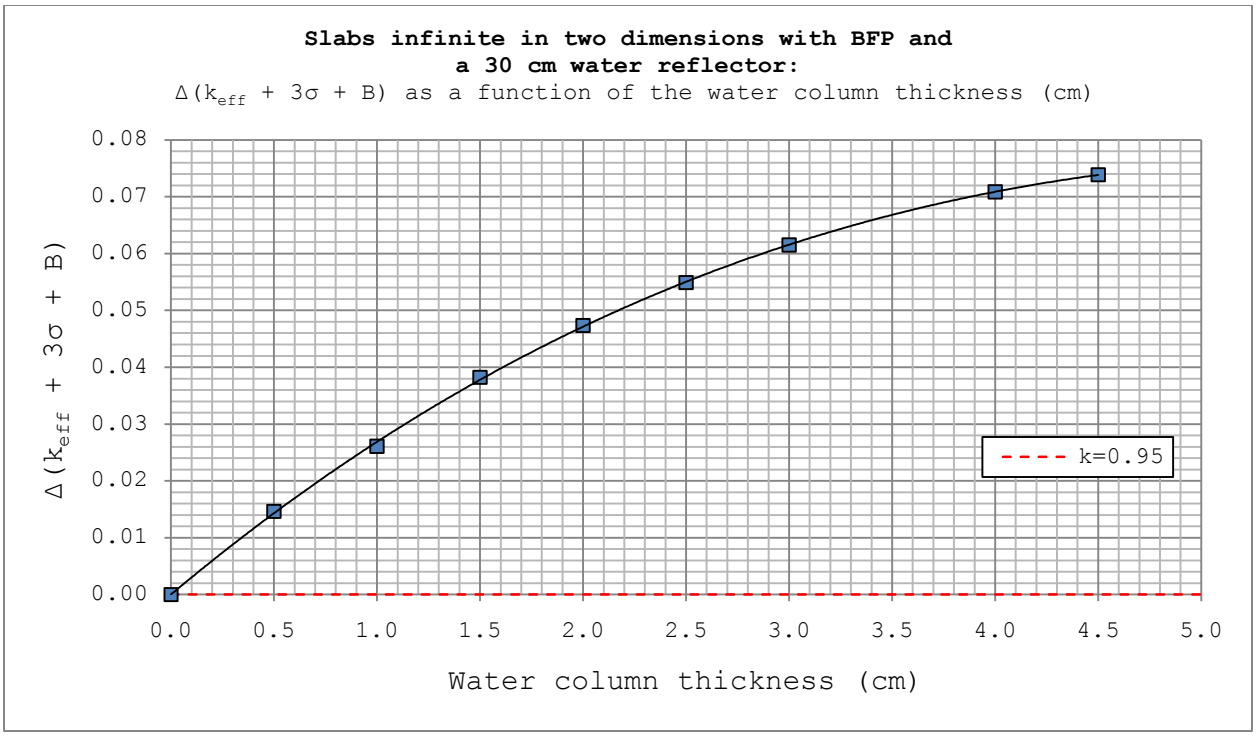


**Figure 4-23.** A slab infinite in depth and height with BFP as an absorber, reflected by 30 cm water.

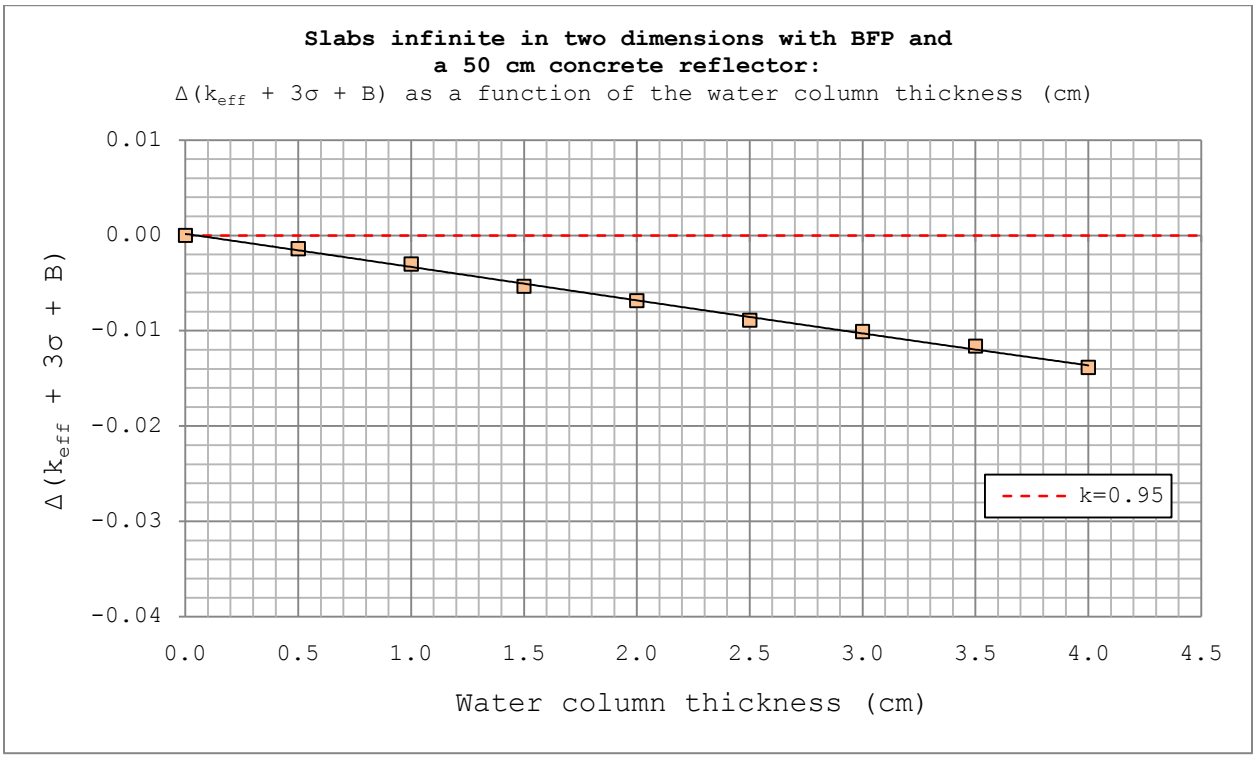


**Figure 4-24.** A slab infinite in depth and height with BFP as an absorber, reflected by 50 cm concrete.

For both the cylinder and slab systems reflected by water, an increasingly thicker water column leads to an increasingly higher value of $k_{eff}$ due to additional moderation and reflection. The effect is greater for the slab system.

The situation is more complex for concrete, since concrete is a more reflecting but at the same time less absorbing material than water [33]. Depending on which effect that is dominating, the value of $k_{eff}$ may either increase or decrease with an increasingly thicker water column. The previous figures show that the slab systems reflected by concrete has a decreasing trend in $k_{eff}$ while it is difficult to see a clear trend in the cylinder systems reflected by concrete.

#### 4.1.7.2 PVC

The effect of varying the steel thickness of the tank that contains the $UO_2$ + $H_2O$ mixture is investigated for PVC. The results for cylinders and slabs are shown in Figure 4-25 and Figure 4-26 below.

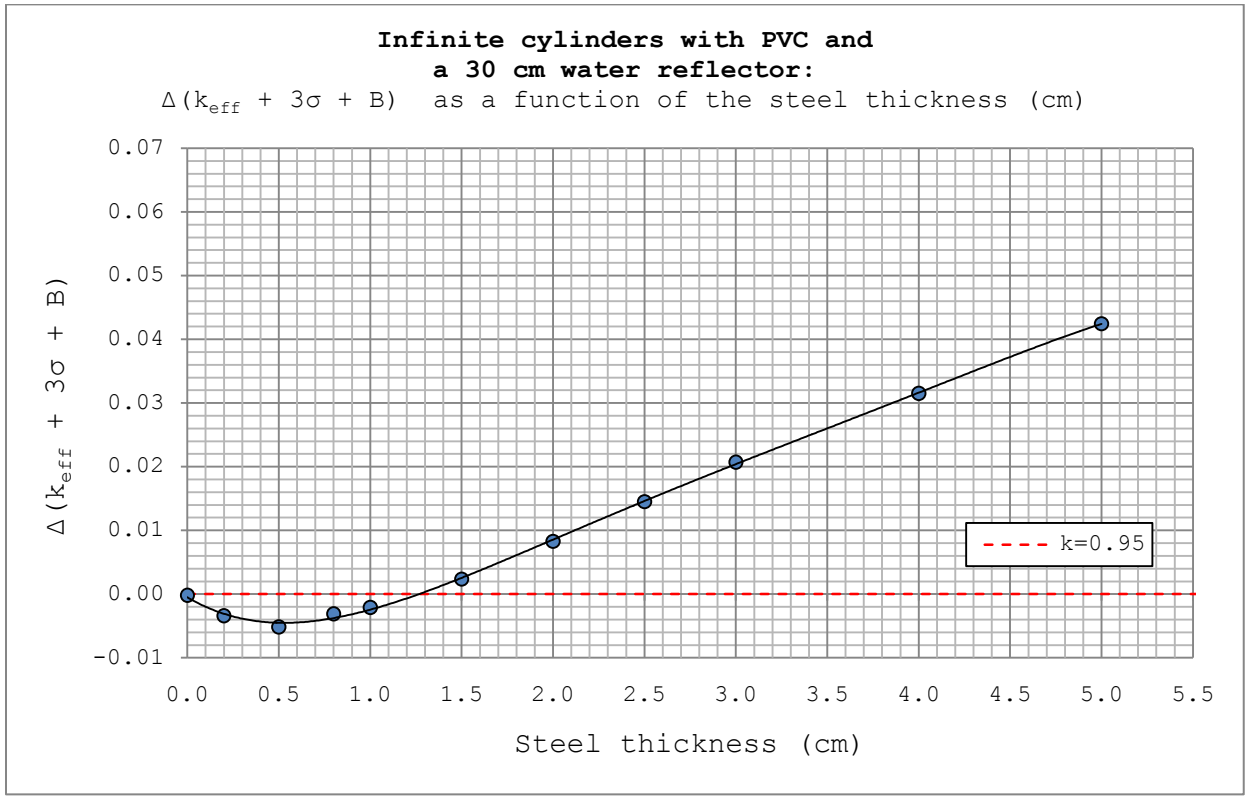


**Figure 4-25.** An infinite cylinder with PVC as an absorber, reflected by 30 cm water.

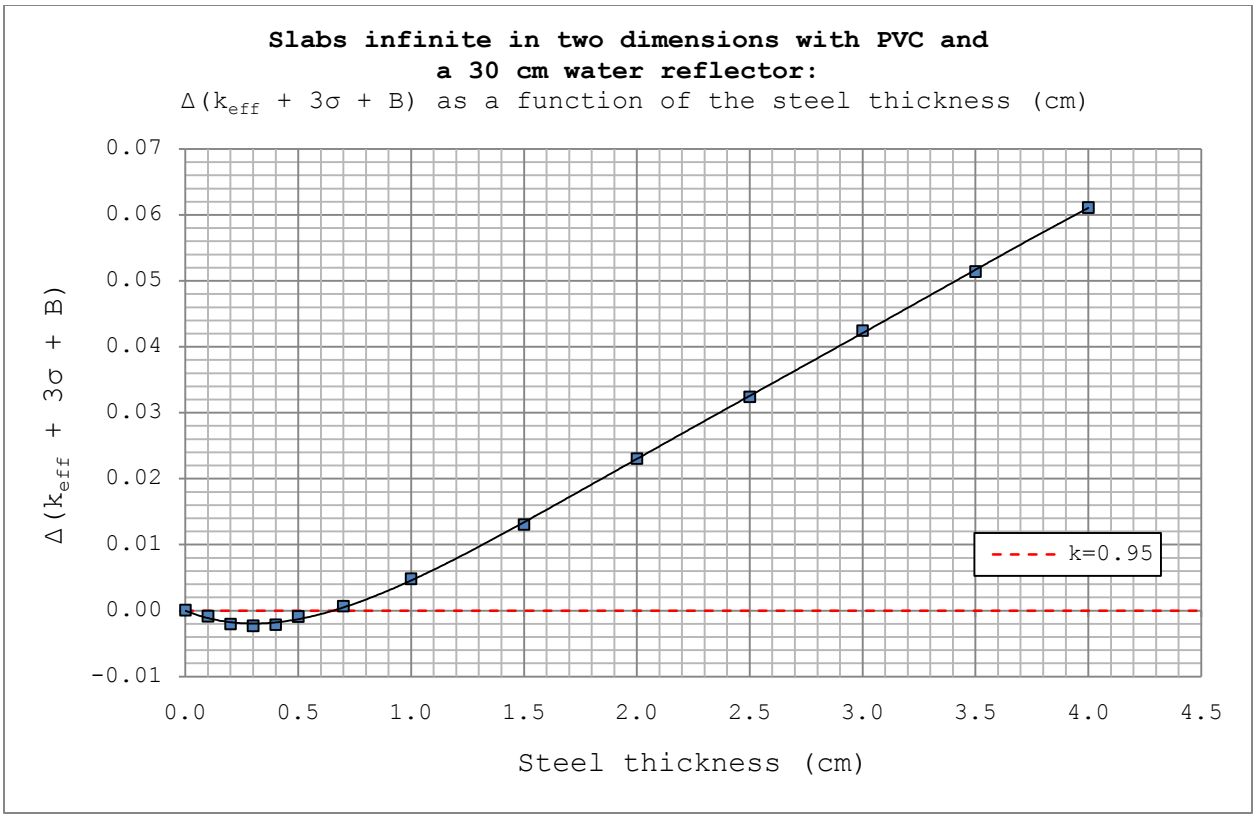


**Figure 4-26.** A slab infinite in depth and height with PVC as an absorber, reflected by 30 cm water.

The results in the previous figures show that for infinite cylinders and slabs infinite in two dimensions with PVC, the addition of steel initially decreases the value of $k_{eff}$. This result was not anticipated in advance, as previous work on KSH 12.6 with a different PVC composition showed an increasing value of $k_{eff}$ with the addition of steel similar to the corresponding parametric study with BFP presented earlier.

The new PVC composition is less neutron absorbing than the previous composition, and a similar trend as in the previous figures has been seen for other systems with weak absorbers at WSE e.g. slabs with BFP on only one side. This behavior is the result of a complex interaction between a number of materials with different cross sections for absorption and reflection with a geometry that is changing in discrete steps, and while it is possible to offer an explanation that fits with the results it may not be applicable to other cases. The current recommendation at WSE is to be careful in assessing the effect of the steel on the neutron multiplication factor since there can be a problem dependence that is hard to predict. [18]

The results for a water column of a varying thickness between the $UO_2$ mixture and the absorber are shown in Figure 4-27 and Figure 4-28 below.

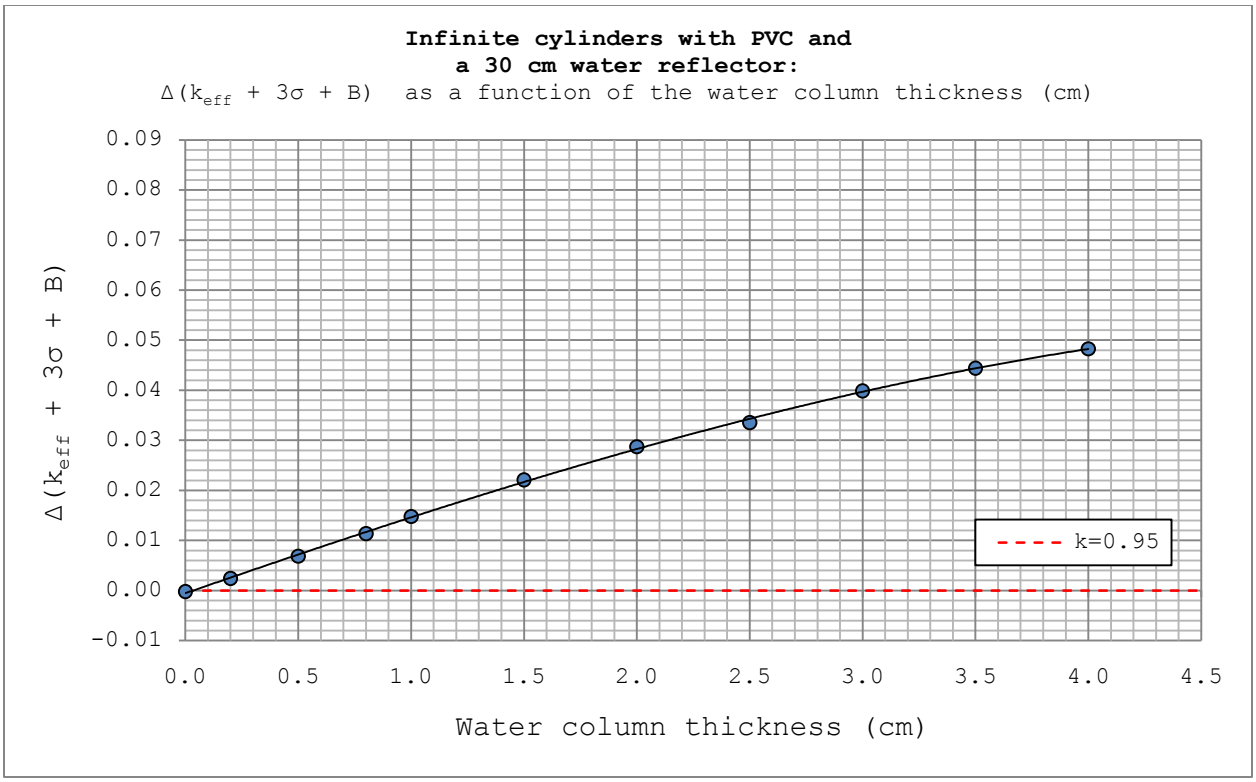


**Figure 4-27.** An infinite cylinder with PVC as an absorber, reflected by 30 cm water.

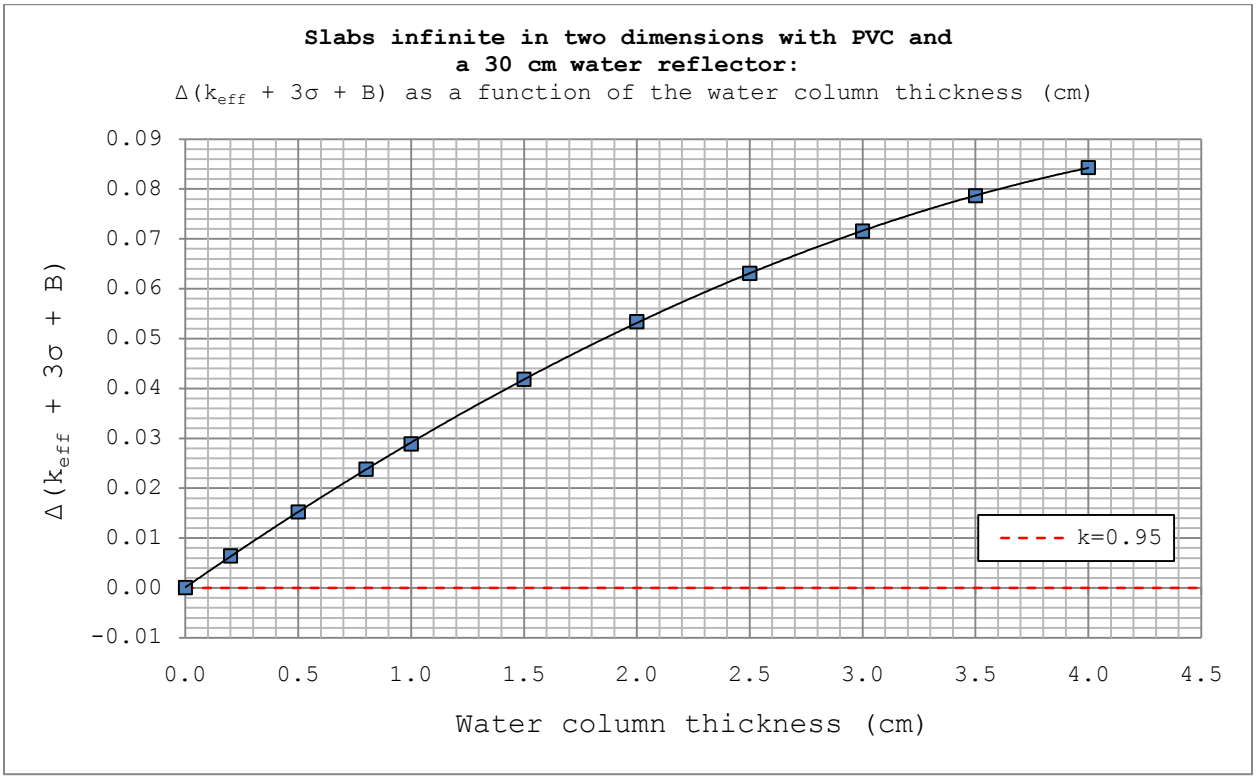


**Figure 4-28.** A slab infinite in depth and height with PVC as an absorber, reflected by 30 cm water.

The effect of a water column is similar to the BFP cases with a water reflector, $k_{eff}$ increases with an increasing water column thickness and the effect is larger for the slabs infinite in two dimensions than for infinite cylinders.

The chlorine content of PVC has been varied to assess the effect on $k_{eff}$ due to fluctuations in the PVC composition. The results are shown in Figure 4-29 and Figure 4-30.

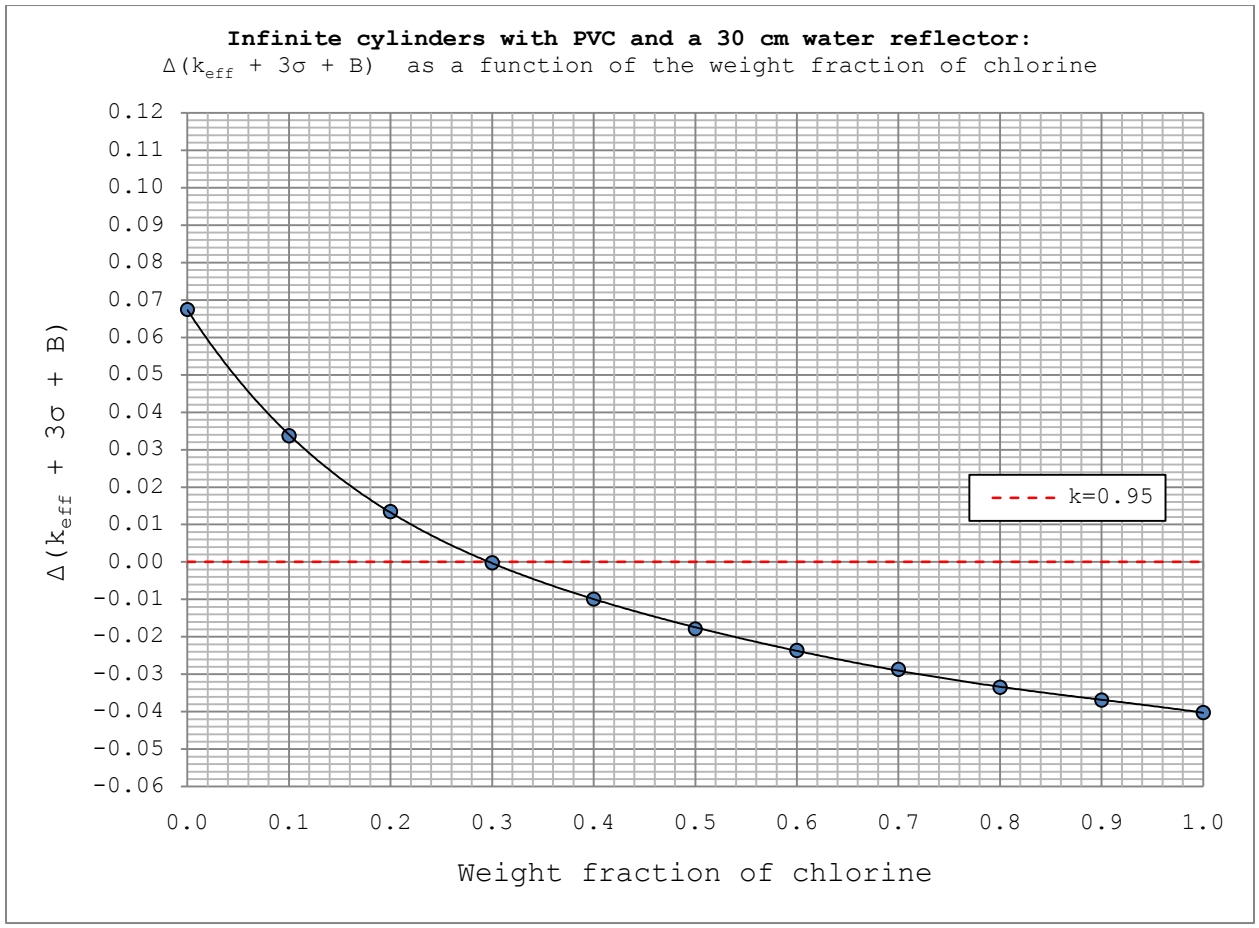


**Figure 4-29.** An infinite cylinder with PVC as an absorber, reflected by 30 cm water.

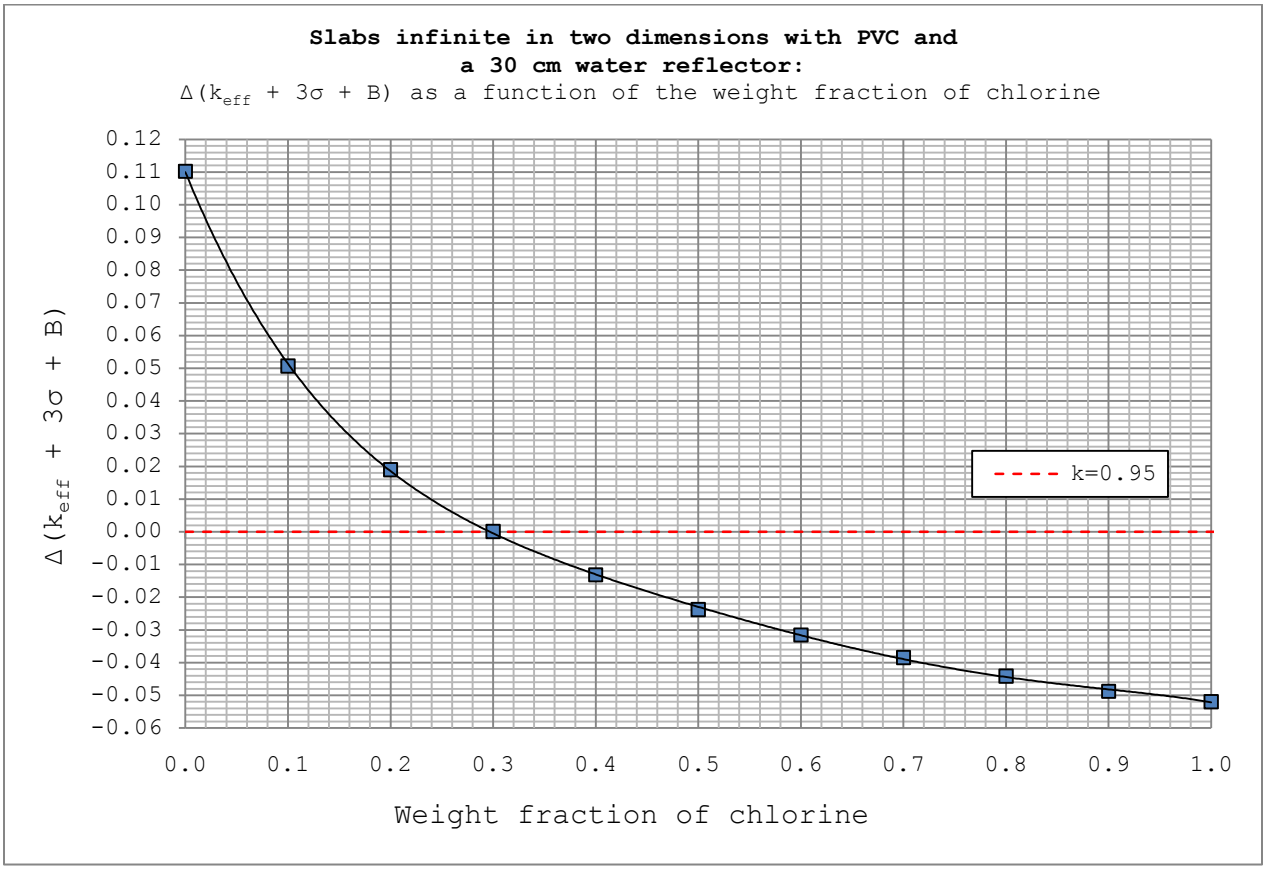


**Figure 4-30.** A slab infinite in depth and height with PVC as an absorber, reflected by 30 cm water.

The results verify that a decreasing amount of chlorine leads to less neutron absorption and thus a higher value of $k_{eff}$. A decreasing chlorine concentration also implies an increasing concentration of hydrogen and carbon, leading to increased neutron reflection. The effect is greater for the slabs infinite in two dimensions, which apart from the differences in geometry may be explained by the fact that the slabs have been modeled with a greater amount of PVC (1.3 cm for slabs compared to 0.9 cm for cylinders).

Difficulties in quantitatively determining how different additives in the PVC manufacturing process affect the hydrogen to carbon atom ratio has lead to an interest in studying the effect on $k_{eff}$ from varying this parameter. The results are shown in Figure 4-31 and Figure 4-32.

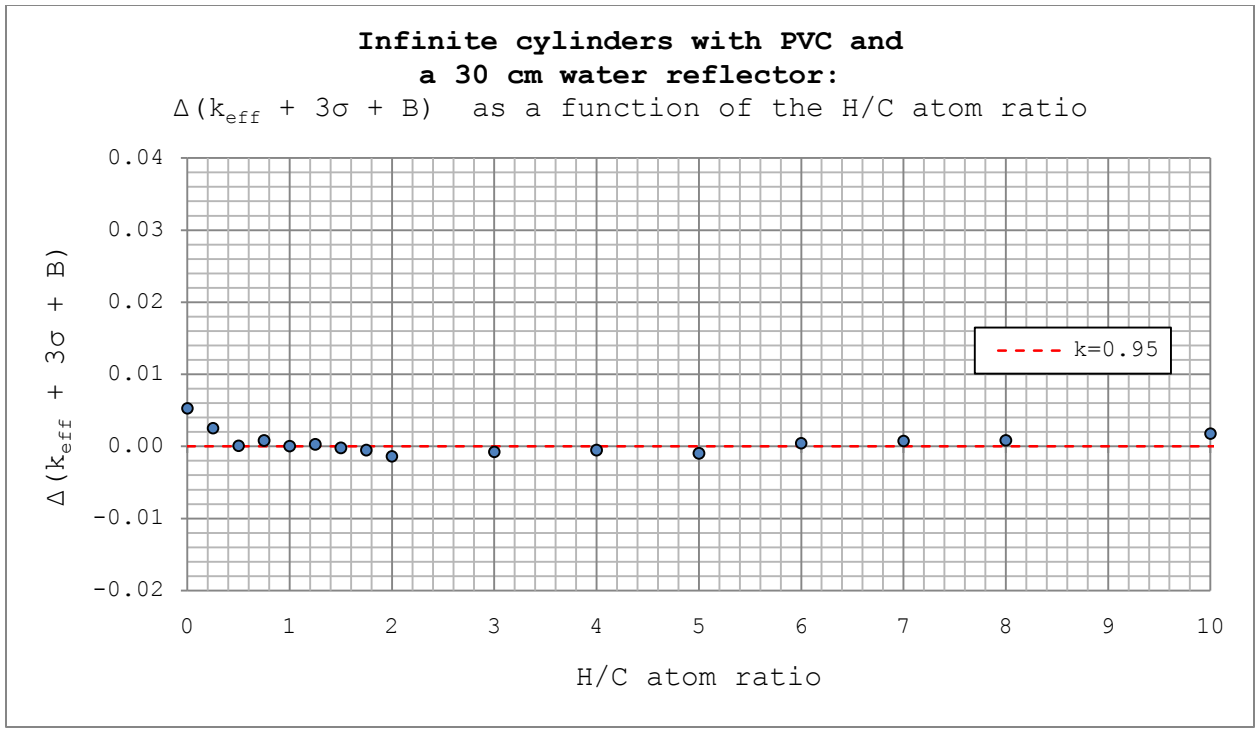


**Figure 4-31.** An infinite cylinder with PVC as an absorber, reflected by 30 cm water.

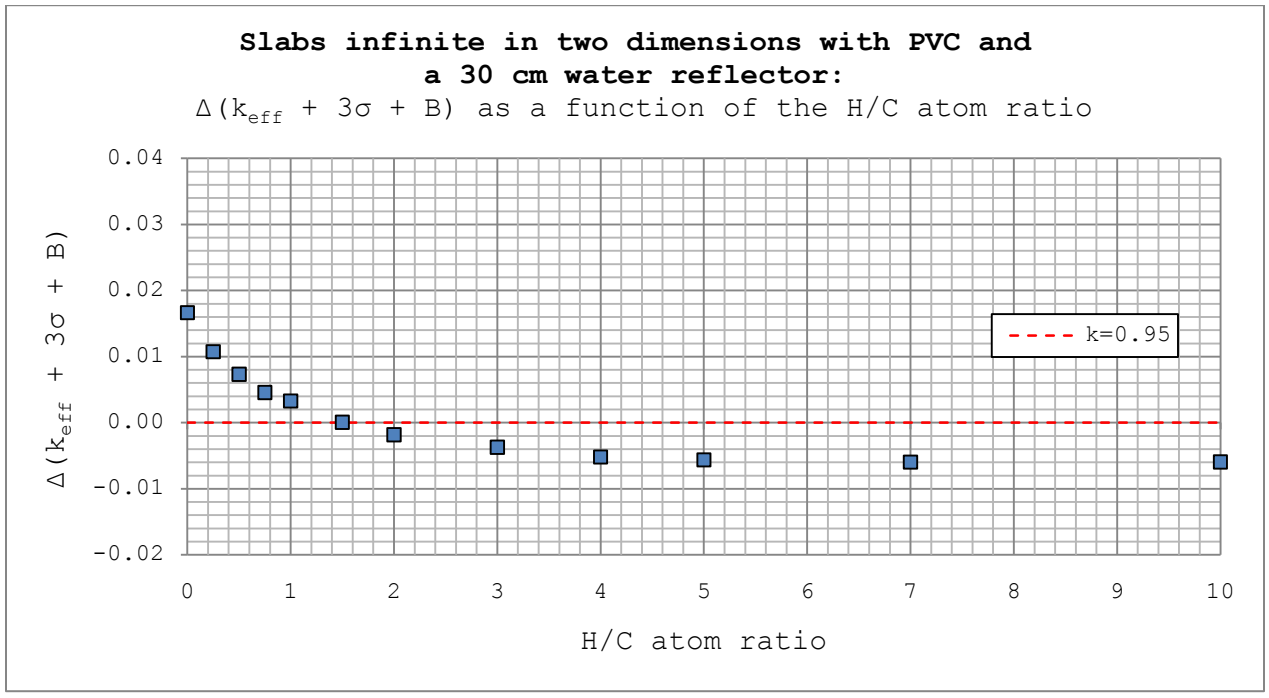


**Figure 4-32.** A slab infinite in depth and height with PVC as an absorber, reflected by 30 cm water.

The results in Figure 4-32 show that $k_{eff}$ increases with an increasing amount of carbon, which may be explained by greater reflection and less neutron absorption from carbon

compared to hydrogen [34]. A similar trend can be discerned for the infinite cylinders although it is less evident, possibly due to both the differences in geometry and that less PVC is used for the cylinders.

Another parameter that may vary in the PVC manufacturing process is the density. The results for varying the PVC density are shown in Figure 4-33 and Figure 4-34.

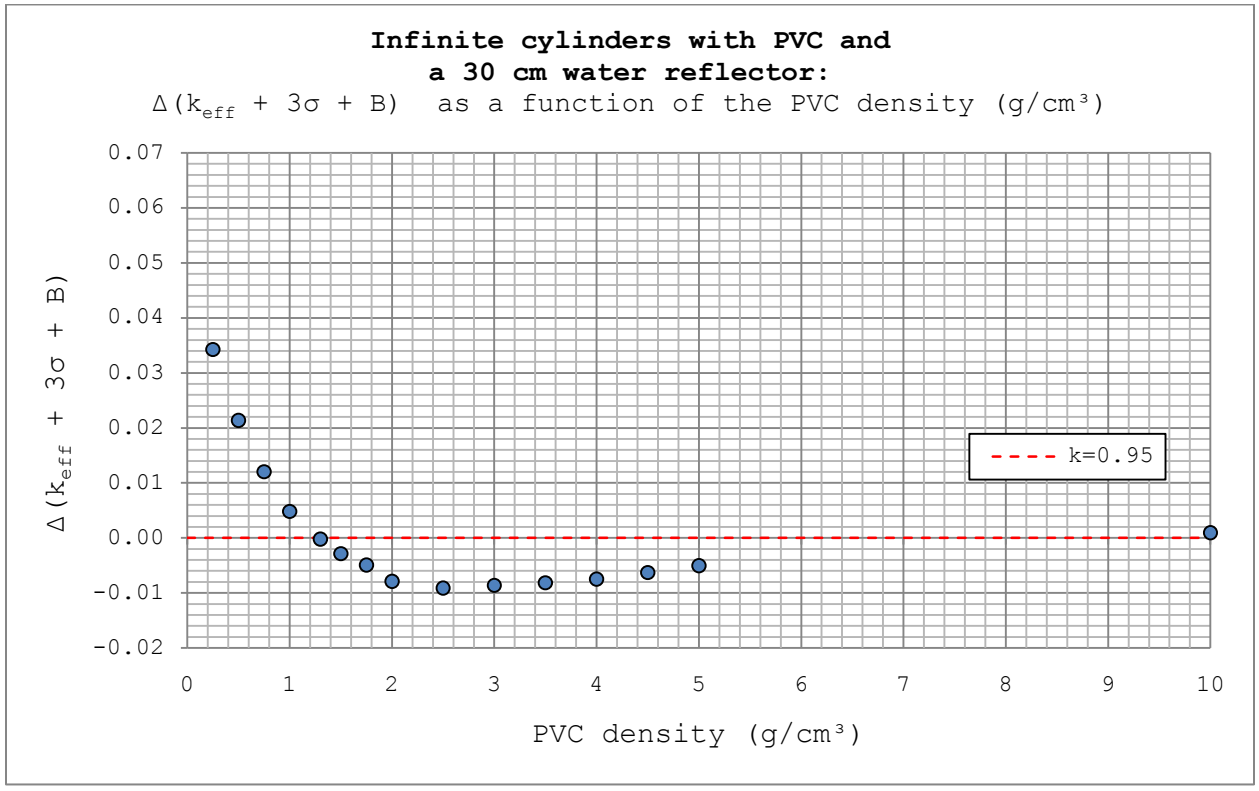


**Figure 4-33.** An infinite cylinder with PVC as an absorber, reflected by 30 cm water.

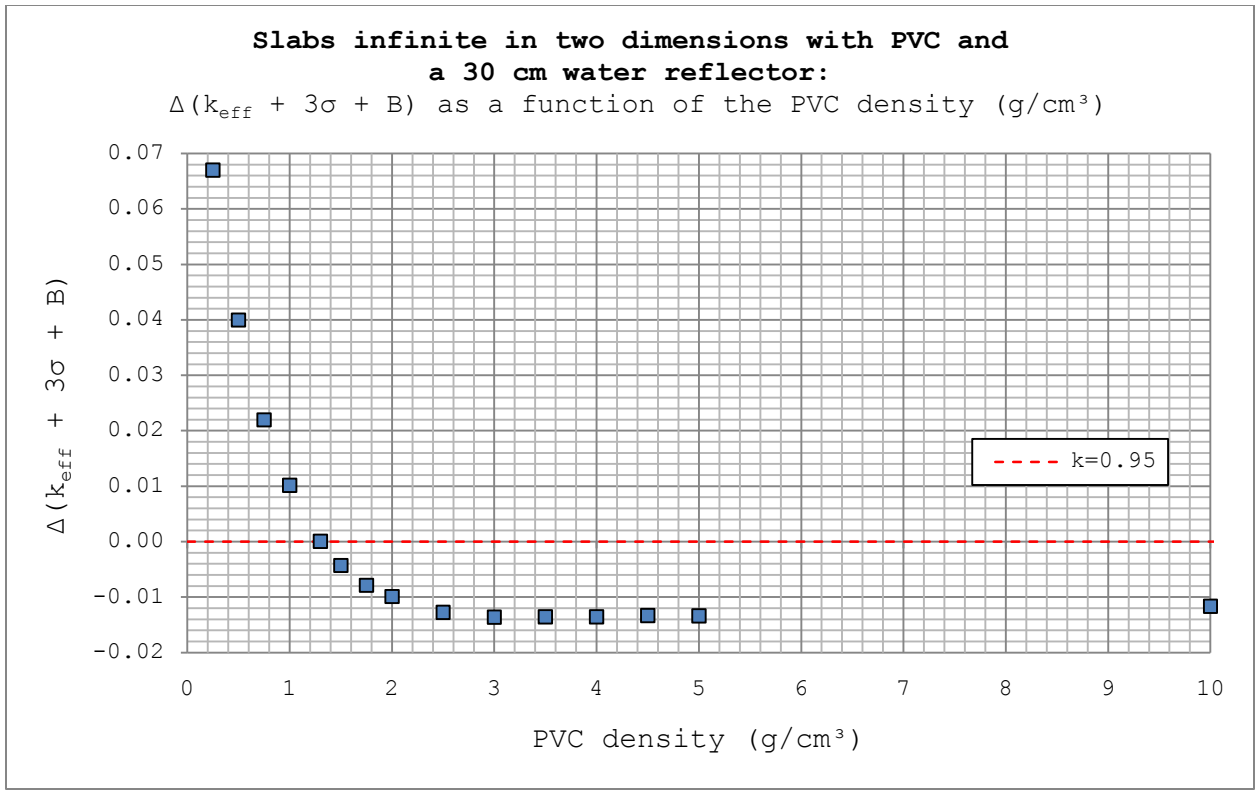


**Figure 4-34.** A slab infinite in depth and height with PVC as an absorber, reflected by 30 cm water.

Measurements of the composition of the PVC that is used in the fuel factory have shown that the density varies between roughly 1.3-1.5 g/cm$^3$ [20]. The previous two figures thus cover a substantially larger interval than what can be expected to occur in the actual installations at WSE, and it may not even be possible to manufacture PVC with such high densities.

The results show that $k_{eff}$ initially decreases sharply with an increasing PVC density, and then it increases. The effect is more pronounced for the infinite cylinders than for the slabs infinite in two dimensions. The effect can possibly be explained by counteracting mechanisms; both increasing neutron absorption due to a higher density of chlorine but also an increasing amount of reflection due to a higher density of hydrogen and carbon.

The last parameter that is studied for PVC is the thickness. The results are shown in Figure 4-35 and Figure 4-36.

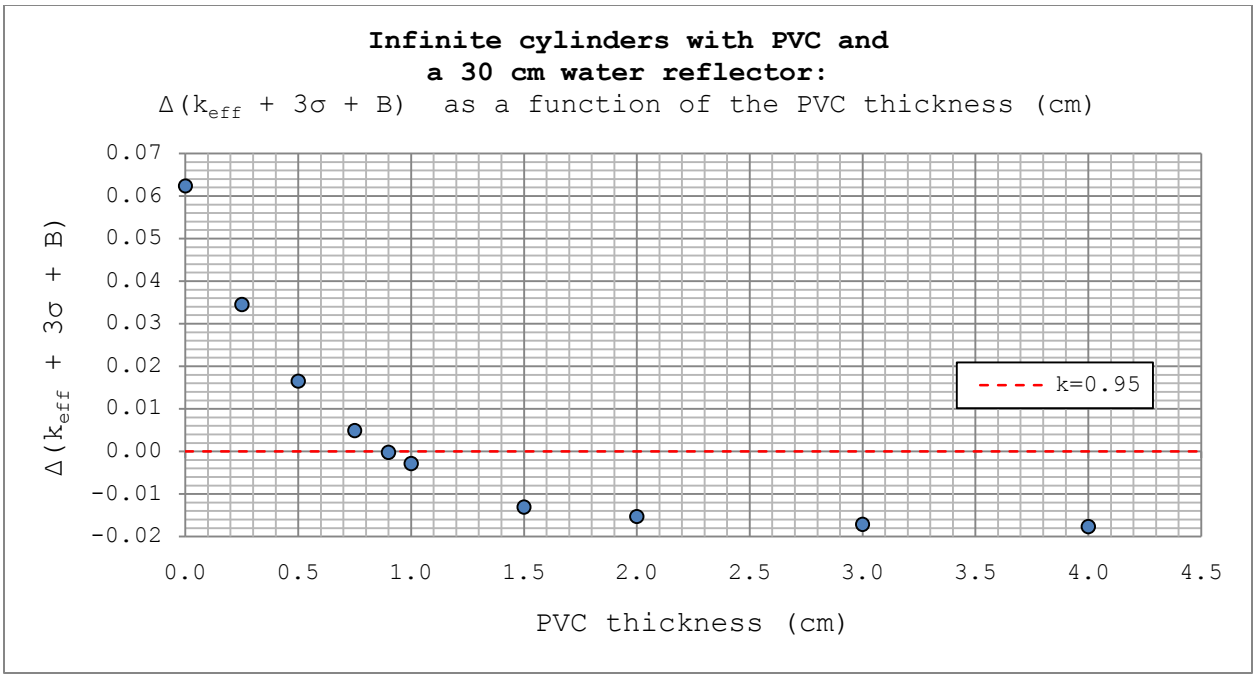


**Figure 4-35.** An infinite cylinder with PVC as an absorber, reflected by 30 cm water.

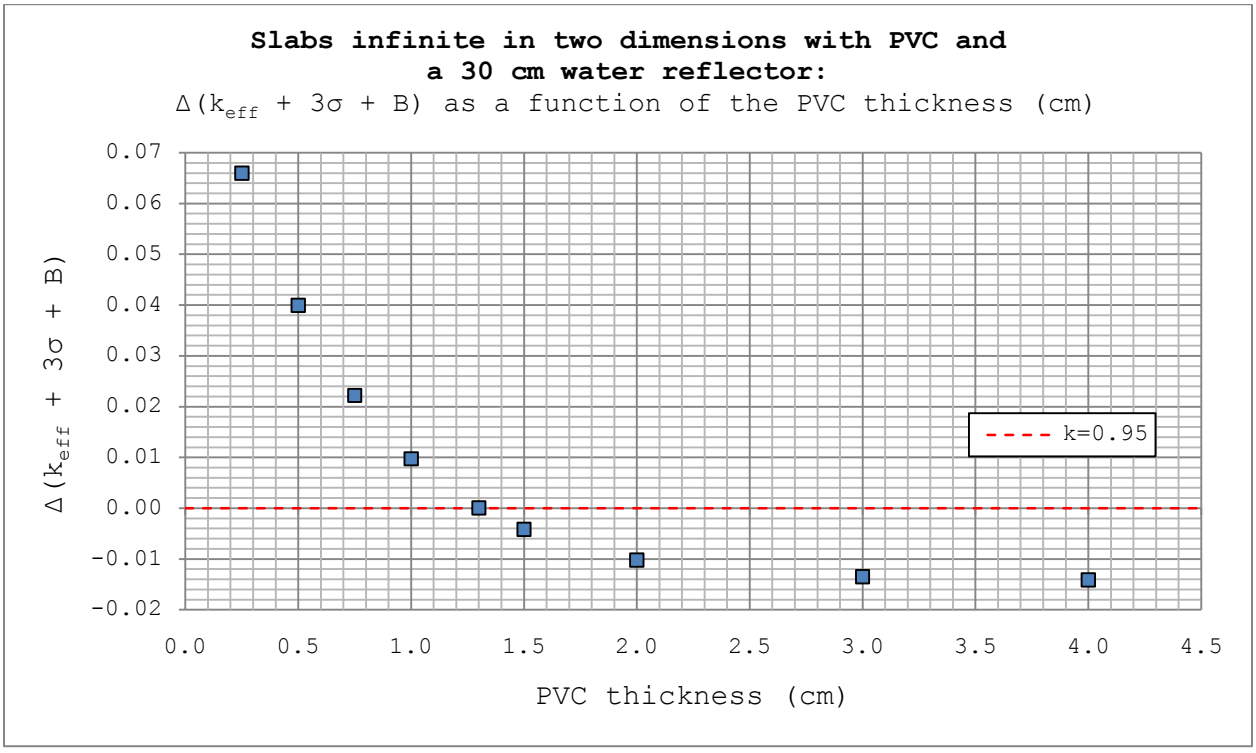


**Figure 4-36.** A slab infinite in depth and height with PVC as an absorber, reflected by 30 cm water.

The initial effect on $k_{eff}$ from increasing the thickness of the PVC is substantial, but the trend flattens out as more and more PVC is added.

## 4.2 KSH 12.6

The results in KSH 12.6 are divided into subchapters according to the system being studied. Just as in KSH 12.3, the parametric study is presented in a separate subchapter.

As mentioned in Section 3, the results in KSH 12.6 are presented in a different way than in KSH 12.3. In KSH 12.6, the critically safe dimension of the slab (i.e. the thickness $z$ corresponding to the critically safe limit) is plotted as a function of a certain quadratic base area as presented in Figure 3-6. For slabs infinite in two dimensions, i.e. with an infinite base area, the results are plotted as dashed asymptotes. The data for the slabs infinite in two dimensions is summarized in Table A2-12 in Appendix II. The data for slabs without absorbers come from section 12.5 of the KSH [22]. This data does not cover all the cases with absorbers, but still serve as a fair comparison.

The PVC simulations have been run with enough precision to ensure that the standard deviation $\sigma$ has been less than 20 pcm. The B-term (see Section 2.5.3) for PVC is 0.0122 for the conditions being used. The BFP results exist from previous calculations with older cross section libraries, the standard deviation for BFP is less than 50 pcm and the B-term is 0.0130. The term $k_{eff}$ referenced only in the parametric study in KSH 12.6 refers to the calculated value of $k_{eff}$, $k_{calc}$.

### 4.2.1 $UO_2$ + $H_2O$ with a 30 cm water reflector

The results for slabs containing a $UO_2$ + $H_2O$ mixture with different absorbers, reflected by 30 cm water are presented in Figure 4-37.

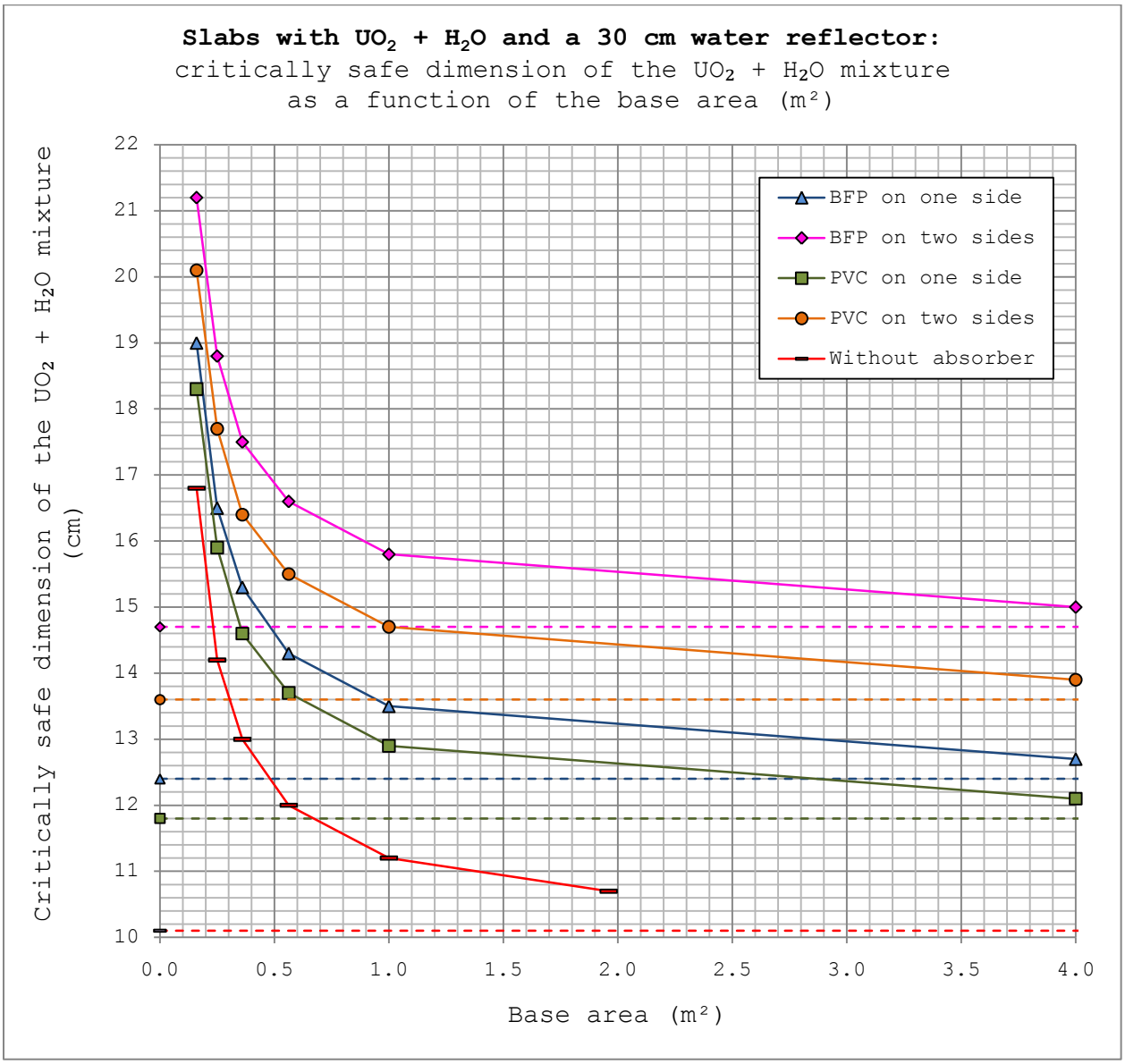


**Figure 4-37.** Critically safe dimensions for slabs surrounded by a 30 cm water reflector, containing a $UO_2$ + $H_2O$ mixture with BFP or PVC as an absorber on one or two sides for different base areas.

As anticipated, the largest dimensions can be allowed when BFP is used as an absorber on both sides. Figure 4-37 also shows that even though PVC is a comparatively weak absorber, it is more effective to use 1.3 cm PVC on both sides of the slab than to use 0.64 cm BFP on only one side. The data points above are summarized in Table A2-13 in Appendix II.

### 4.2.2 UNH + $H_2O$ with a 30 cm water reflector

The results for slabs containing a UNH + $H_2O$ mixture with different absorbers, reflected by 30 cm water are presented in Figure 4-38.

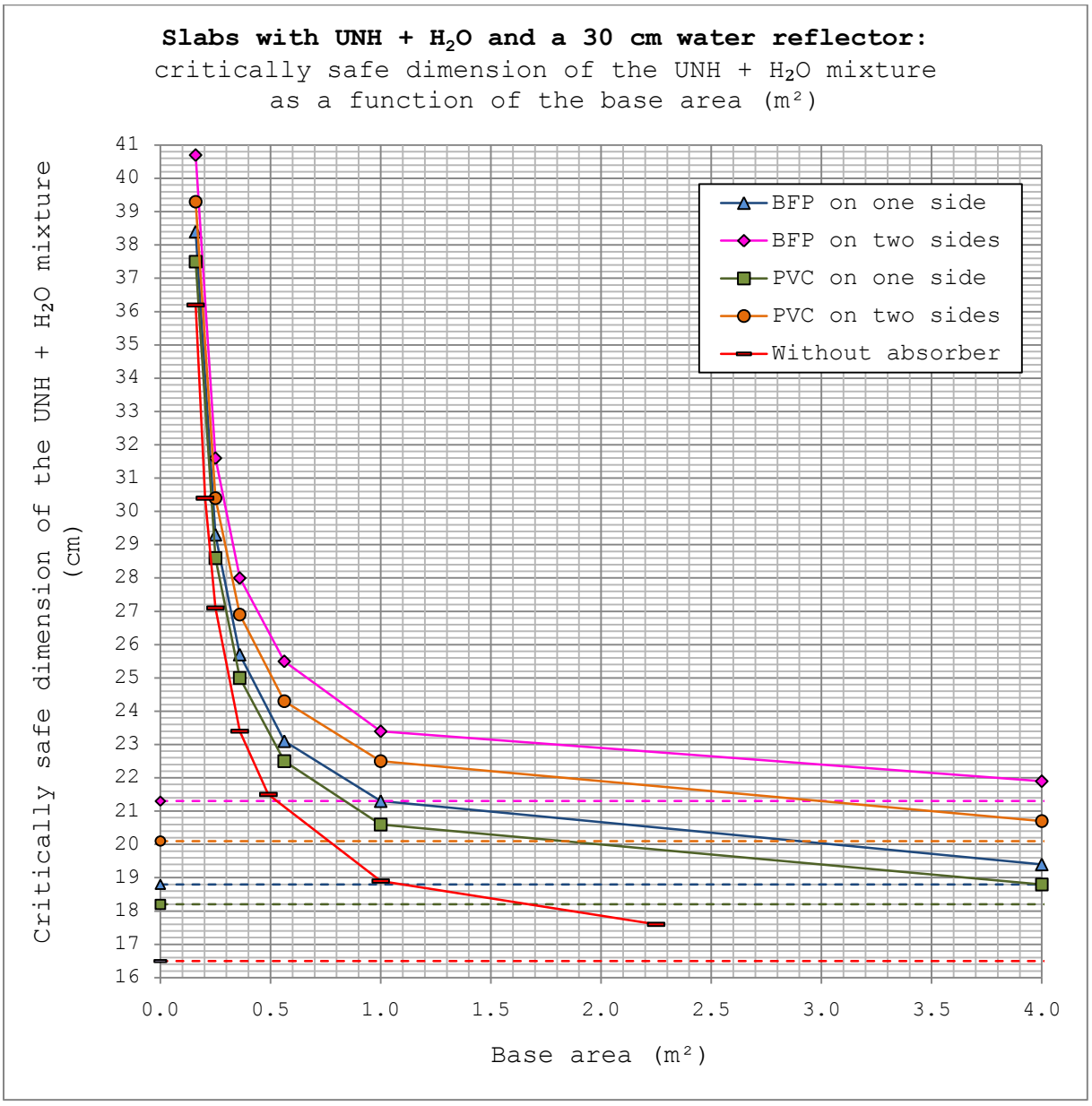


**Figure 4-38.** Critically safe dimensions for slabs surrounded by a 30 cm water reflector, containing a UNH + $H_2O$ mixture with BFP or PVC as an absorber on one or two sides for different base areas.

The general trend is similar to the corresponding $UO_2$ + $H_2O$ system, but a greater dimension can be permitted for a given base area when UNH + $H_2O$ is used since less uranium is present in the same volume of liquid. The data points above are summarized in Table A2-14 in Appendix II.

### 4.2.3 $UO_2$ + $H_2O$ placed in a concrete corner

The results for slabs containing a $UO_2$ + $H_2O$ mixture with PVC on different sides, placed in a concrete corner with water on the sides that are not concrete are shown in Figure 4-39.

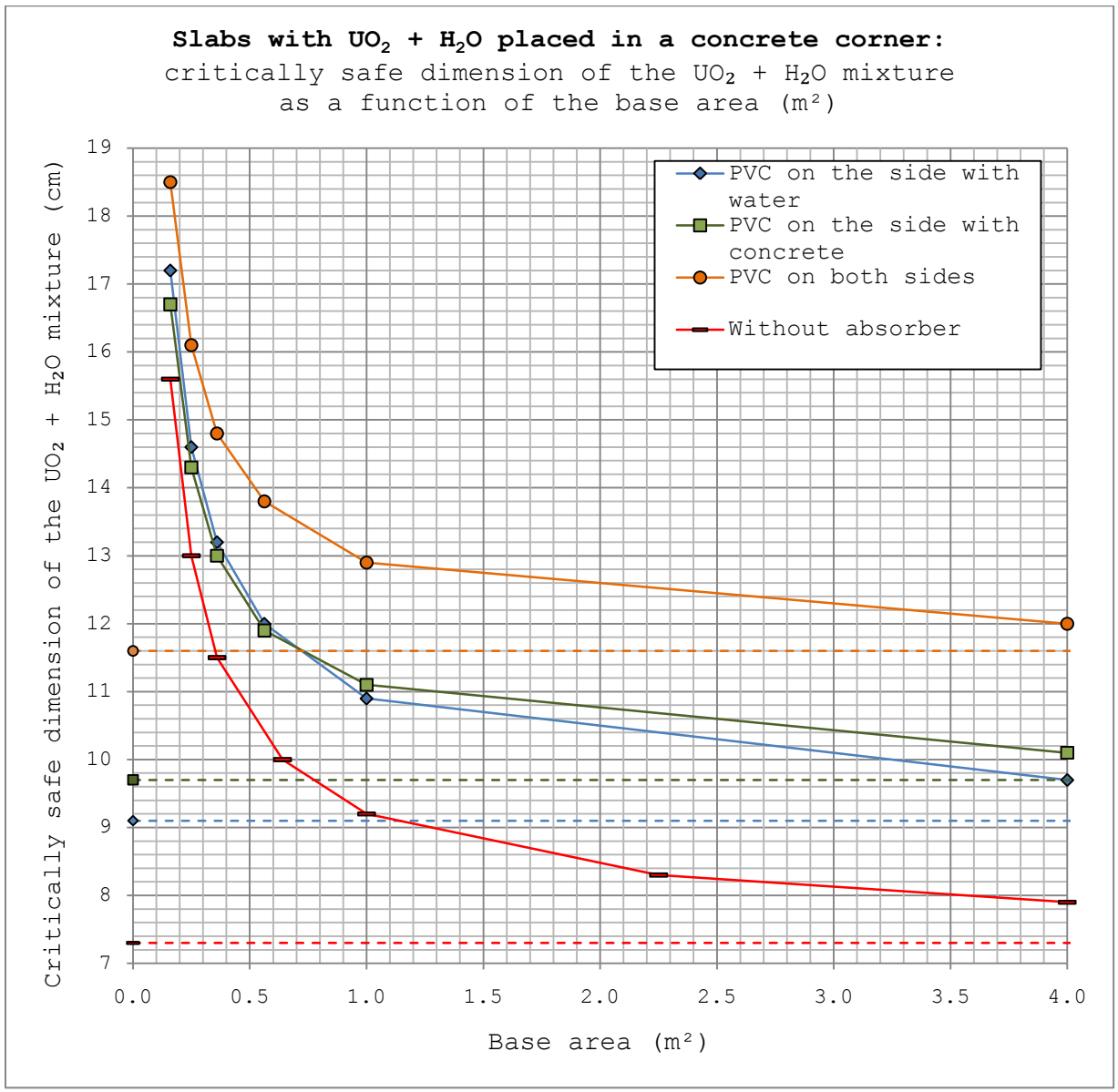


**Figure 4-39.** Critically safe dimensions for slabs placed in a concrete corner, containing a $UO_2$ + $H_2O$ mixture with BFP or PVC as an absorber on one or two sides for different base areas.

The results in Figure 4-39 show a decrease in the permitted dimensions when the system is placed in a concrete corner compared to having a water reflector all around the slab, owing to the more reflecting (and less absorbing) properties of concrete compared to water

as previously explained. The curves for PVC on the side with water and PVC on the side with concrete cross each other; for small base areas it is slightly better to have the PVC on the side not facing the wall or the floor while for larger base areas it is better to have the PVC on the side facing the concrete. The data points above are summarized in Table A2-15 in Appendix II.

### 4.2.4 Removing part of an absorber

When using an absorber such as PVC, it may be unsuitable to cover the entire surface of the tank. Some installations require instruments such as level sensors to be installed, requiring a piece of the absorber to be removed.

As mentioned in Section 3.2.2, the removed part of an absorber has been modeled by varying the area of a $UO_2 + H_2O$ cylinder protruding from the center of the slab. A factor is determined which can then be used to calculate the critically safe dimensions of a slab with a part of the absorber removed according to the following formula:

$$z_{tank} \cdot F = z_{tank,hole} \quad (16)$$

Where $z_{tank}$ is the maximum thickness for slabs with absorbers covering the entire surface, $F$ is the factor and $z_{tank,hole}$ is the maximum thickness for slabs with a part of an absorber removed.

The results in Figure 4-40 show the most conservative factors for each base area (0.16 $m^2$ and 4.00 $m^2$) plotted against the area of the hole. The factors for a base area of 0.16 $m^2$ conservatively cover factors with a larger base area than 0.16 $m^2$, and in the same manner the factors for 4.00 $m^2$ conservatively cover base areas larger than 4.00 $m^2$.

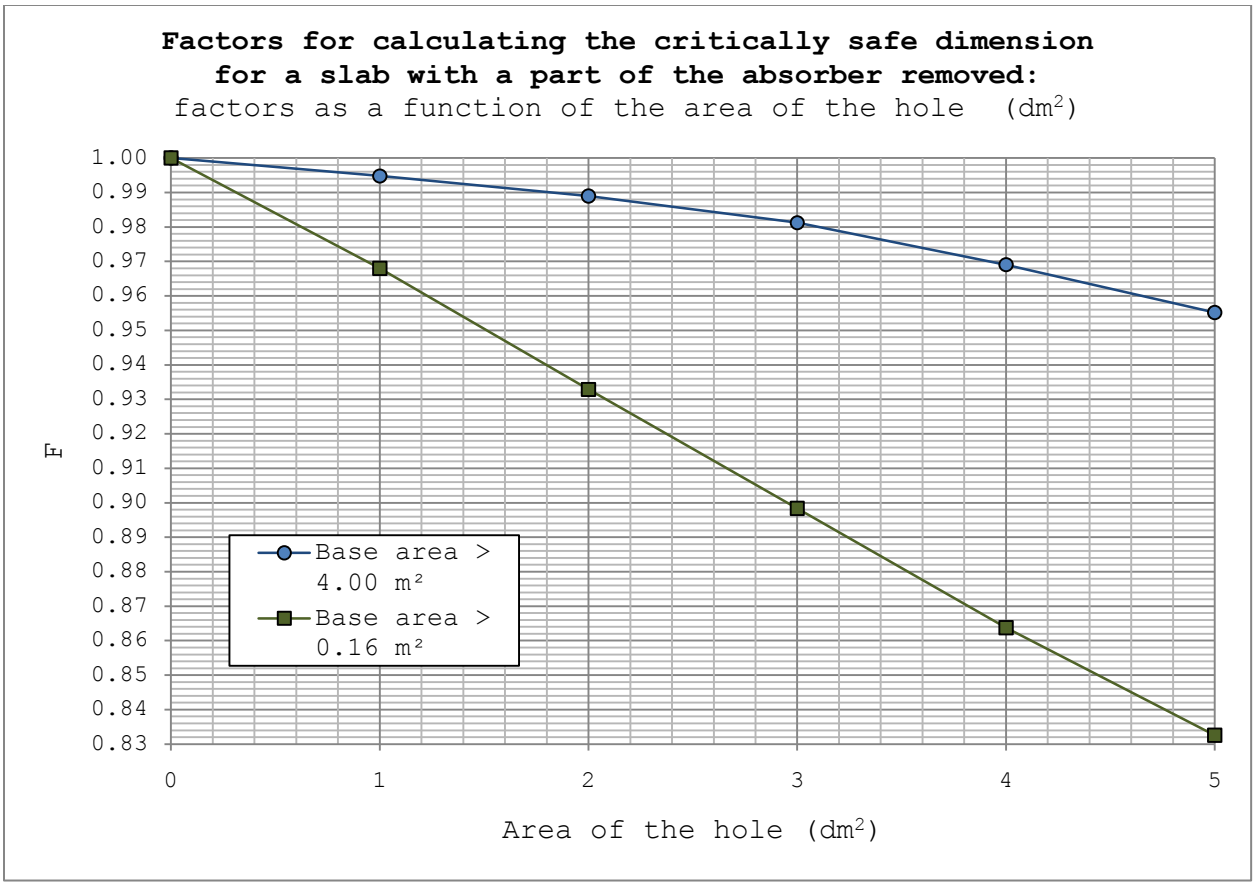


**Figure 4-40.** Factors for calculating the maximum thickness of a slab with a part of the absorber removed as a function of the area of the hole, for finite slabs with a base area of at least 0.16 $m^2$.

The data points above are summarized in Table A2-16 in Appendix II.

### 4.2.5 Comparison between the new and old PVC results

There are fewer differences between the new and the old PVC simulations in KSH 12.6 compared to KSH 12.3. The magnitude of the standard deviation is known for KSH 12.6; it is approximately 30 pcm larger than in the new simulations. A B-term is used in both the new and the old simulations, although for the cross section libraries and conditions used in the old version it is 80 pcm larger. The new PVC simulations have been run both with and without steel, and the most conservative slab thickness has been chosen for each quadratic base area. The old simulations use steel for all the cases.

A comparison between the new and the old PVC results for systems of a different base area containing a $UO_2 + H_2O$ mixture with a 30 cm water reflector is presented in Table 4-3.

**Table 4-3.** Comparison between the new and old PVC composition for $UO_2$ + $H_2O$ systems reflected by water.

| $UO_2$ + $H_2O$, water refl. | Maximum thickness KSH 12.6 (old) (cm) | | Maximum thickness KSH 12.6 (new) (cm) | | Difference new-old (cm) | |
|---|---|---|---|---|---|---|
| Area ($m^2$) | PVC on one side | PVC on two sides | PVC on one side | PVC on two sides | PVC on one side | PVC on two sides |
| 0.1600 | 18.6 | 20.5 | 18.3 | 20.1 | -0.3 | -0.4 |
| 0.2500 | 16.2 | 18.1 | 15.9 | 17.7 | -0.3 | -0.4 |
| 0.3600 | 14.9 | 16.9 | 14.6 | 16.4 | -0.3 | -0.5 |
| 0.5625 | 13.9 | 15.9 | 13.7 | 15.5 | -0.2 | -0.4 |
| 1.0000 | 13.1 | 15.1 | 12.9 | 14.7 | -0.2 | -0.4 |
| 4.0000 | 12.3 | 14.3 | 12.1 | 13.9 | -0.2 | -0.4 |
| Infinite | 12.1 | 14.0 | 11.8 | 13.6 | -0.3 | -0.4 |

A comparison between the new and the old PVC results for systems of a different base area containing a UNH + $H_2O$ mixture with a 30 cm water reflector is presented in Table 4-4.

**Table 4-4.** Comparison between the new and old PVC composition for UNH + $H_2O$ systems reflected by water.

| UNH + $H_2O$, water refl. | Maximum thickness KSH 12.6 (old) (cm) | | Maximum thickness KSH 12.6 (new) (cm) | | Difference new-old (cm) | |
|---|---|---|---|---|---|---|
| Area ($m^2$) | PVC on one side | PVC on two sides | PVC on one side | PVC on two sides | PVC on one side | PVC on two sides |
| 0.1600 | 38.0 | 40.0 | 37.5 | 39.3 | -0.5 | -0.7 |
| 0.2500 | 28.9 | 30.9 | 28.6 | 30.4 | -0.3 | -0.5 |
| 0.3600 | 25.3 | 27.3 | 25.0 | 26.9 | -0.3 | -0.4 |
| 0.5625 | 22.7 | 24.8 | 22.5 | 24.3 | -0.2 | -0.5 |
| 1.0000 | 20.8 | 22.9 | 20.6 | 22.5 | -0.2 | -0.4 |
| 4.0000 | 19.1 | 21.1 | 18.8 | 20.7 | -0.3 | -0.4 |
| Infinite | 18.5 | 20.5 | 18.2 | 20.1 | -0.3 | -0.6 |

A comparison between the new and the old PVC results for systems of a different base area containing a $UO_2$ + $H_2O$ mixture placed in a concrete corner is presented in Table 4-5.

**Table 4-5.** Comparison between the new and old PVC composition for $UO_2$ + $H_2O$ systems placed in a concrete corner.

| $UO_2$ + $H_2O$, concrete corner | Maximum thickness KSH 12.6 (old) (cm) | | | Maximum thickness KSH 12.6 (new) (cm) | | | Difference new-old (cm) | | |
|---|---|---|---|---|---|---|---|---|---|
| Area ($m^2$) | PVC on water side | PVC on concrete side | PVC on two sides | PVC on water side | PVC on concrete side | PVC on two sides | PVC on water side | PVC on concrete sides | PVC on two sides |
| 0.1600 | 17.5 | 17.2 | 19.1 | 17.2 | 16.7 | 18.5 | -0.3 | -0.5 | -0.6 |
| 0.2500 | 14.9 | 14.8 | 16.7 | 14.6 | 14.3 | 16.1 | -0.3 | -0.5 | -0.6 |
| 0.3600 | 13.5 | 13.5 | 15.5 | 13.2 | 13.0 | 14.8 | -0.3 | -0.5 | -0.7 |
| 0.5625 | 12.2 | 12.4 | 14.4 | 12.0 | 11.9 | 13.8 | -0.2 | -0.5 | -0.6 |
| 1.0000 | 11.2 | 11.6 | 13.6 | 10.9 | 11.1 | 12.9 | -0.3 | -0.5 | -0.7 |
| 4.0000 | 9.9 | 10.6 | 12.7 | 9.7 | 10.1 | 12.0 | -0.2 | -0.5 | -0.7 |
| Infinite | 9.3 | 10.3 | 12.3 | 9.1 | 9.7 | 11.6 | -0.2 | -0.6 | -0.7 |

A comparison between the new and the old PVC results for systems of a specific base area containing a $UO_2$ + $H_2O$ mixture with a certain area of a circular hole representing the removal of a piece of an absorber is presented in Table 4-6. The results for different thicknesses and factors for the new simulations are omitted for readability, but these are available in Table A2-16 in Appendix II.

**Table 4-6.** Comparison between the new and old PVC composition for $UO_2$ + $H_2O$ systems with a piece of the absorber removed.

| $UO_2$ + $H_2O$ water refl. | | PVC on one side (old) | | PVC on two sides (old) | | Difference PVC on one side (new-old) | | Difference PVC on two sides (new-old) | |
|---|---|---|---|---|---|---|---|---|---|
| Area ($m^2$) | Area of the hole ($dm^2$) | Thickness (cm) | Factor (-) | Thickness (cm) | Factor (-) | Thickness (cm) | Factor (-) | Thickness (cm) | Factor (-) |
| >0.16 | 0 | 18.6 | 1.000 | 20.5 | 1.000 | -0.3 | 0.000 | -0.4 | 0.000 |
| | 1 | 18.1 | 0.973 | 20.0 | 0.975 | -0.4 | -0.005 | -0.6 | -0.006 |
| | 2 | 17.5 | 0.942 | 19.4 | 0.945 | -0.4 | -0.009 | -0.6 | -0.007 |
| | 3 | 16.9 | 0.907 | 18.8 | 0.916 | -0.5 | -0.009 | -0.6 | -0.009 |
| | 4 | 16.3 | 0.874 | 18.1 | 0.885 | -0.5 | -0.010 | -0.5 | -0.009 |
| | 5 | 15.7 | 0.841 | 17.5 | 0.855 | -0.5 | -0.008 | -0.5 | -0.008 |
| >4.00 | 0 | 12.3 | 1.000 | 14.3 | 1.000 | -0.2 | 0.000 | -0.4 | 0.000 |
| | 1 | 12.3 | 0.997 | 14.3 | 0.998 | -0.3 | -0.002 | -0.5 | -0.002 |
| | 2 | 12.2 | 0.992 | 14.2 | 0.993 | -0.3 | -0.003 | -0.4 | -0.002 |
| | 3 | 12.1 | 0.985 | 14.1 | 0.986 | -0.3 | -0.004 | -0.4 | -0.002 |
| | 4 | 12.0 | 0.975 | 14.0 | 0.978 | -0.3 | -0.006 | -0.5 | -0.004 |
| | 5 | 11.8 | 0.962 | 13.8 | 0.968 | -0.3 | -0.007 | -0.4 | -0.006 |

The results presented in the previous tables verify that the new PVC composition is more conservative, thus decreasing the allowed thicknesses and factors for all the cases studied.

### 4.2.6 Parametric study

A number of parametric studies have been performed as a complement to the parametric study in KSH 12.3. The studies are made for finite slabs with a base area of 0.16 $m^2$ and for slabs with an infinite base area, both containing UNH + $H_2O$ with 1.3 cm PVC used as an absorber on both sides of the slab. Both systems have critically safe dimensions and are reflected by a 30 cm water reflector.

The following parameters have been varied to study the effect on $k_{eff}$:

- Steel tank thickness between the UNH + $H_2O$ mixture and the absorber
- Water column thickness between the steel tank and the absorber

As with KSH 12.3, the results show the difference in $k_{eff} + 3\sigma + B$ from 0.95 by varying a certain parameter.

In Figure 4-41, the steel tank whose thickness is varied is shown.

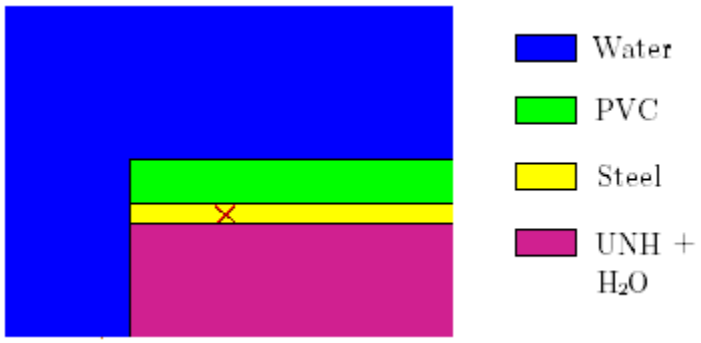


**Figure 4-41.** Close up of a slab infinite in depth and height with PVC as an absorber. The red cross marks the steel layer whose thickness has been varied.

The results for slabs with a base area of 0.16 $m^2$ and for slabs with an infinite base area are shown in Figure 4-42 and Figure 4-43.

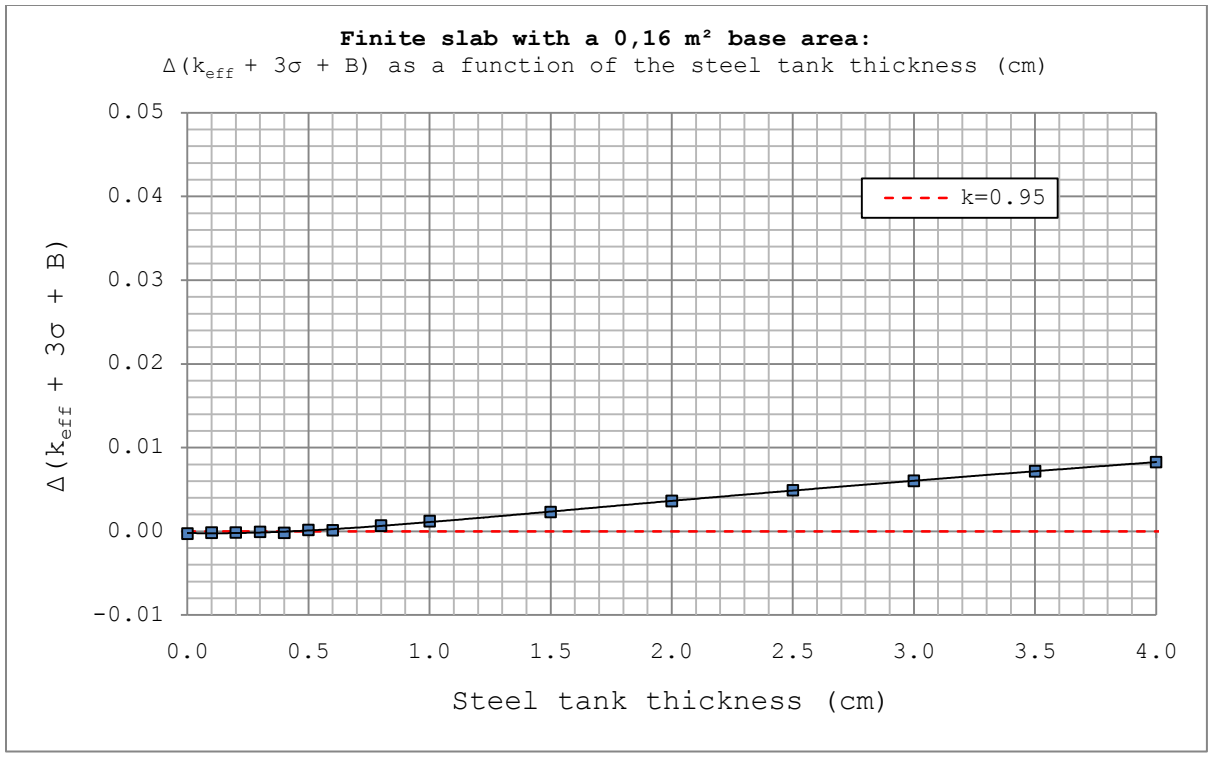


**Figure 4-42.** A finite slab with a base area of 0.16 $m^2$ containing a UNH + $H_2O$ mixture, surrounded by PVC on two sides and reflected by 30 cm water.

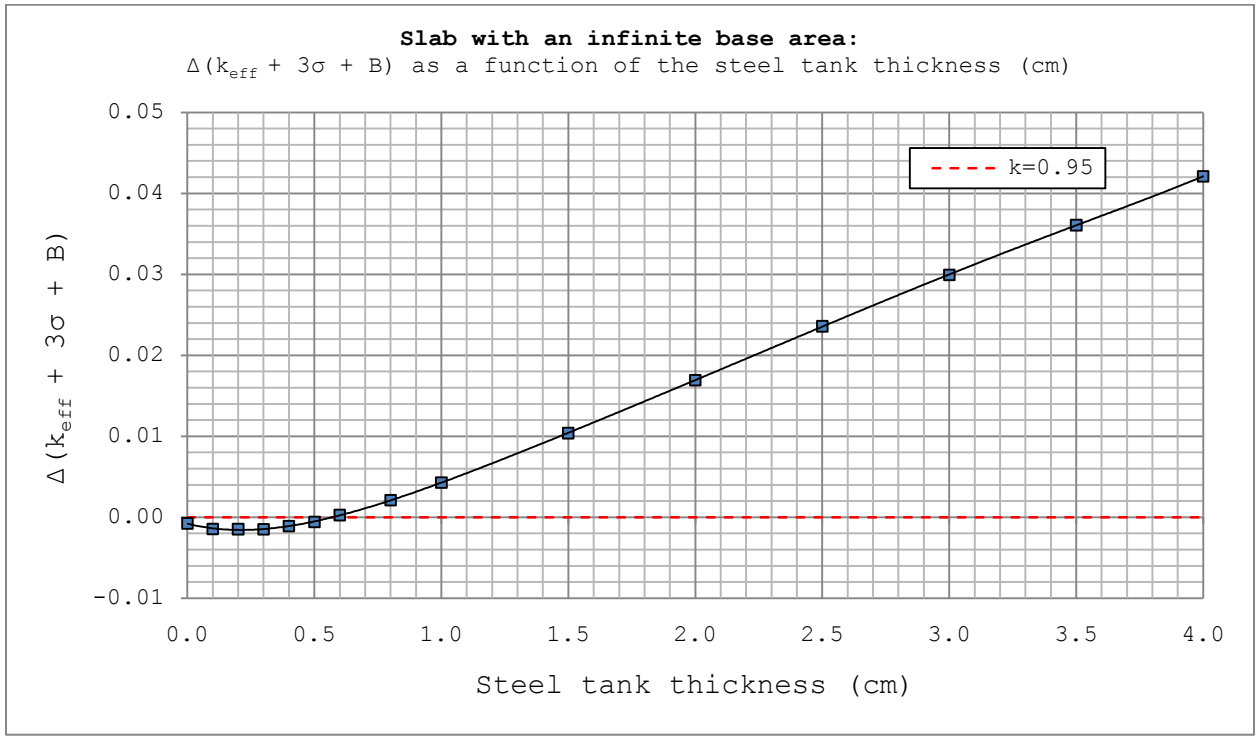


**Figure 4-43.** A slab infinite in two dimensions containing a UNH + $H_2O$ mixture surrounded by PVC on two sides and reflected by 30 cm water.

Figure 4-43 above clearly shows a trend similar to the corresponding parametric study in KSH 12.3, where the value of $k_{eff}$ initially decreases but then increases for increasing thicknesses of steel. The same trend is present in Figure 4-42 but it is much less pronounced for smaller base areas. It is seen that the effect of adding steel is significantly greater for the system with an infinite base area.

The water column that has been modeled is shown in Figure 4-44.

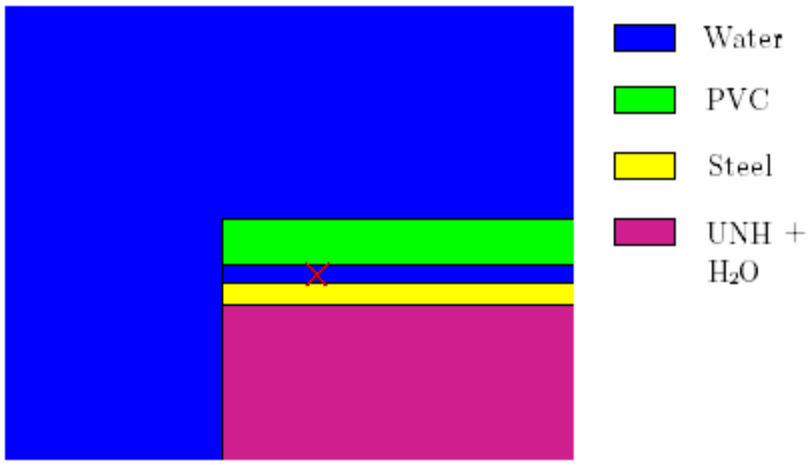


**Figure 4-44.** Close up of a slab infinite in depth and height with PVC as an absorber. The red cross marks the water column whose thickness has been varied.

The results for slabs with a base area of 0.16 $m^2$ and for slabs with an infinite base area are shown in Figure 4-45 and Figure 4-46.

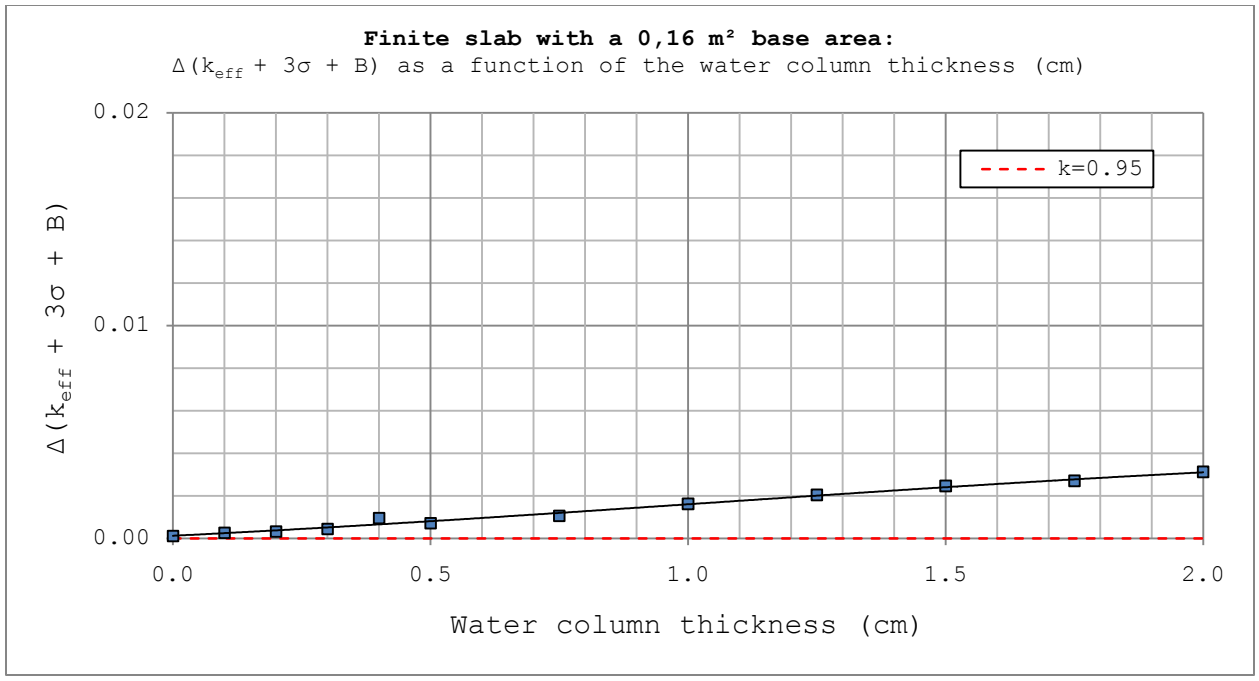


**Figure 4-45.** A finite slab with a base area of 0.16 $m^2$ containing a UNH + $H_2O$ mixture, surrounded by PVC on two sides and reflected by 30 cm water.

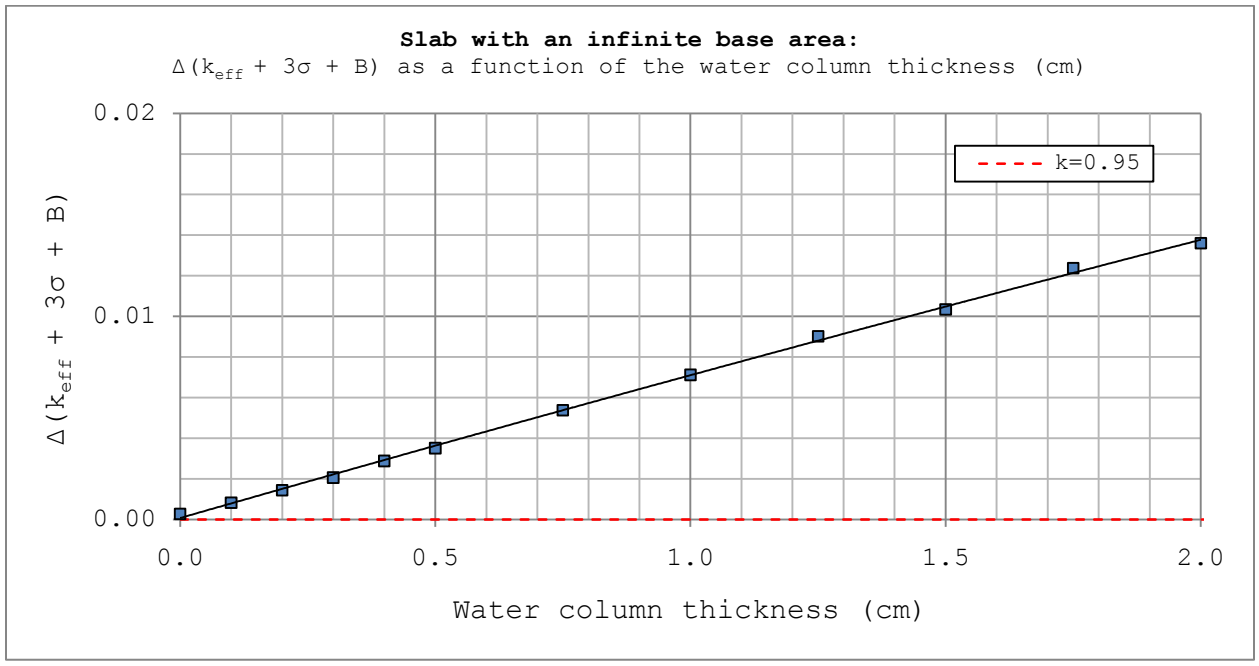


**Figure 4-46.** A slab infinite in two dimensions containing a UNH + $H_2O$ mixture surrounded by PVC on two sides and reflected by 30 cm water.

Similarly to the varying steel tank thickness study, $k_{eff}$ increases with an increasing thickness of the water column and the effect is greater for bigger base areas. A larger amount of flooding can be allowed for the UNH + $H_2O$ case than the $UO_2$ + $H_2O$ case.

## 4.3 Validation results

Table 4-7 and Table 4-8 show the raw calculation results together with the EALF for each of the critical experiments considered in this validation suite. For the cases where information about $\sigma_{exp}$ is missing this value is estimated using the recommendations in [1]. Figure 4-47 shows the deviation from criticality for each result.

**Table 4-7.** Raw calculation results for the IHECSBE cases

| Case LCT[2]- | $k_{calc}$ | $k_{exp}$ | $k_{norm}$ | $\sigma_{calc}$ | $\sigma_{exp}$ | $\sigma_i$ | EALF (eV) | Strong absorber present | Case description In Section |
|---|---|---|---|---|---|---|---|---|---|
| 001-1 | 0.99984 | 0.99980 | 1.00004 | 0.00010 | 0.00300 | 0.00300 | 0.09901 | No | |
| 001-2 | 0.99930 | 0.99980 | 0.99950 | 0.00009 | 0.00300 | 0.00300 | 0.09834 | No | |
| 001-3 | 0.99892 | 0.99980 | 0.99912 | 0.00009 | 0.00300 | 0.00300 | 0.09746 | No | |
| 001-4 | 0.99947 | 0.99980 | 0.99967 | 0.00009 | 0.00300 | 0.00300 | 0.09808 | No | 3.3.2.1.1 |
| 001-5 | 0.99742 | 0.99980 | 0.99762 | 0.00009 | 0.00300 | 0.00300 | 0.09675 | No | |
| 001-6 | 0.99935 | 0.99980 | 0.99955 | 0.00009 | 0.00300 | 0.00300 | 0.09771 | No | |
| 001-7 | 0.99866 | 0.99980 | 0.99886 | 0.00009 | 0.00310 | 0.00310 | 0.09598 | No | |
| 001-8 | 0.99766 | 0.99980 | 0.99786 | 0.00009 | 0.00300 | 0.00300 | 0.09706 | No | |
| 002-1 | 0.99875 | 0.99970 | 0.99905 | 0.00011 | 0.00200 | 0.00200 | 0.11609 | No | |
| 002-2 | 1.00011 | 0.99970 | 1.00041 | 0.00010 | 0.00200 | 0.00200 | 0.11598 | No | |
| 002-3 | 0.99931 | 0.99970 | 0.99961 | 0.00010 | 0.00200 | 0.00200 | 0.11577 | No | 3.3.2.1.2 |
| 002-4 | 0.99912 | 0.99970 | 0.99942 | 0.00011 | 0.00180 | 0.00180 | 0.11481 | No | |
| 002-5 | 0.99781 | 0.99970 | 0.99811 | 0.00010 | 0.00190 | 0.00190 | 0.11310 | No | |
| 008-1 | 0.99957 | 1.00070 | 0.99887 | 0.00009 | 0.00120 | 0.00120 | 0.28627 | Yes | |
| 008-2 | 0.99971 | 1.00070 | 0.99901 | 0.00009 | 0.00120 | 0.00120 | 0.25248 | Yes | |
| 008-3 | 1.00037 | 1.00070 | 0.99967 | 0.00009 | 0.00120 | 0.00120 | 0.25221 | Yes | |
| 008-11 | 0.99992 | 1.00070 | 0.99922 | 0.00010 | 0.00120 | 0.00120 | 0.26099 | Yes | 3.3.2.1.3 |
| 008-12 | 0.99956 | 1.00070 | 0.99886 | 0.00010 | 0.00120 | 0.00120 | 0.25478 | Yes | |
| 008-14 | 0.99951 | 1.00070 | 0.99881 | 0.00009 | 0.00120 | 0.00120 | 0.25684 | Yes | |
| 008-16 | 0.99912 | 1.00070 | 0.99842 | 0.00009 | 0.00120 | 0.00120 | 0.23384 | Yes | |
| 008-17 | 0.99822 | 1.00070 | 0.99752 | 0.00009 | 0.00120 | 0.00120 | 0.20436 | Yes | |
| 009-1 | 0.99962 | 1.00000 | 0.99962 | 0.00011 | 0.00210 | 0.00210 | 0.11566 | No | |
| 009-2 | 0.99918 | 1.00000 | 0.99918 | 0.00011 | 0.00210 | 0.00210 | 0.11523 | No | |
| 009-3 | 0.99889 | 1.00000 | 0.99889 | 0.00010 | 0.00210 | 0.00210 | 0.11549 | No | |
| 009-4 | 0.99942 | 1.00000 | 0.99942 | 0.00010 | 0.00210 | 0.00210 | 0.11507 | No | |
| 009-5 | 1.00004 | 1.00000 | 1.00004 | 0.00010 | 0.00210 | 0.00210 | 0.11654 | Yes | |
| 009-6 | 0.99946 | 1.00000 | 0.99946 | 0.00010 | 0.00210 | 0.00210 | 0.11565 | Yes | 3.3.2.1.4 |
| 009-7 | 1.00005 | 1.00000 | 1.00005 | 0.00010 | 0.00210 | 0.00210 | 0.11668 | Yes | |
| 009-8 | 0.99930 | 1.00000 | 0.99930 | 0.00011 | 0.00210 | 0.00210 | 0.11579 | Yes | |
| 009-9 | 0.99974 | 1.00000 | 0.99974 | 0.00011 | 0.00210 | 0.00210 | 0.11647 | Yes | |
| 009-16 | 0.99916 | 1.00000 | 0.99916 | 0.00011 | 0.00210 | 0.00210 | 0.11666 | Yes | |
| 009-17 | 0.99989 | 1.00000 | 0.99989 | 0.00011 | 0.00210 | 0.00210 | 0.11581 | Yes | |
| 009-18 | 0.99880 | 1.00000 | 0.99880 | 0.00011 | 0.00210 | 0.00210 | 0.11660 | Yes | |
| 009-19 | 0.99997 | 1.00000 | 0.99997 | 0.00011 | 0.00210 | 0.00210 | 0.11585 | Yes | |

[2] LEU-COMP-THERM

| Case LCT[2]- | $k_{calc}$ | $k_{exp}$ | $k_{norm}$ | $\sigma_{calc}$ | $\sigma_{exp}$ | $\sigma_i$ | EALF (eV) | Strong absorber present | Case description In Section |
|---|---|---|---|---|---|---|---|---|---|
| 009-20 | 0.99924 | 1.00000 | 0.99924 | 0.00010 | 0.00210 | 0.00210 | 0.11670 | Yes | |
| 009-21 | 0.99998 | 1.00000 | 0.99998 | 0.00011 | 0.00210 | 0.00210 | 0.11579 | Yes | |
| 009-22 | 0.99943 | 1.00000 | 0.99943 | 0.00010 | 0.00210 | 0.00210 | 0.11683 | Yes | 3.3.2.1.4 |
| 009-23 | 1.00024 | 1.00000 | 1.00024 | 0.00010 | 0.00210 | 0.00210 | 0.11589 | Yes | |
| 009-26 | 0.99988 | 1.00000 | 0.99988 | 0.00010 | 0.00210 | 0.00210 | 0.11497 | No | |
| 009-27 | 0.99976 | 1.00000 | 0.99976 | 0.00011 | 0.00210 | 0.00210 | 0.11470 | No | |
| 011-1 | 0.99942 | 1.00100 | 0.99842 | 0.00010 | 0.00180 | 0.00180 | 0.17286 | No | |
| 011-2 | 1.00020 | 1.00090 | 0.99930 | 0.00010 | 0.00320 | 0.00320 | 0.25087 | Yes | |
| 011-3 | 0.99973 | 1.00090 | 0.99883 | 0.00009 | 0.00320 | 0.00320 | 0.19745 | Yes | |
| 011-4 | 1.00022 | 1.00090 | 0.99932 | 0.00009 | 0.00320 | 0.00320 | 0.19787 | Yes | |
| 011-5 | 0.99991 | 1.00090 | 0.99901 | 0.00010 | 0.00320 | 0.00320 | 0.19865 | Yes | 3.3.2.1.5 |
| 011-6 | 0.99981 | 1.00090 | 0.99891 | 0.00010 | 0.00320 | 0.00320 | 0.09992 | Yes | |
| 011-7 | 0.99986 | 1.00090 | 0.99896 | 0.00010 | 0.00320 | 0.00320 | 0.20103 | Yes | |
| 011-8 | 1.00020 | 1.00090 | 0.99930 | 0.00010 | 0.00320 | 0.00320 | 0.20207 | Yes | |
| 011-9 | 0.99979 | 1.00090 | 0.99889 | 0.00010 | 0.00320 | 0.00320 | 0.20312 | Yes | |
| 016-1 | 0.99918 | 1.00000 | 0.99918 | 0.00009 | 0.00310 | 0.00310 | 0.09823 | No | |
| 016-2 | 0.99798 | 1.00000 | 0.99798 | 0.00009 | 0.00310 | 0.00310 | 0.09794 | No | |
| 016-3 | 0.99894 | 1.00000 | 0.99894 | 0.00009 | 0.00310 | 0.00310 | 0.09791 | No | |
| 016-4 | 0.99797 | 1.00000 | 0.99797 | 0.00009 | 0.00310 | 0.00310 | 0.09808 | No | |
| 016-5 | 0.99873 | 1.00000 | 0.99873 | 0.00009 | 0.00310 | 0.00310 | 0.09780 | No | |
| 016-6 | 0.99884 | 1.00000 | 0.99884 | 0.00009 | 0.00310 | 0.00310 | 0.09867 | No | |
| 016-7 | 0.99892 | 1.00000 | 0.99892 | 0.00009 | 0.00310 | 0.00310 | 0.09847 | No | |
| 016-8 | 0.99920 | 1.00000 | 0.99920 | 0.00009 | 0.00310 | 0.00310 | 0.09954 | Yes | |
| 016-9 | 0.99968 | 1.00000 | 0.99968 | 0.00010 | 0.00310 | 0.00310 | 0.09879 | Yes | |
| 016-10 | 0.99881 | 1.00000 | 0.99881 | 0.00009 | 0.00310 | 0.00310 | 0.09953 | Yes | |
| 016-11 | 0.99930 | 1.00000 | 0.99930 | 0.00009 | 0.00310 | 0.00310 | 0.09886 | Yes | |
| 016-12 | 0.99857 | 1.00000 | 0.99857 | 0.00009 | 0.00310 | 0.00310 | 0.10009 | Yes | 3.3.2.1.6 |
| 016-13 | 0.99928 | 1.00000 | 0.99928 | 0.00009 | 0.00310 | 0.00310 | 0.09912 | Yes | |
| 016-14 | 0.99932 | 1.00000 | 0.99932 | 0.00009 | 0.00310 | 0.00310 | 0.10007 | Yes | |
| 016-21 | 0.99945 | 1.00000 | 0.99945 | 0.00009 | 0.00310 | 0.00310 | 0.09958 | Yes | |
| 016-22 | 0.99933 | 1.00000 | 0.99933 | 0.00009 | 0.00310 | 0.00310 | 0.09934 | Yes | |
| 016-23 | 0.99901 | 1.00000 | 0.99901 | 0.00009 | 0.00310 | 0.00310 | 0.09884 | Yes | |
| 016-24 | 0.99905 | 1.00000 | 0.99905 | 0.00009 | 0.00310 | 0.00310 | 0.09928 | Yes | |
| 016-25 | 0.99918 | 1.00000 | 0.99918 | 0.00009 | 0.00310 | 0.00310 | 0.09887 | Yes | |
| 016-26 | 0.99959 | 1.00000 | 0.99959 | 0.00010 | 0.00310 | 0.00310 | 0.09937 | Yes | |
| 016-27 | 0.99924 | 1.00000 | 0.99924 | 0.00009 | 0.00310 | 0.00310 | 0.09888 | Yes | |
| 016-31 | 0.99927 | 1.00000 | 0.99927 | 0.00009 | 0.00310 | 0.00310 | 0.09752 | No | |
| 016-32 | 0.99898 | 1.00000 | 0.99898 | 0.00009 | 0.00310 | 0.00310 | 0.09744 | No | |
| 042-1 | 0.99883 | 1.00000 | 0.99883 | 0.00010 | 0.00160 | 0.00160 | 0.17342 | No | |
| 042-2 | 0.99885 | 1.00000 | 0.99885 | 0.00009 | 0.00160 | 0.00160 | 0.17971 | Yes | 3.3.2.1.7 |
| 042-3 | 0.99968 | 1.00000 | 0.99968 | 0.00010 | 0.00160 | 0.00160 | 0.18661 | Yes | |
| 042-5 | 1.00008 | 1.00000 | 1.00008 | 0.00010 | 0.00330 | 0.00330 | 0.18196 | Yes | |

**Table 4-8.** Raw calculation results for the NUREG/CR-6361 cases

| Case | $k_{calc}$ | $k_{exp}$ | $k_{norm}$ | $\sigma_{calc}$ | $\sigma_{exp}$ | $\sigma_i$ | EALF (eV) | Strong absorber present | Case description In Section |
|---|---|---|---|---|---|---|---|---|---|
| B1645SO1 | 1.00246 | 1.00000 | 1.00246 | 0.00010 | 0.00318[3] | 0.00318 | 0.42962 | Yes | 3.3.2.2.1 |
| B1645SO2 | 1.00256 | 1.00000 | 1.00256 | 0.00010 | 0.00318 | 0.00318 | 0.41117 | Yes | |
| BW1231B1 | 0.99945 | 1.00000 | 0.99945 | 0.00011 | 0.00318 | 0.00318 | 0.70573 | Yes | 3.3.2.2.2 |
| BW1231B2 | 0.99993 | 1.00000 | 0.99993 | 0.00010 | 0.00318 | 0.00318 | 1.15230 | Yes | |
| BW1237M | 0.99880 | 1.00000 | 0.99880 | 0.00009 | 0.00318 | 0.00318 | 0.49469 | Yes | 3.3.2.2.3 |
| BW1810A | 1.00383 | 1.00000 | 1.00383 | 0.00009 | 0.00318 | 0.00318 | 0.25022 | Yes | 3.3.2.2.4 |
| BW1810B | 1.00363 | 1.00000 | 1.00363 | 0.00009 | 0.00318 | 0.00318 | 0.24920 | Yes | |
| BW1810C | 1.00296 | 1.00000 | 1.00296 | 0.00010 | 0.00318 | 0.00318 | 0.33473 | Yes | |
| BW1810D | 1.00254 | 1.00000 | 1.00254 | 0.00010 | 0.00318 | 0.00318 | 0.34124 | Yes | |
| BW1810E | 1.00269 | 1.00000 | 1.00269 | 0.00010 | 0.00318 | 0.00318 | 0.33460 | Yes | |
| BW1810F | 1.00382 | 1.00000 | 1.00382 | 0.00010 | 0.00318 | 0.00318 | 0.25196 | Yes | |
| BW1810G | 1.00243 | 1.00000 | 1.00243 | 0.00010 | 0.00318 | 0.00318 | 0.36132 | Yes | |
| BW1810H | 1.00182 | 1.00000 | 1.00182 | 0.00009 | 0.00318 | 0.00318 | 0.36266 | Yes | |
| BW1810I | 1.00313 | 1.00000 | 1.00313 | 0.00010 | 0.00318 | 0.00318 | 0.25116 | Yes | |
| EPRU65 | 1.00306 | 1.00000 | 1.00306 | 0.00010 | 0.00259 | 0.00259 | 0.25500 | No | 3.3.2.2.5 |
| EPRU65B | 1.00600 | 1.00000 | 1.00600 | 0.00010 | 0.00318 | 0.00318 | 0.31189 | Yes | |
| EPRU75 | 1.00208 | 1.00000 | 1.00208 | 0.00009 | 0.00259 | 0.00259 | 0.11561 | No | |
| EPRU75B | 1.00393 | 1.00000 | 1.00393 | 0.00009 | 0.00318 | 0.00318 | 0.14348 | Yes | |
| EPRU87 | 1.00146 | 1.00000 | 1.00146 | 0.00009 | 0.00259 | 0.00259 | 0.08518 | No | |
| EPRU87B | 1.00327 | 1.00000 | 1.00327 | 0.00009 | 0.00318 | 0.00318 | 0.09482 | Yes | |
| W3269A | 0.99958 | 1.00000 | 0.99958 | 0.00011 | 0.00318 | 0.00318 | 0.30736 | Yes | 3.3.2.2.6 |
| W3269B1 | 0.99858 | 1.00000 | 0.99858 | 0.00010 | 0.00318 | 0.00318 | 0.44734 | Yes | |
| W3269B2 | 0.99808 | 1.00000 | 0.99808 | 0.00010 | 0.00318 | 0.00318 | 0.44241 | Yes | |
| W3269B3 | 0.99733 | 1.00000 | 0.99733 | 0.00010 | 0.00318 | 0.00318 | 0.47390 | Yes | |
| W3269C | 0.99801 | 1.00000 | 0.99801 | 0.00010 | 0.00318 | 0.00318 | 0.25762 | Yes | |

[3] Experimental uncertainty estimated from similar experiments is used for all NUREG/CR-6361 cases

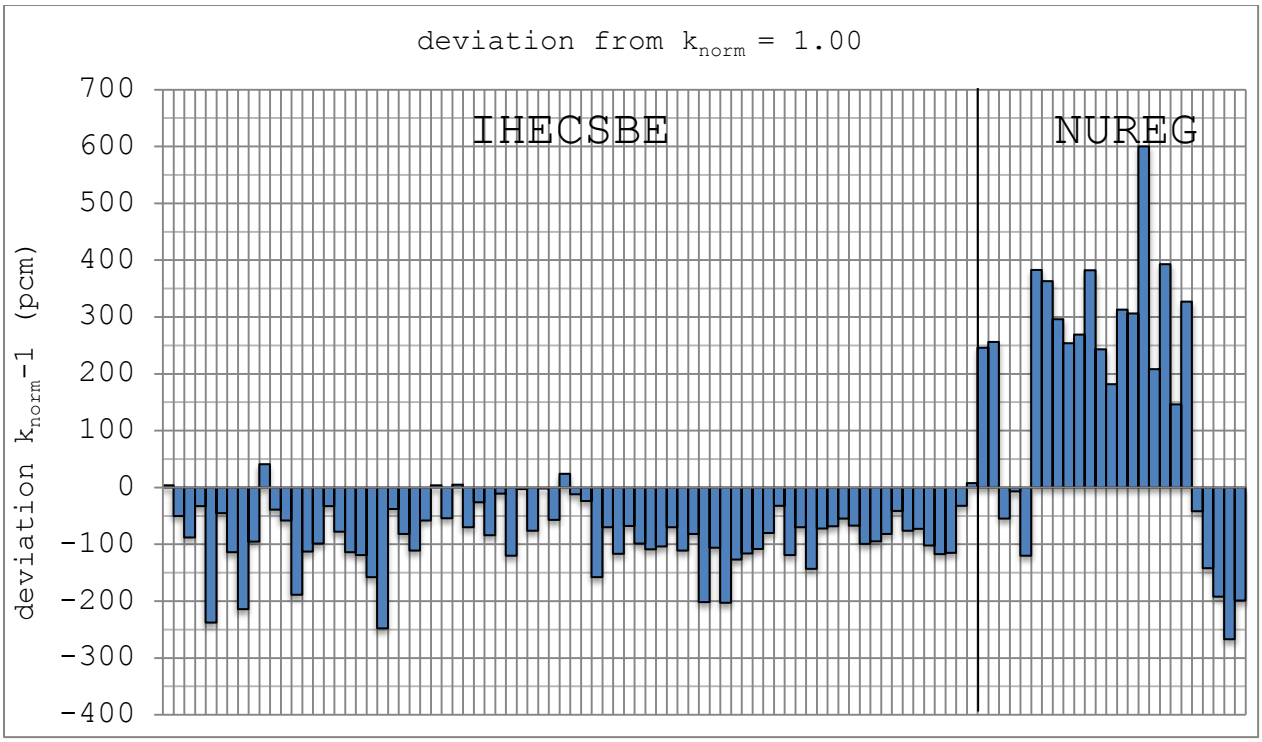


**Figure 4-47.** Deviation from criticality for the calculation results. IHECSBE and NUREG (denoting NUREG/CR-6361) refer to the different collections of benchmark experiments used.

### 4.3.1 Summary of calculation results

The average $k_{norm}$ from the calculations is 0.99979 with the standard deviation 0.00163. This is the simple average of the normalized $k_{eff}$ values that does not include weighting factors to correct for the differences in data uncertainty. The weighted average $k_{norm}$ is presented in the following section.

### 4.3.2 Bias, bias uncertainty and normality check

The full calculation results are analyzed group wise in two subsets, designed to reflect common situations in storage of spent LWR fuel, described in Section 3.4.1. The chosen subsets are:

- Experiments which contained fresh fuel and strong absorbers (68 experiments)
- Experiments which contained fresh fuel without strong absorbers (33 experiments)

Experiments containing the absorbers listed in Section 3.3.1 belong to the first group and remaining experiments belong to the second group. Best estimate, untrended, bias and bias uncertainty is determined for each group using the method presented in section 2.5. The validation results for fresh fuel experiments containing strong absorbers are presented in Table 4-9 and in Table 4-10 for experiments without strong absorbers. The best

estimate untrended bias is presented with a bias uncertainty that equals the square root of the pooled variance.

As the data set for fresh fuel without absorber contains less than 50 experiments, the Shapiro-Wilk normality test is performed in addition to the USLSTATS normality test. The method for this test and the necessary coefficients are found in [1].

**Table 4-9.** Validation results for fresh fuel experiments with strong absorbers.

| | |
|---|---|
| Variance about the mean $s^2$ | 2.018E-06 |
| Average total uncertainty $\bar{\sigma}^2$ | 4.948E-06 |
| Weighted mean $k_{norm}$ value $\bar{k}_{norm}$ | 0.999513 |
| Square root of the pooled variance $S_P$ | 0.002639 |
| Number of experiments | 68 |
| USLSTATS Normality test result $\chi^2$ | 52.735 |
| USLSTATS Normality test conclusion | Not normal |
| Best estimate, untrended, bias and bias uncertainty | -0.000487±0.00264 |

**Table 4-10.** Validation results for fresh fuel experiments without strong absorbers.

| | |
|---|---|
| Variance about the mean $s^2$ | 1.151E-06 |
| Average total uncertainty $\bar{\sigma}^2$ | 5.842E-06 |
| Weighted mean $k_{norm}$ value $\bar{k}_{norm}$ | 0.999355 |
| Square root of the pooled variance $S_P$ | 0.002644 |
| Number of experiments | 33 |
| USLSTATS Normality test result $\chi^2$ | 5.9394 |
| USLSTATS Normality test conclusion | Normal |
| Shapiro-Wilk test result (Wt) | 0.87174 |
| Shapiro-Wilk normality test lower bound | 0.931 |
| Shapiro-Wilk normality test conclusion | Not normal |
| Best estimate, untrended, bias and bias uncertainty | -0.000645±0.00264 |

It can be seen from the tables that neither of the two data sets passed the tests for normal distribution. The subset with fresh fuel without strong absorbers passed the USLSTATS normality test but failed the Shapiro-Wilk test. For non-normally distributed subsets the most conservative approach is to use a non-parametric treatment to determine bias and bias uncertainty. No formal trend analysis will be performed in these cases.

### 4.3.3 Trending analysis

Regression fit and goodness of fit tests should be applied to each set or subset of normal data for the following parameters:

- Energy of Average Lethargy Causing Fission, EALF (eV)
- Enrichment (wt% $^{235}$U/U)
- Pin Pitch (cm)
- Soluble Boron Concentration (ppm)
- $^{10}$B Areal Density of Poison Plates (g/cm$^2$)

In Section 4.3.3.1 and Section 4.3.3.2 the results are shown graphically to display possible trends. As neither data set proved to be normally distributed, no formal trend analysis will be performed.

#### 4.3.3.1 Trend results for fresh fuel with strong absorbers

The scatter plots in Figure 4-48 through Figure 4-52 shows the variation in $k_{norm}$ values as a function of EALF, enrichment, pitch, soluble boron concentration and $^{10}$B areal density. A visual inspection of Figure 4-49 indicates that $k_{norm}$ may be a weak function of the enrichment of the fuel. Figure 4-51 indicates that $k_{norm}$ may also be a weak function of soluble boron concentration. As the data set is not normally distributed, a non-parametric treatment will be performed in Section 4.3.4 in order to determine the USL and B-term.

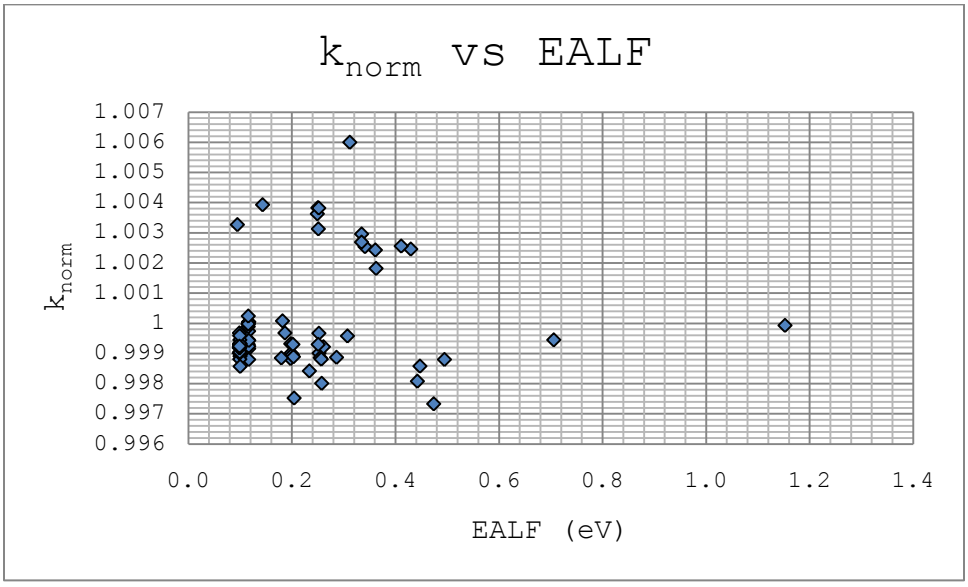


**Figure 4-48.** $k_{norm}$ versus EALF for fresh fuel with strong absorbers.

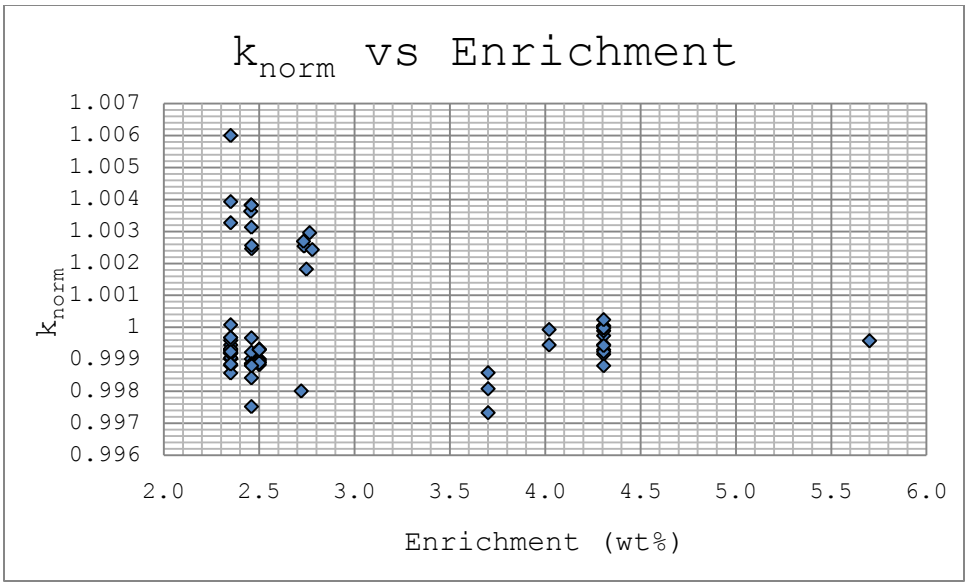


**Figure 4-49.** $k_{norm}$ versus $^{235}$U enrichment for fresh fuel with strong absorbers.

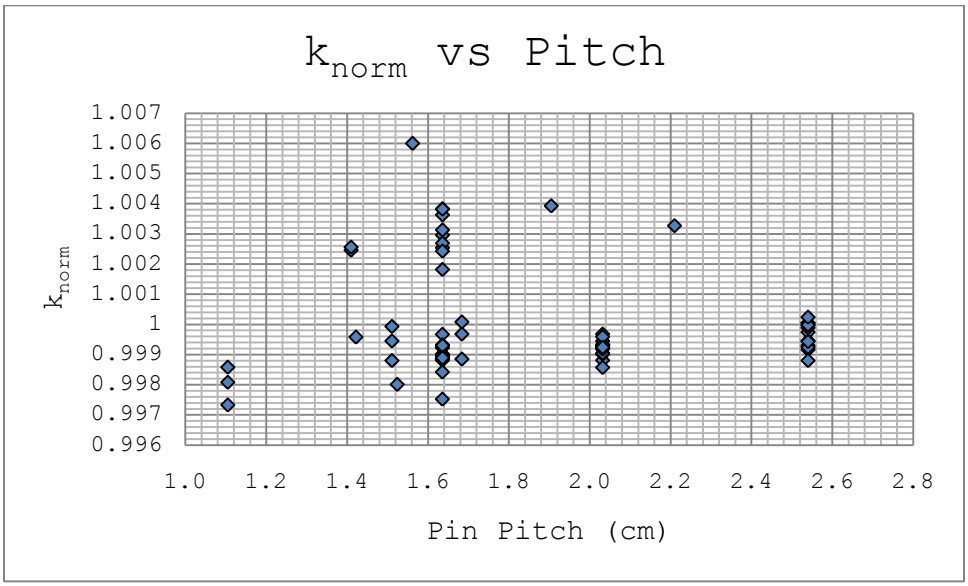


**Figure 4-50.** $k_{norm}$ versus pin pitch for fresh fuel with strong absorbers.

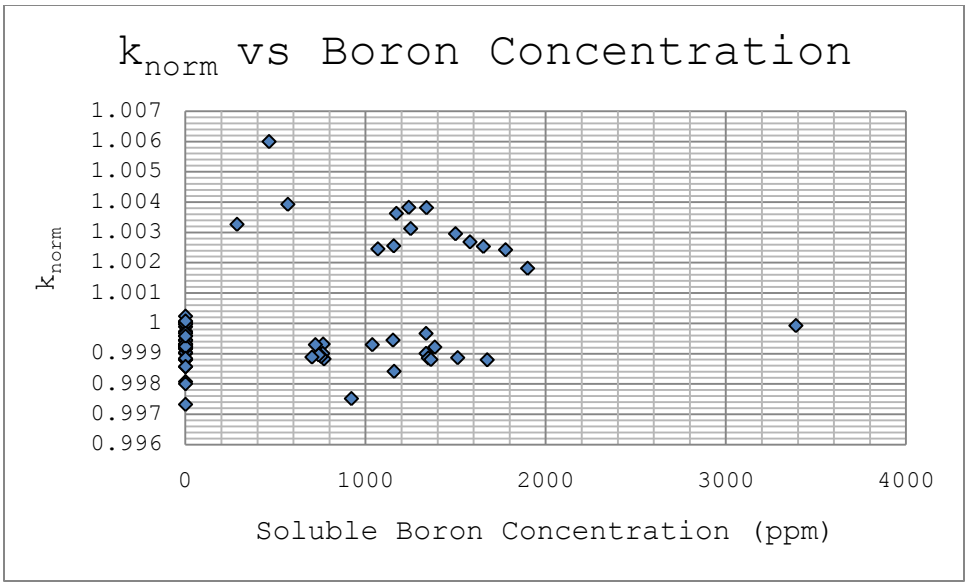


**Figure 4-51.** $k_{norm}$ versus soluble boron concentration for fresh fuel with strong absorbers.

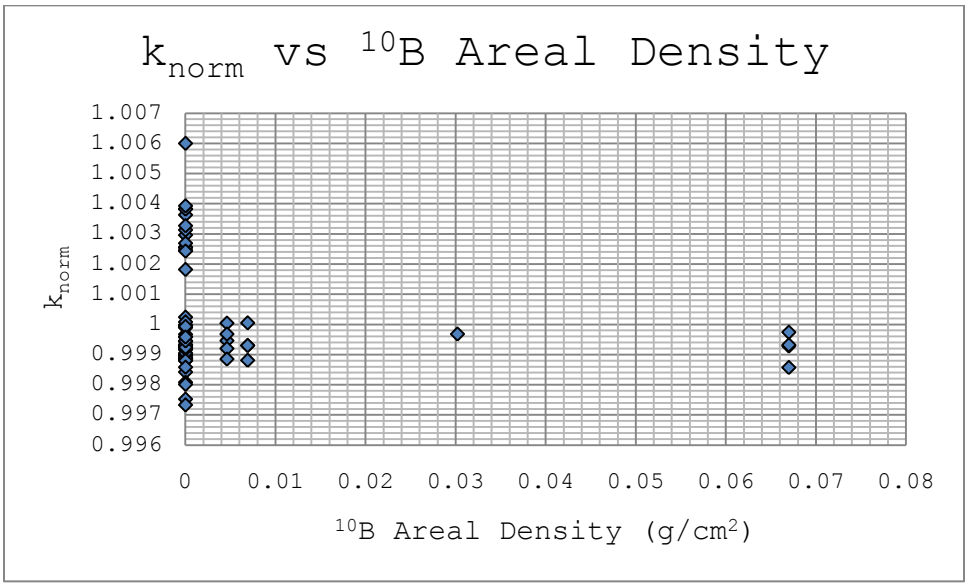


**Figure 4-52.** $k_{norm}$ versus $^{10}$B areal density for fresh fuel with strong absorbers.

#### 4.3.3.2 Trend results for fresh fuel experiments without strong absorber

The scatter plots in Figure 4-53, Figure 4-54 and Figure 4-55 shows the variation in $k_{norm}$ values as a function of EALF, enrichment and pitch. The scatter plot in Figure 4-53 indicates that $k_{norm}$ may be a weak function of EALF. As the data set is not normally distributed, a non-parametric treatment will be performed in order to determine the USL and B-term.

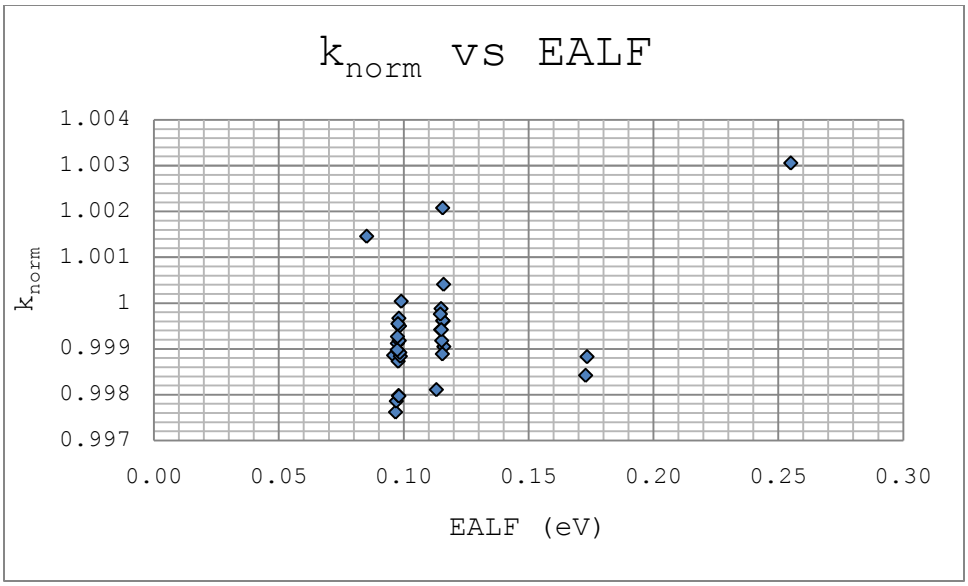


**Figure 4-53.** $k_{norm}$ versus EALF for fresh fuel without strong absorbers.

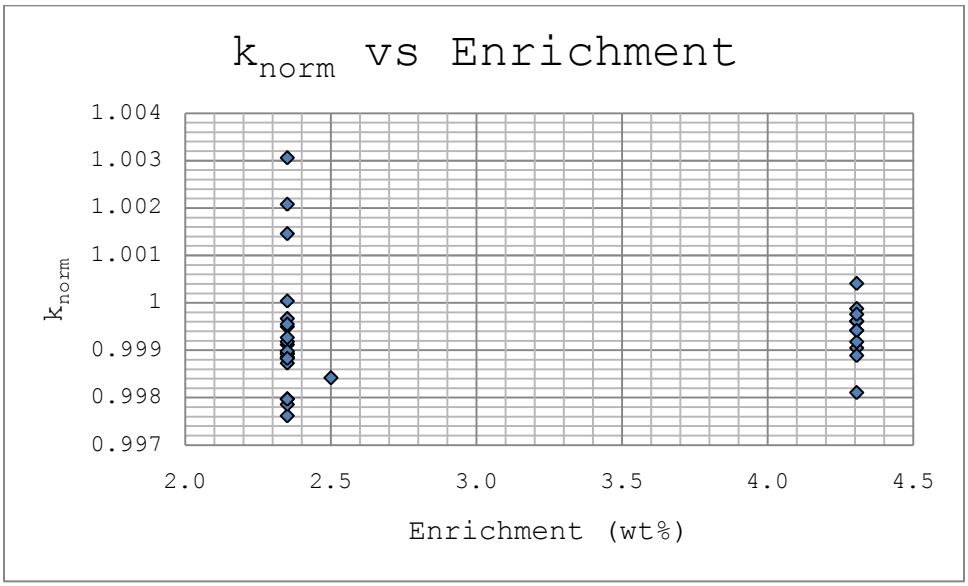


**Figure 4-54.** $k_{norm}$ versus $^{235}$U enrichment for fresh fuel without strong absorbers.

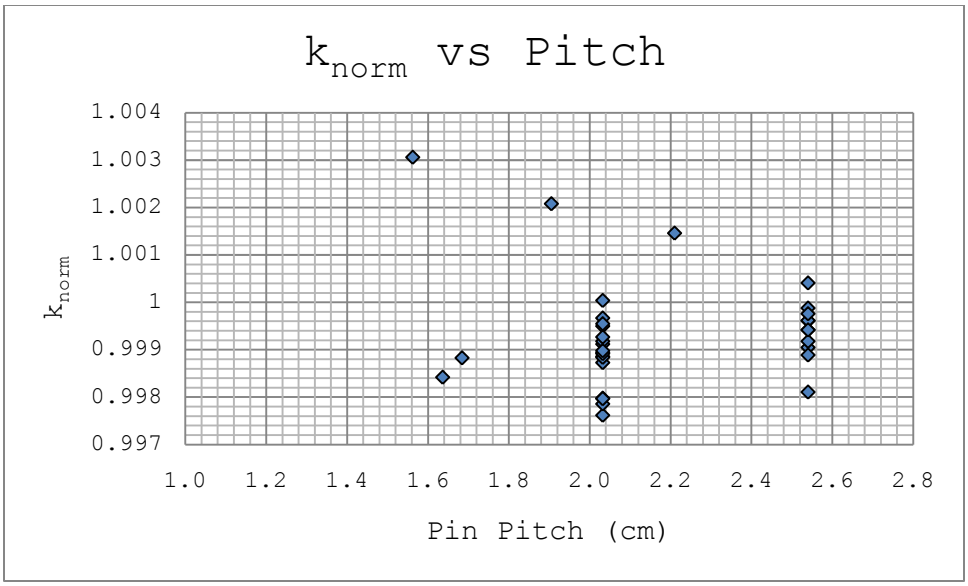


**Figure 4-55.** $k_{norm}$ versus pin pitch for fresh fuel without strong absorbers.

### 4.3.4 Non-parametric treatment

For the data sets failing the normality test, a non-parametric treatment is used. The non-parametric treatment used is described in 2.5.2 and the results produced may be seen in Table 4-11.

**Table 4-11.** USL and the corresponding B-term for the non-normally distributed data sets.

| | Fresh fuel with absorber | Fresh fuel without absorber |
|---|---|---|
| $K_L$ | 0.99415 | 0.98462 |
| USL | 0.94415 | 0.93462 |
| B | 0.00585 | 0.01538 |

As seen in Table 4-11, the B-term for fresh fuel without absorber is notably higher than for fresh fuel with absorbers. This is due to the non-parametric margin of 0.01 that is added due to the lack of data points.

### 4.3.5 Area of Applicability Definition

The AOA of this benchmark is defined by the range of parameters featured in the validation suite. The area of applicability for this MCNP5 validation covers heterogeneous systems with low enriched uranium oxide fuel rod assemblies in array configurations moderated and reflected by water with and without absorbers present with some restrictions detailed below.

A summary of the AOA is tabulated in Table 4-12. This table may be used to determine the B-term to be used for a specific system. Although the B-terms are calculated from experiments with fresh fuel, these may be used in spent fuel pools calculations without burnable absorbers and depletion credited.

The obtained values are deemed to be conservative within the AOA. Possible trends such as the one seen in Figure 4-49 have not been investigated and this should be kept in mind when extrapolating outside the AOA. If the B-term is to be used outside of the designated AOA this should be accounted for as described in Section 2.5.

**Table 4-12.** Area of applicability (AOA).

| | Fresh fuel with strong absorbers | Fresh fuel without strong absorbers |
|---|---|---|
| Fissionable material | $^{235}$U | $^{235}$U |
| Isotopic composition of fuel (wt% $^{235}$U/U) | 2.35-5.70 | 2.35-4.31 |
| Physical form of fuel | $UO_2$ | $UO_2$ |
| Moderation material | $H_2O$ @~1 g/cm$^3$ | $H_2O$ @~1 g/cm$^3$ |
| Reflector material | $H_2O$ @~1 g/cm$^3$ | $H_2O$ @~1 g/cm$^3$ |
| Structural material | steel, aluminum, zirconium based materials | steel, aluminum, zirconium based materials |
| Absorber material | Boron, Ag-In-Cd, Cadmium, Gadolinium | N/A |
| Physical form of absorbers | Soluble boron, $B_4C$plates, Ag-In-Cd rods, Cd plates, $UO_2$-Gd rods | N/A |
| Soluble boron concentration (ppm) | 0-3389 | 0 |
| $^{10}$B areal density (g/cm$^2$) | 0-0.07 | 0 |
| Geometry | Square lattice | Square lattice |
| Pin pitch (cm) | 1.11-2.54 | 1.56-2.54 |
| EALF (eV) | 0.095-1.152 | 0.085-0.255 |

# 5 Conclusion

The KSH has been updated with a new PVC composition. Steel has been incorporated into the models when it has been conservative to do so, and parametric studies have been performed to evaluate the effect of a number of parameters on the neutron multiplication factor.

MCNP5 version 1.51 has been validated against 101 heterogeneous critical experiments and a B-term including the bias and its uncertainty has been determined. In the validation the cross-section files used all come from the source B-VII.0.

The conclusions specific for the KSH update and the MCNP5 validation are highlighted in the following subsections.

## 5.1 The criticality safety handbook

The postulated assertion that the updated PVC composition would be more conservative than the old composition has been verified in both KSH 12.3 and KSH 12.6. For one of the cases highlighted in the comparison section of KSH 12.3, a difference of as much as 4700 pcm is observed. While this might sound alarming, this update is based on a number of conservative assumptions. For instance, the composition of the concrete used in the MCNP simulations has been optimized for neutron reflection. The PVC chlorine content and density has been chosen to result in less absorption than what can be expected based on the analyses of the PVC used in the factory. All the calculations assume optimal moderation, while in reality there is typically either too much or too little uranium in the solution for that condition to be fulfilled. Apart from the B-term, three standard deviations are added to ensure that it is highly unlikely that the actual value of $k_{eff}$ would be higher than the calculated value. In the design process of new installations, the dimensions are also selected in a conservative way to ensure that the value of $k_{eff}$ is below the critical safety limit as defined in chapter 2.5.3. All design decision that are made based on the KSH have to be verified by a criticality safety engineer at WSE, and in any doubtful cases a more thorough analysis will be performed.

The addition of steel resulted in ambiguous results. For the cases with BFP in KSH 12.3, the addition of steel was conservative as anticipated from existing work on KSH 12.6. For the infinite systems with PVC in KSH 12.3, the parametric studies showed that it would not be conservative to include steel with a thickness corresponding to what can be expected to occur at the fuel factory. The subsequent analyses of finite and infinite slabs in KSH 12.6 revealed that it would sometimes be conservative to include steel and

sometimes not, leading to the decision to perform dual calculations where steel was included when it was conservative to do so. These findings are supported by previous advice given in KSH 11.1 to be cautious in assessing the effect of steel on the neutron multiplication factor due to a problem dependence that is hard to predict.

Parametric studies were performed for the first time for the systems in KSH 12.3 and KSH 12.6. Besides the aforementioned effect of varying the steel thickness, a visual aid has been provided for a number of other parameters and their effect on the neutron multiplication factor. The results can be used to get a qualitative description of how fluctuations in the composition of PVC affect the neutron multiplication factor, and also to evaluate the criticality safety in events such as flooding.

Updating the KSH is an ever ongoing process. As this thesis has shown, regular updates are needed to ensure that the information provided in the KSH reflects the conditions in the factory in a conservative way. The KSH can always be expanded to cover more cases with different reflectors and parameters. New geometries with updated material compositions and newer cross section libraries for MCNP, and new releases of MCNP, will have to be incorporated to more accurately describe the behavior of the neutrons in fissile materials. The work done in this thesis is meant to address the most pressing of these matters in the KSH as of now.

## 5.2 Validation

Looking at the simulation results seen in Figure 4-47, it can be noted that the normalized calculated $k_{norm}$ values for the IHECSBE cases deviate less than 300 pcm from $k_{exp}$. The NUREG/CR-6361 cases on the other hand deviate up to 600 pcm and these values also show a broader range. This is likely due to the lack of information available about these experiments. For instance the composition of different aluminum alloys used is fully specified in IHECSBE but unknown for most NUREG/CR-6361 cases. In these cases standard compositions from SCALE have been utilized which may or may not be the same as the actual materials used. Weighted analysis has been used to reduce the influence of results with a high uncertainty but the real uncertainty of the NUREG/CR-6361 cases remains unknown. Sensitivity studies to investigate the actual effect on $k_{eff}$ of these uncertainties as is done in the IHECSBE may provide a more correct estimation of the experimental uncertainty. Such a task would however be well outside the scope of this thesis.

As seen in Section 4.3.4, the B-term for fresh fuel without absorber is notably higher than for fresh fuel with absorbers. This is due to the non parametric margin of 0.01 that is

added due to the lack of data points. If 12 more experiments without strong absorbers present would be included in this validation suite the non-parametric margin would be reduced to zero and the resulting bias and B-term would likely decrease. This may also be achieved if this validation suite would be combined with the experiments featured in the previous WSE validation report [15].

It is possible to compare the obtained B-term with the results in the previous WSE validation report [15] that covers a part of the AOA of this report. In that report all heterogeneous systems investigated are analyzed as one group with the resulting B = 0.012 for uranium enriched between 3.26 wt% and 5.06 wt% and B = 0.012 to B = 0.015 at enrichments 3.26 wt% to 2.35 wt%. This value falls in between the B-terms calculated in this report which could be expected for similar validation suites. The lower B-term for the subset of fresh fuel with strong absorbers present can be explained by the high quality of the IHECSBE cases that are dominating this validation suite.

In addition to the possible future work mentioned above, the project of producing a comprehensive methodology description for criticality safety analysis continues after this thesis is finished. The remaining work includes expanding the AOA of this validation suite to spent fuel conditions with burnable absorbers and depletion credited and much more additional work mainly including other codes.

# References


[1] J.C. Dean and R.W. Tayloe, “Guide for validation of Nuclear Critical Safety Calculation Methodology”, NUREG/CR-6698, Science Applications International Corporation, Oak Ridge, TN, January 2001.

[2] World Nuclear Association, ”Nuclear Fuel Fabrication” http://world-nuclear.org/info/Nuclear-Fuel-Cycle/Conversion-Enrichment-and-Fabrication/Fuel-Fabrication/#.UYz6tkrBcoF (Updated September 2011)

[3] NUREG-0800,”Standard Review Plan for the Review of Safety Analysis Reports for Nuclear Power Plants: LWR Edition”, Section 9.1.1, “Criticality Safety of the Fresh and Spent Fuel Storage and Handling”, Revision 3, March 2007.

[4] M. W. Allsopp and G. Vianello, "Poly(Vinyl Chloride)", Ullmann's Encyclopedia of Industrial Chemistry, Wiley-VCH, Weinheim , 2012.

[5] "Substance Details CAS Registry Number: 9002-86-2", Common chemistry. CAS. http://www.commonchemistry.org/ChemicalDetail.aspx?ref=9002-86-2&terms=Polyvinyl%20chloride . Retrieved July 12, 2012

[6] National Institute of Standards and Technology, “Neutron scattering lengths and cross sections”, http://www.ncnr.nist.gov/resources/n-lengths/ (January 17 - 2013)

[7] D.F. Cadogan and C.J. Howick "Plasticizers", Ullmann's Encyclopedia of Industrial Chemistry, Wiley-VCH, Weinheim, 2000

[8] S. Glasstone and A. Sesonske, “Nuclear Reactor Engineering.” Van Nostrand Reinhold Company, New York, NY, 1981.

[9] International Atomic Energy Agency, “Survey of wet and dry spent fuel storage”, IAEA-TECDOC-1100, http://www-pub.iaea.org/MTCD/publications/PDF/te_0944_scr.pdf (1999)

[10] U. Lindelöw, WSE, Personal communication, 14 May 2013.

[11] Kärnkraftsäkerhet och Utbildning AB, ”Reaktorfysik, grundkurs”, July 2007.

[12] X-5 Monte Carlo Team, “MCNP — A General Monte Carlo N-Particle Transport Code, Version 5”, Los Alamos National Laboratory, NM, January 2008

[13] C. Demaziere “Physics of Nuclear Reactors: Lecture notes”, Chalmers University of Technology, Gothenburg, 2011.

[14] SCALE: A Modular Code System for Performing Standardized Computer Analyses for Licensing Evaluations, ORNL/TM-2005/39, Version 5.1, Vols. I–III, November 2006. Available from Radiation Safety Information Computational Center at Oak Ridge National Laboratory as CCC-732.

[15] R. Fridström, “MCNP5 Validation for Criticality Calculations: Heterogeneous Systems”, BTE-10-1493 rev 2, WSE, December 2012

[16] J.J. Lichtenwalter et al “Criticality Benchmark Guide for Light-Water-Reactor Fuel in Transportation and Storage Packages”, NUREG/CR-6361, Oak Ridge National Laboratory, Oak Ridge, TN, March 1997.

[17] G. Dodig-Crnkovic,”Metoder för kriticitetssäkerhetsanalyser”, KSH-4.1 rev1, Westinghouse Electric Sweden AB, December 2002.

[18] G. Dodig-Crnkovic, “Reflektion.”, KSH-11.1 rev 2, Westinghouse Electric Sweden AB, December 2004.

[19] G. Dodig-Crnkovic, “Materialsammansättningar som används i kriticitetssäkerhetsanalyser.”, KSH-9 rev 3 , Westinghouse Electric Sweden AB, February 2011.

[20] E. Lundin, “Sammanställning provresultat – klorhalt och densitet i PVC-plattor/insatser (fasta neutronabsorbatorer)”, BL-11-167 rev 1, Westinghouse Electric Sweden AB, July 2012.

[21] A. Libal, Principal Criticality Safety Engineer, Personal communication, WSE, 15 May 2013.

[22] A. Tronsén, ”Kritiskt säkra dimensioner för ändliga homogena system med cylindrisk eller kvadratisk bas”, KSH 12.5,WSE, February 2008.

[23] “International Handbook of Evaluated Criticality Safety Benchmark Experiments”, NEA/NCS/DOC(95)03/IV, 2009 Edition.

[24] LEU-COMP-THERM-008 “Critical Lattices of UO2 Fuel Rods and Perturbing Rods in Borated Water”, NEA/NCS/DOC(95)03/IV, 2009 Edition.

[25] LEU-COMP-THERM-001 “Water-Moderated U(2.35)O2, Fuel Rods in 2.032-cm Square-Pitched Arrays”, NEA/NCS/DOC(95)03/IV, 2009 Edition.

[26] LEU-COMP-THERM-016 “Water-Moderated Rectangular Clusters of U(2.35)O2, Fuel Rods (2.032-cm Pitch) Separated by Steel, Boral, Copper, Cadmium, Aluminum or Zircaloy-4 Plates”, NEA/NCS/DOC(95)03/IV, 2009 Edition.

[27] LEU-COMP-THERM-002 “Water-Moderated U(4.31)O2, Fuel Rods in 2.54-cm Square-Pitched Array”, NEA/NCS/DOC(95)03/IV, 2009 Edition.

[28] LEU-COMP-THERM-009 “Water-Moderated Rectangular Clusters of U(4.31)O2 Fuel Rods (2.54-cm Pitch) Separated by Steel, Boral, Copper, Cadmium, Aluminum or Zircaloy-4 Plates”, NEA/NCS/DOC(95)03/IV, 2009 Edition.

[29] LEU-COMP-THERM-011 “Critical Experiments Supporting Close Proximity Water Storage of Power Reactor Fuel. Part 1 – Absorber Rods”, NEA/NCS/DOC(95)03/IV, 2009 Edition.

[30] LEU-COMP-THERM-042 “Water-Moderated Rectangular Clusters of U(2.35)O2, Fuel Rods(1.684-cm Pitch) Separated by Steel, Boral, Boraflex, Cadmium, or Copper Plates with Steel Reflecting Walls”, NEA/NCS/DOC(95)03/IV, 2009 Edition.

[31] R.D. Leamer, D.F. Hanlen, G.N. Hamilton and E.G. Taylor, “Critical Experiments Performed with Clustered & Uniform Arrays of Rodded Absorbers”, WCAP-3269-39. Westinghouse Electric Corp., November 1965.

[32] National Nuclear Data Center, “Cross Section Evaluation Working Group (CSEWG)” http://www.nndc.bnl.gov/csewg/, (April 21 – 2013).

[33] P. Behrenz,”Kriticitetssäkerhet – jämförelse mellan olika reflektorer.”, ASEA-ATOM, 1985.

[34] G. Choppin, J. Rydberg and J-O. Liljenzin, “Radiochemistry and Nuclear Chemistry”, 3rd Ed, Butterworth-Heinemann, Woburn, MA, November 2001.

# Appendix I – Critical conditions for the validated benchmarking experiments

The tables below summarize the critical conditions for the experiments included in the validation suite. Critical data for LEU-COMP THERM-001 through -042 are given in Table A1-1 through A1-6. The critical conditions for the NUREG/CR-6361 cases are given in Table A1-7.

Note that while aluminum, zircaloy-4 and stainless steel are entered as absorber materials in Table A1-3, Table A1-5 and Table A1-7, these materials are weak absorbers and are listed as structural materials in Section 3.3.1 and Table 4-12. Experiments that only use these materials and none of the absorbers listed in 3.3.1 belong to the fresh fuel without strong absorbers category.

**Table A1-1.** Critical data for LEU-COMP-THERM-001 and -002. Data from [23].

| LEU-COMP-THERM- | Number of clusters | Cluster size | Enrichment (wt%$^{235}$U/U) | Pitch (cm) | Separation between clusters (mm) |
|---|---|---|---|---|---|
| 001-1 | 1 | 20x18.08[4] | 2.35 | 2.032 | - |
| 001-2 | 3 | 20x17 | 2.35 | 2.032 | 119.2 |
| 001-3 | 3 | 20x16 | 2.35 | 2.032 | 84.1 |
| 001-4 | 3 | 20x16 (center) 22x16 (outer) | 2.35 | 2.032 | 100.5 |
| 001-5 | 3 | 20x15 | 2.35 | 2.032 | 63.9 |
| 001-6 | 3 | 20x15 (center) 24x15 (outer) | 2.35 | 2.032 | 80.1 |
| 001-7 | 3 | 20x14 | 2.35 | 2.032 | 44.6 |
| 001-8 | 3 | 19x16 | 2.35 | 2.032 | 75.7 |
| 002-1 | 1 | 10x11.51[4] | 4.306 | 2.54 | - |
| 002-2 | 1 | 9x13.35[4] | 4.306 | 2.54 | - |
| 002-3 | 1 | 8x16.37[4] | 4.306 | 2.54 | - |
| 002-4 | 3 | 15x8 | 4.306 | 2.54 | 106.2 |

[4] Partial row

**Table A1-2.** Critical data for LEU-COMP-THERM-008. Data from [24].

| LEU-COMP-THERM- | Enrichment (wt% $^{235}$U/U) | Pitch (cm) | Number of fuel rods | Number of water holes | Number of $Al_2O_3$ rods | Soluble Boron Concentration (ppm) |
|---|---|---|---|---|---|---|
| 008-1 | 2.459 | 1.63576 | 4961 | 0 | 0 | 1511 |
| 008-2 | 2.459 | 1.63576 | 4808 | 153 | 0 | 1335.5 |
| 008-3 | 2.459 | 1.63576 | 4808 | 153 | 0 | 1335.5 |
| 008-11 | 2.459 | 1.63576 | 4808 | 9 | 144 | 1384 |
| 008-12 | 2.459 | 1.63576 | 4808 | 117 | 36 | 1348 |
| 008-14 | 2.459 | 1.63576 | 4808 | 81 | 72 | 1362.5 |
| 008-16 | 2.459 | 1.63576 | 4691 | 270 | 0 | 1158 |
| 008-17 | 2.459 | 1.63576 | 4457 | 504 | 0 | 921 |

**Table A1-3.** Critical data for LEU-COMP-THERM-009. Data from [28].

| LEU-COMP-THERM-009- | Number of clusters | Cluster size | Enrichment (wt%) | Pitch (cm) | Absorber Plate Material | plate thickness (mm) | Separation between clusters (mm) | Separation between plates and center cluster (mm) | $^{10}$B-areal density (g/cm$^2$) |
|---|---|---|---|---|---|---|---|---|---|
| 1 | 3 | 15x8 | 4.306 | 2.54 | SS | 4.85 | 85.8 | 2.45 | 0.0 |
| 2 | 3 | 15x8 | 4.306 | 2.54 | SS | 4.85 | 96.5 | 32.77 | 0.0 |
| 3 | 3 | 15x8 | 4.306 | 2.54 | SS | 3.02 | 92.2 | 4.28 | 0.0 |
| 4 | 3 | 15x8 | 4.306 | 2.54 | SS | 3.02 | 97.6 | 32.77 | 0.0 |
| 5 | 3 | 15x8 | 4.306 | 2.54 | SS 1.05wt%B | 2.98 | 61.0 | 4.32 | 0.0046 |
| 6 | 3 | 15x8 | 4.306 | 2.54 | SS 1.05wt%B | 2.98 | 80.8 | 32.77 | 0.0046 |
| 7 | 3 | 15x8 | 4.306 | 2.54 | SS 1.05wt%B | 2.98 | 57.6 | 4.32 | 0.0069 |
| 8 | 3 | 15x8 | 4.306 | 2.54 | SS 1.05wt%B | 2.98 | 79.0 | 32.77 | 0.0069 |
| 9 | 3 | 15x8 | 4.306 | 2.54 | Boral | 7.13[5] | 67.2 | 32.77 | 0.067 |
| 16 | 3 | 15x8 | 4.306 | 2.54 | Cadmium | 0.291 | 59.3 | 7.009 | 0.0 |
| 17 | 3 | 15x8 | 4.306 | 2.54 | Cadmium | 0.291 | 74.2 | 32.77 | 0.0 |
| 18 | 3 | 15x8 | 4.306 | 2.54 | Cadmium | 0.610 | 59.6 | 6.69 | 0.0 |
| 19 | 3 | 15x8 | 4.306 | 2.54 | Cadmium | 0.610 | 74.2 | 32.77 | 0.0 |
| 20 | 3 | 15x8 | 4.306 | 2.54 | Cadmium | 0.901 | 58.7 | 6.40 | 0.0 |
| 21 | 3 | 15x8 | 4.306 | 2.54 | Cadmium | 0.901 | 73.8 | 32.77 | 0.0 |
| 22 | 3 | 15x8 | 4.306 | 2.54 | Cadmium | 2.006 | 56.8 | 5.29 | 0.0 |
| 23 | 3 | 15x8 | 4.306 | 2.54 | Cadmium | 2.006 | 72.8 | 32.77 | 0.0 |
| 26 | 3 | 15x8 | 4.306 | 2.54 | Aluminum | 6.52 | 109.2 | 0.78 | 0.0 |
| 27 | 3 | 15x8 | 4.306 | 2.54 | Aluminum | 6.52 | 108.6 | 32.77 | 0.0 |

[5] The Boral plate thickness includes aluminum cladding

**Table A1-4.** Critical data for LEU-COMP-THERM-011. Data from [29].

| LEU-COMP-THERM-011- | Number of clusters | cluster size | Enrichment (wt% $^{235}$U/U) | pitch (cm) | boron concentration (ppm) | Water level (cm) |
|---|---|---|---|---|---|---|
| 1 | 1 | 438 | 2.5 | 1.636 | 0 | 143.88 |
| 2 | 9 | 14x14 | 2.5 | 1.636 | 1037 | 144.29 |
| 3 | 9 | 14x14 | 2.5 | 1.636 | 769 | 148.63 |
| 4 | 9 | 14x14 | 2.5 | 1.636 | 764 | 144.88 |
| 5 | 9 | 14x14 | 2.5 | 1.636 | 762 | 140.38 |
| 6 | 9 | 14x14 | 2.5 | 1.636 | 753 | 131.32 |
| 7 | 9 | 14x14 | 2.5 | 1.636 | 739 | 120.64 |
| 8 | 9 | 14x14 | 2.5 | 1.636 | 721 | 110.04 |
| 9 | 9 | 14x14 | 2.5 | 1.636 | 702 | 100.32 |

**Table A1-5.** Critical conditions for the experiment suite LEU-COMP-THERM-016. Data from [26].

| LEU-COMP-THERM-016- | Number of clusters | Cluster size | Enrichment wt% $^{235}U/U$ | Pitch (cm) | Absorber Plate Material | plate thickness (mm) | Separation between clusters (mm) | Distance plate to center cluster (mm) | $^{10}B$-areal density (g/cm$^2$) |
|---|---|---|---|---|---|---|---|---|---|
| 1 | 3 | 20x16 | 2.35 | 2.032 | SS | 4.85 | 68.8 | 6.45 | 0.0 |
| 2 | 3 | 20x16 | 2.35 | 2.032 | SS | 4.85 | 76.4 | 27.32 | 0.0 |
| 3 | 3 | 20x16 | 2.35 | 2.032 | SS | 4.85 | 75.1 | 40.42 | 0.0 |
| 4 | 3 | 20x16 | 2.35 | 2.032 | SS | 3.02 | 74.2 | 6.45 | 0.0 |
| 5 | 3 | 20x16 | 2.35 | 2.032 | SS | 3.02 | 77.6 | 40.42 | 0.0 |
| 6 | 3 | 20x17 | 2.35 | 2.032 | SS | 3.02 | 104.4 | 6.45 | 0.0 |
| 7 | 3 | 20x17 | 2.35 | 2.032 | SS | 3.02 | 114.7 | 40.42 | 0.0 |
| 8 | 3 | 20x17 | 2.35 | 2.032 | SS 1.05 wt%B | 2.98 | 75.6 | 6.45 | 0.0046 |
| 9 | 3 | 20x17 | 2.35 | 2.032 | SS 1.05 wt%B | 2.98 | 96.2 | 40.42 | 0.0046 |
| 10 | 3 | 20x17 | 2.35 | 2.032 | SS 1.62 wt%B | 2.98 | 73.6 | 6.45 | 0.0069 |
| 11 | 3 | 20x17 | 2.35 | 2.032 | SS 1.62 wt%B | 2.98 | 95.2 | 40.42 | 0.0069 |
| 12 | 3 | 20x17 | 2.35 | 2.032 | Boral | 7.13[6] | 63.3 | 6.45 | 0.067 |
| 13 | 3 | 20x17<br>20x16<br>(center)<br>22x16 | 2.35 | 2.032 | Boral | 7.13[6] | 90.3 | 44.42 | 0.067 |
| 14 | 3 | (outer) | 2.35 | 2.032 | Boral | 7.13[6] | 50.5 | 6.45 | 0.067 |
| 21 | 3 | 20x17 | 2.35 | 2.032 | Cadmium | 0.610 | 67.4 | 6.45 | 0.0 |
| 22 | 3 | 20x17 | 2.35 | 2.032 | Cadmium | 0.610 | 76.0 | 14.82 | 0.0 |
| 23 | 3 | 20x17 | 2.35 | 2.032 | Cadmium | 0.610 | 93.7 | 40.42 | 0.0 |
| 24 | 3 | 20x17 | 2.35 | 2.032 | Cadmium | 0.291 | 77.8 | 14.82 | 0.0 |
| 25 | 3 | 20x17 | 2.35 | 2.032 | Cadmium | 0.291 | 94.0 | 40.42 | 0.0 |
| 26 | 3 | 20x17 | 2.35 | 2.032 | Cadmium | 0.901 | 75.4 | 14.82 | 0.0 |
| 27 | 3 | 20x17 | 2.35 | 2.032 | Cadmium | 0.901 | 93.9 | 40.42 | 0.0 |
| 31 | 3 | 20x16 | 2.35 | 2.032 | Zircaloy-4 | 6.52 | 87.9 | 6.45 | 0.0 |
| 32 | 3 | 20x16 | 2.35 | 2.032 | Zircaloy-4 | 6.52 | 87.8 | 40.42 | 0.0 |

[6] Boral plate thickness includes aluminum cladding

**Table A1-6.** Critical conditions for the experiment suite LEU-COMP-THERM-042. Data from [30].

| LEU-COMP-THERM-042- | Number of clusters | Cluster size | Enrichment wt% $^{235}$U/U | Pitch (cm) | Plate Material | plate thickness (mm) | Separation between clusters (mm) | $^{10}$B-areal density (g/cm$^2$) |
|---|---|---|---|---|---|---|---|---|
| 1 | 3 | 25x18 (center)<br>20x18 (outer) | 2.35 | 1.684 | SS | 3.02 | 78.66 | 0.0 |
| 2 | 3 | 25x18 (center)<br>20x18 (outer) | 2.35 | 1.684 | SS<br>1.05 wt%B | 2.98 | 43.86 | 0.0046 |
| 3 | 3 | 25x18 (center)<br>20x18 (outer) | 2.35 | 1.684 | Boral B | 2.16[7] | 22.76 | 0.0302 |
| 5 | 3 | 25x18 (center)<br>20x18 (outer) | 2.35 | 1.684 | Cadmium | 0.610[8] | 34.46 | 0.0 |

[7] Boral B plate thickness includes aluminum cladding

[8] Cadmium plate thickness includes Plexiglas plates that the cadmium plates are mounted on.

**Table A1-7.** Critical conditions for the featured experiments from the Criticality Benchmark Guide for Light-Water-Reactor Fuel in Transportation and Storage Packages, NUREG/CR-6361. Data from [16]

| Experiment | Enrichment (wt%$^{235}$U/U) | Pitch (cm) | Absorber Material | Boron Concentration (ppm) | Number of rods or assemblies (rods) | Number of water holes | Water Level[9] (cm) |
|---|---|---|---|---|---|---|---|
| B1645SO1 | 2.459 | 1.4097 | Aluminum | 1068 | 25(13x13)[10] | - | 101.81[11] |
| B1645SO2 | 2.459 | 1.4097 | Aluminum | 1156 | 25(13x13) [10] | - | 144.85[11] |
| BW1231B1 | 4.020 | 1.511 | - | 1152 | 936 | - | 167.5[11] |
| BW1231B2 | 4.020 | 1.511 | - | 3389 | 4904 | - | 146.65[11] |
| BW1237M | 2.459 | 1.511 | - | 1675 | 5137 | - | 93.2[11] |
| BW1810A | 2.457 | 1.636 | - | 1239.3 | 4788[12]+ 20[13] | 153 | 145 |
| BW1810B | 2.455 | 1.636 | - | 1170.7 | 4772[12]+36[13] | 153 | 145 |
| BW1810C | 2.764 | 1.636 | - | 1499 | 3676[12]+912[14]+32[13] | 180 | 145 |
| BW1810D | 2.735 | 1.636 | - | 1653.8 | 3920[12]+860[14]+28[13] | 153 | 145 |
| BW1810E | 2.732 | 1.636 | - | 1579.4 | 3920[12]+852[14]+36[13] | 153 | 145 |
| BW1810F | 2.459 | 1.636 | - | 1337.9 | 4808[12] | 153 | 145 |
| BW1810G | 2.778 | 1.636 | - | 1776.8 | 3676[12]+944[14] | 180 | 145 |
| BW1810H | 2.747 | 1.636 | - | 1899.3 | 3920[12]+888[14] | 153 | 145 |
| BW1810I | 2.459 | 1.636 | Ag-In-Cd | 1250 | 4808[12] | 137 | 145 |
| EPRU65 | 2.35 | 1.562 | - | 0.9 | 708 | - | 111.76 |
| EPRU65B | 2.35 | 1.562 | - | 463.8 | 1201 | - | 111.76 |
| EPRU75 | 2.35 | 1.905 | - | 0.5 | 383 | - | 112.08 |
| EPRU75B | 2.35 | 1.905 | - | 568.1 | 1201 | - | 112.08 |
| EPRU87 | 2.35 | 2.21 | - | 0.9 | 342 | - | 111.76 |
| EPRU87B | 2.35 | 2.21 | - | 285.8 | 885 | - | 111.76 |
| W3269A | 5.7 | 1.422 | Ag-In-Cd | 0 | 453 | - | 88.27[11] |
| W3269B1 | 3.7 | 1.105 | Ag-In-Cd | 0 | 2221 | - | 55.41[11] |
| W3269B2 | 3.7 | 1.105 | Ag-In-Cd | 0 | 2209 | - | 64.56[11] |
| W3269B3 | 3.7 | 1.105 | Ag-In-Cd | 0 | 2185 | - | 57.00[11] |
| W3269C | 2.72 | 1.524 | Ag-In-Cd | 0 | 945 | - | 89.75[11] |

[9] Measured from top of base plate (unless otherwise stated)

[10] With corner Al-rods

[11] Measured from bottom of fuel

[12] Enrichment: 2.459 wt%

[13] Enrichment: 1.944 wt% with 4.00 wt% $Gd_2O_3$

[14] Enrichment: 4.020 wt%

# Appendix II – Tables of results for KSH 12.3 and 12.6

The following tables summarize the information presented in the figures for KSH 12.3 and 12.6.

## KSH 12.3

The results for the critically safe dimensions (the intersection of the curves with the k = 0.95 line) from KSH 12.3 are summarized in the tables below. The critically safe dimensions have been rounded down to one decimal.
The results for the infinite cylinders are shown in Table A2-1.

**Table A2-1.** Critically safe inner diameters for infinite cylinders filled with optimally moderated $UO_2$ in water with/without absorbers surrounded by water/concrete reflectors.

| Reflector | Absorber | Critically safe inner diameter (cm) |
|---|---|---|
| Concrete | None | 19.1 |
| Water | None | 22.2 |
| Concrete | 0.64 cm BFP | 23.9 |
| Water | 0.64 cm BFP | 27.2 |
| Concrete | 0.9 cm PVC | 21.6 |
| Water | 0.9 cm PVC | 25.4 |

The results for the finite cylinders are shown in Table A2-2 through A2-4.

**Table A2-2.** Critically safe inner diameters for finite cylinders filled with optimally moderated $UO_2$ in water without absorber, surrounded by water/concrete reflectors.

| Reflector | Absorber | Height (cm) | Critically safe inner diameter (cm) |
|---|---|---|---|
| Concrete | None | 50 | 22.9 |
| Concrete | None | 100 | 20.5 |
| Concrete | None | 200 | 19.6 |
| Water | None | 50 | 24.9 |
| Water | None | 100 | 23.1 |
| Water | None | 200 | 22.5 |

**Table A2-3.** Critically safe inner diameters for finite cylinders filled with optimally moderated $UO_2$ in water with BFP as an absorber, surrounded by water/concrete reflectors.

| Reflector | Absorber | Height (cm) | Critically safe inner diameter (cm) |
|---|---|---|---|
| Concrete | 0.64 cm BFP | 50 | 26.8 |
| Concrete | 0.64 cm BFP | 100 | 24.8 |
| Concrete | 0.64 cm BFP | 200 | 24.2 |
| Water | 0.64 cm BFP | 50 | 29.9 |
| Water | 0.64 cm BFP | 100 | 27.9 |
| Water | 0.64 cm BFP | 200 | 27.4 |

**Table A2-4.** Critically safe inner diameters for finite cylinders filled with optimally moderated $UO_2$ in water with PVC as an absorber, surrounded by water/concrete reflectors.

| Reflector | Absorber | Height (cm) | Critically safe inner diameter (cm) |
|---|---|---|---|
| Concrete | 0.9 cm PVC | 50 | 24.8 |
| Concrete | 0.9 cm PVC | 100 | 22.7 |
| Concrete | 0.9 cm PVC | 200 | 22.0 |
| Water | 0.9 cm PVC | 50 | 28.1 |
| Water | 0.9 cm PVC | 100 | 26.2 |
| Water | 0.9 cm PVC | 200 | 25.6 |

The results for slabs infinite in two dimensions are shown in Table A2-5.

**Table A2-5.** Critically safe inner widths for slabs infinite in two dimensions filled with optimally moderated $UO_2$ and surrounded by water/concrete reflectors.

| Reflector | Absorber | Critically safe inner width (cm) |
|---|---|---|
| Concrete | None | 4.5 |
| Water | None | 9.9 |
| Water + Concrete | None | 7.2 |
| Concrete | 0.64 cm BFP | 11.3 |
| Water | 0.64 cm BFP | 14.9 |
| Concrete | 1.3 cm PVC | 9.5 |
| Water | 1.3 cm PVC | 13.6 |

The results for slabs infinite in one dimension are shown in Table A2-6 through A2-11.

**Table A2-6.** Critically safe inner widths for slabs infinite in one dimension filled with optimally moderated $UO_2$ in water, without absorbers and surrounded by water reflectors.

| Reflector | Absorber | Depth (cm) | Critically safe inner width (cm) |
|---|---|---|---|
| Water | None | 5 | [Critically safe up to 140 cm] |
| Water | None | 7 | [Critically safe up to 140 cm] |
| Water | None | 9 | [Critically safe up to 140 cm] |
| Water | None | 11 | 69.9 |
| Water | None | 13 | 37.8 |
| Water | None | 15 | [Not critically safe] |

**Table A2-7.** Critically safe inner widths for slabs infinite in one dimension filled with optimally moderated $UO_2$ in water, without absorbers and surrounded by concrete reflectors.

| Reflector | Absorber | Depth (cm) | Critically safe inner width (cm) |
|---|---|---|---|
| Concrete | None | 5 | [Critically safe up to 140 cm] |
| Concrete | None | 6 | 91.2 |
| Concrete | None | 7 | 62.8 |
| Concrete | None | 8 | 48.1 |
| Concrete | None | 9 | 38.9 |

**Table A2-8.** Critically safe inner widths for slabs infinite in one dimension filled with optimally moderated $UO_2$ in water, with BFP as an absorber and surrounded by water reflectors.

| Reflector | Absorber | Depth (cm) | Critically safe inner width (cm) |
|---|---|---|---|
| Water | 0.64 cm BFP | 10 | [Critically safe up to 140 cm] |
| Water | 0.64 cm BFP | 12 | [Critically safe up to 140 cm] |
| Water | 0.64 cm BFP | 14 | [Critically safe up to 140 cm] |
| Water | 0.64 cm BFP | 16 | 67.7 |
| Water | 0.64 cm BFP | 18 | 36.9 |

**Table A2-9.** Critically safe inner widths for slabs infinite in one dimension filled with optimally moderated $UO_2$ in water, with BFP as an absorber and surrounded by concrete reflectors.

| Reflector | Absorber | Depth (cm) | Critically safe inner width (cm) |
|---|---|---|---|
| Concrete | 0.64 cm BFP | 8 | [Critically safe up to 140 cm] |
| Concrete | 0.64 cm BFP | 10 | [Critically safe up to 140 cm] |
| Concrete | 0.64 cm BFP | 12 | 96.8 |
| Concrete | 0.64 cm BFP | 14 | 41.0 |
| Concrete | 0.64 cm BFP | 16 | [Not critically safe] |
| Concrete | 0.64 cm BFP | 18 | [Not critically safe] |

**Table A2-10.** Critically safe inner widths for slabs infinite in one dimension filled with optimally moderated $UO_2$ in water, with PVC as an absorber and surrounded by water reflectors.

| Reflector | Absorber | Depth (cm) | Critically safe inner width (cm) |
|---|---|---|---|
| Water | 1.3 cm PVC | 10 | [Critically safe up to 140 cm] |
| Water | 1.3 cm PVC | 12 | [Critically safe up to 140 cm] |
| Water | 1.3 cm PVC | 14 | 128.6 |
| Water | 1.3 cm PVC | 16 | 42.9 |
| Water | 1.3 cm PVC | 18 | 30.2 |

**Table A2-11.** Critically safe inner widths for slabs infinite in one dimension filled with optimally moderated $UO_2$ in water, with PVC as an absorber and surrounded by concrete reflectors.

| Reflector | Absorber | Depth (cm) | Critically safe inner width (cm) |
|---|---|---|---|
| Concrete | 1.3 cm PVC | 8 | [Critically safe up to 140 cm] |
| Concrete | 1.3 cm PVC | 10 | [Critically safe up to 140 cm] |
| Concrete | 1.3 cm PVC | 12 | 46.6 |
| Concrete | 1.3 cm PVC | 14 | 30.5 |
| Concrete | 1.3 cm PVC | 16 | [Not critically safe] |
| Concrete | 1.3 cm PVC | 18 | [Not critically safe] |

# KSH 12.6

In a similar way to KSH 12.3, the critically safe thicknesses for infinite and finite systems are presented below.

The results for the infinite systems (the dashed lines in the results section) are shown in Table A2-12 below.

**Table A2-12**. Critically safe dimensions for systems with an infinite base area containing different uranium compounds with BFP or PVC as an absorber on one or two sides, reflected by either concrete and/or water.

| System | Reflector | UO2 + H2O (cm U-compound) | UNH + H2O (cm U-compound) |
|---|---|---|---|
| 0.64 cm BFP on one side | 30 cm water | 12.4 | 18.8 |
| 0.64 cm BFP on two sides | 30 cm water | 14.7 | 21.3 |
| 1.3 cm PVC on one side | 30 cm water | 11.8 | 18.2 |
| 1.3 cm PVC on two sides | 30 cm water | 13.6 | 20.1 |
| 1.3 cm PVC on the concrete side | 50 cm concrete corner | 9.7 | - |
| 1.3 cm PVC on the water side | 50 cm concrete corner | 9.1 | - |
| 1.3 cm PVC on two sides | 50 cm concrete corner | 11.6 | - |

The results for the finite systems are shown in Table A2-13 through A2-15 below.

**Table A2-13.** Critically safe dimensions for finite slabs containing $UO_2$ + $H_2O$ with BFP or PVC as an absorber on one or two sides, surrounded by a 30 cm water reflector.

| Area ($m^2$) | 0.64 cm BFP on one side (cm U-compound) | 0.64 cm BFP on two sides (cm U-compound) | 1.3 cm PVC on one side (cm U-compound) | 1.3 cm PVC on two sides (cm U-compound) |
|---|---|---|---|---|
| 0.1600 | 19.0 | 21.2 | 18.3 | 20.1 |
| 0.2500 | 16.5 | 18.8 | 15.9 | 17.7 |
| 0.3600 | 15.3 | 17.5 | 14.6 | 16.4 |
| 0.5625 | 14.3 | 16.6 | 13.7 | 15.5 |
| 1.0000 | 13.5 | 15.8 | 12.9 | 14.7 |
| 4.0000 | 12.7 | 15.0 | 12.1 | 13.9 |
| Infinite | 12.4 | 14.7 | 11.8 | 13.6 |

**Table A2-14.** Critically safe dimensions for finite slabs containing UNH + $H_2O$ with BFP or PVC as an absorber on one or two sides, surrounded by a 30 cm water reflector.

| Area (m2) | 0.64 cm BFP on one side (cm U-compound) | 0.64 cm BFP on two sides (cm U-compound) | 1.3 cm PVC on one side (cm U-compound) | 1.3 cm PVC on two sides (cm U-compound) |
|---|---|---|---|---|
| 0.1600 | 38.4 | 40.7 | 37.5 | 39.3 |
| 0.2500 | 29.3 | 31.6 | 28.6 | 30.4 |
| 0.3600 | 25.7 | 28.0 | 25.0 | 26.9 |
| 0.5625 | 23.1 | 25.5 | 22.5 | 24.3 |
| 1.0000 | 21.3 | 23.4 | 20.6 | 22.5 |
| 4.0000 | 19.4 | 21.9 | 18.8 | 20.7 |
| Infinite | 18.8 | 21.3 | 18.2 | 20.1 |

**Table A2-15.** Critically safe dimensions for finite slabs containing $UO_2$ + $H_2O$ placed in a concrete corner with PVC as an absorber on one or two sides.

| Area (m2) | 1.3 cm PVC on the side with concrete (cm U-compound) | 1.3 cm PVC on the side with water (cm U-compound) | 1.3 cm PVC on two sides (cm U-compound) |
|---|---|---|---|
| 0.1600 | 16.7 | 17.2 | 18.5 |
| 0.2500 | 14.3 | 14.6 | 16.1 |
| 0.3600 | 13.0 | 13.2 | 14.8 |
| 0.5625 | 11.9 | 12.0 | 13.8 |
| 1.0000 | 11.1 | 10.9 | 12.9 |
| 4.0000 | 10.1 | 9.7 | 12.0 |
| Infinite | 9.7 | 9.1 | 11.6 |

The results for the systems with a missing piece of an absorber (the factors that are plotted against a certain area of the hole in the absorber) are shown in Table A2-16 below.

**Table A2-16.** Critically safe dimensions for finite slabs with or without a missing piece of an absorber with BFP or PVC as an absorber on one or two sides. Factors for calculating the maximum thickness for different areas of the holes given a certain base area of the slab are also presented. Values in bold text conservatively cover the other factors for a given area.

| | | BFP on one side | | BFP on two sides | | PVC on one side | | PVC on two sides | |
|---|---|---|---|---|---|---|---|---|---|
| Area ($m^2$) | Area of the hole ($dm^2$) | Thickness (cm) | Factor (-) | Thickness (cm) | Factor (-) | Thickness (cm) | Factor (-) | Thickness (cm) | Factor (-) |
| >0.16 | 0 | 19.0 | 1.000 | 21.2 | 1.000 | 18.3 | 1.000 | 20.1 | 1.000 |
| | 1 | 18.5 | 0.976 | 20.7 | 0.978 | 17.7 | **0.968** | 19.4 | 0.969 |
| | 2 | 17.9 | 0.943 | 20.2 | 0.951 | 17.1 | **0.933** | 18.8 | 0.938 |
| | 3 | 17.3 | 0.912 | 19.5 | 0.920 | 16.4 | **0.898** | 18.2 | 0.907 |
| | 4 | 16.7 | 0.877 | 18.9 | 0.891 | 15.8 | **0.864** | 17.6 | 0.876 |
| | 5 | 16.1 | 0.846 | 18.3 | 0.865 | 15.2 | **0.833** | 17.0 | 0.847 |
| >4.00 | 0 | 12.7 | 1.000 | 15.0 | 1.000 | 12.1 | 1.000 | 13.9 | 1.000 |
| | 1 | 12.7 | 0.997 | 15.0 | 0.999 | 12.0 | **0.995** | 13.8 | 0.996 |
| | 2 | 12.6 | 0.991 | 14.9 | 0.994 | 11.9 | **0.989** | 13.8 | 0.991 |
| | 3 | 12.5 | 0.984 | 14.8 | 0.989 | 11.8 | **0.981** | 13.7 | 0.984 |
| | 4 | 12.3 | 0.972 | 14.7 | 0.980 | 11.7 | **0.969** | 13.5 | 0.974 |
| | 5 | 12.2 | 0.960 | 14.5 | 0.970 | 11.5 | **0.955** | 13.4 | 0.962 |

# Appendix III - Cross-Section Libraries for 293.6 Kelvin

**Table A3-1.** Cross section libraries for 293.6 Kelvin.

| Table | Data file | Table | Data file |
|---|---|---|---|
| 1001.70c | endf70a/ B-VII.0:x | 22048.70c | endf70a/ B-VII.0 |
| 5010.70c | endf70a/ B-VII.0 | 22049.70c | endf70a/ B-VII.0 |
| 5011.70c | endf70a/ B-VII.0 | 22050.70c | endf70a/ B-VII.0 |
| 6000.70c | endf70a/ B-VII.0 | 23000.70c | endf70a/ B-VII.0 |
| 7014.70c | endf70a/ B-VII.0 | 24050.70c | endf70b/ B-VII.0 |
| 7015.70c | endf70a/ B-VII.0 | 24052.70c | endf70b/ B-VII.0 |
| 8016.70c | endf70a/ B-VII.0 | 24053.70c | endf70b/ B-VII.0 |
| 9019.70c | endf70a/ B-VII.0 | 24054.70c | endf70b/ B-VII.0 |
| 11023.70c | endf70a/ B-VII.0 | 25055.70c | endf70b/ B-VII.0 |
| 12024.70c | endf70a/ B-VII.0 | 26054.70c | endf70b/ B-VII.0 |
| 12025.70c | endf70a/ B-VII.0 | 26056.70c | endf70b/ B-VII.0 |
| 12026.70c | endf70a/ B-VII.0 | 26057.70c | endf70b/ B-VII.0 |
| 13027.70c | endf70a/ B-VII.0 | 26058.70c | endf70b/ B-VII.0 |
| 14028.70c | endf70a/ B-VII.0 | 27059.70c | endf70b/ B-VII.0 |
| 14029.70c | endf70a/ B-VII.0 | 28058.70c | endf70b/ B-VII.0 |
| 14030.70c | endf70a/ B-VII.0 | 28060.70c | endf70b/ B-VII.0 |
| 15031.70c | endf70a/ B-VII.0 | 28061.70c | endf70b/ B-VII.0 |
| 16032.70c | endf70a/ B-VII.0 | 28062.70c | endf70b/ B-VII.0 |
| 16033.70c | endf70a/ B-VII.0 | 28064.70c | endf70b/ B-VII.0 |
| 16034.70c | endf70a/ B-VII.0 | 29063.70c | endf70b/ B-VII.0 |
| 16036.70c | endf70a/ B-VII.0 | 29065.70c | endf70b/ B-VII.0 |
| 19039.70c | endf70a/ B-VII.0 | 30000.70c | endf70b/ B-VII.0 |
| 19040.70c | endf70a/ B-VII.0 | 40090.70c | endf70c/ B-VII.0 |
| 19041.70c | endf70a/ B-VII.0 | 40091.70c | endf70c/ B-VII.0 |
| 20040.70c | endf70a/ B-VII.0 | 40092.70c | endf70c/ B-VII.0 |
| 20042.70c | endf70a/ B-VII.0 | 40094.70c | endf70c/ B-VII.0 |
| 20043.70c | endf70a/ B-VII.0 | 40096.70c | endf70c/ B-VII.0:x |
| 20044.70c | endf70a/ B-VII.0 | 42092.70c | endf70c/ B-VII.0 |
| 20046.70c | endf70a/ B-VII.0 | 42094.70c | endf70c/ B-VII.0 |
| 20048.70c | endf70a/ B-VII.0 | 42095.70c | endf70c/ B-VII.0 |
| 22046.70c | endf70a/ B-VII.0 | 42096.70c | endf70c/ B-VII.0 |
| 22047.70c | endf70a/ B-VII.0 | 42097.70c | endf70c/ B-VII.0:x |

**Table A3-2.** Cross section libraries for 293.6 Kelvin.

| Table | Data file | Table | Data file |
|---|---|---|---|
| 42098.70c | endf70c/ B-VII.0 | 72174.70c | endf70i/ B-VII.0 |
| 42100.70c | endf70c/ B-VII.0 | 72176.70c | endf70i/ B-VII.0 |
| 47107.70c | endf70d/ B-VII.0 | 72177.70c | endf70i/ B-VII.0 |
| 47109.70c | endf70d/ B-VII.0 | 72178.70c | endf70i/ B-VII.0 |
| 48106.70c | endf70d/ B-VII.0 | 72179.70c | endf70i/ B-VII.0 |
| 48108.70c | endf70d/ B-VII.0 | 72180.70c | endf70i/ B-VII.0 |
| 48110.70c | endf70d/ B-VII.0 | 74182.70c | endf70i/ B-VII.0 |
| 48111.70c | endf70d/ B-VII.0 | 74183.70c | endf70i/ B-VII.0 |
| 48112.70c | endf70d/ B-VII.0 | 74184.70c | endf70i/ B-VII.0 |
| 48113.70c | endf70d/ B-VII.0 | 74186.70c | endf70i/ B-VII.0 |
| 48114.70c | endf70d/ B-VII.0 | 82204.70c | endf70i/ B-VII.0 |
| 48116.70c | endf70d/ B-VII.0 | 82206.70c | endf70i/ B-VII.0 |
| 49113.70c | endf70e/ B-VII.0 | 82207.70c | endf70i/ B-VII.0 |
| 49115.70c | endf70e/ B-VII.0 | 82208.70c | endf70i/ B-VII.0 |
| 50112.70c | endf70e/ B-VII.0 | 83209.70c | endf70i/ B-VII.0 |
| 50114.70c | endf70e/ B-VII.0 | 92234.70c | endf70j/ B-VII.0 |
| 50115.70c | endf70e/ B-VII.0 | 92235.70c | endf70j/ B-VII.0 |
| 50116.70c | endf70e/ B-VII.0 | 92236.70c | endf70j/ B-VII.0 |
| 50117.70c | endf70e/ B-VII.0 | 92238.70c | endf70j/ B-VII.0 |
| 50118.70c | endf70e/ B-VII.0 | | |
| 50119.70c | endf70e/ B-VII.0 | | |
| 50120.70c | endf70e/ B-VII.0 | | |
| 50122.70c | endf70e/ B-VII.0 | S(α,β) data | Data file |
| 50124.70c | endf70e/ B-VII.0 | u/o2.10t | endf70sab/ endf7.0 |
| 64152.70c | endf70h/ B-VII.0 | o2/u.10t | endf70sab/ endf7.0 |
| 64154.70c | endf70h/ B-VII.0 | lwtr.10t | endf70sab/ endf7.0 |
| 64155.70c | endf70h/ B-VII.0 | poly.10t | endf70sab/ endf7.0 |
| 64156.70c | endf70h/ B-VII.0 | | |
| 64157.70c | endf70h/ B-VII.0 | | |
| 64158.70c | endf70h/ B-VII.0 | | |
| 64160.70c | endf70h/ B-VII.0 | | |